ISTANBUL TECHNICAL UNIVERSITY ★ GRADUATE SCHOOL

FABRICATION AND CHARACTERIZATION OF BIODEGRADABLE FIBROUS WEBS FOR VASCULAR GRAFT STRUCTURES

M.Sc. THESIS

Janset ÖZTEMUR

Department of Textile Engineering

Textile Engineering Programme

JANUARY 2022

ISTANBUL TECHNICAL UNIVERSITY ★ GRADUATE SCHOOL

FABRICATION AND CHARACTERIZATION OF BIODEGRADABLE FIBROUS WEBS FOR VASCULAR GRAFT STRUCTURES

M.Sc. THESIS

Janset ÖZTEMUR

Department of Textile Engineering

Textile Engineering Programme

Thesis Advisor: Assist. Prof. Dr. İpek YALÇIN ENİŞ

JANUARY 2022

ISTANBUL TEKNİK ÜNİVERSİTESİ ★ LİSANSÜSTÜ EĞİTİM ENSTİTÜSÜ

VASKÜLER GREFT YAPILARINA YÖNELİK BİYOBOZUNUR FİBRÖZ YÜZEY ÜRETİMİ VE KARAKTERİZASYONU

YÜKSEK LİSANS TEZİ

Janset ÖZTEMUR

Tekstil Mühendisliği Anabilim Dalı

Tekstil Mühendisliği Programı

Tez Danışmanı: Dr. Öğr. Üyesi İpek YALÇIN ENİŞ

OCAK 2022

Janset Öztemur, a M.Sc. student of ITU Graduate School student ID 503181804, successfully defended the thesis/dissertation entitled "FABRICATION AND CHARACTERIZATION OF BIODEGRADABLE FIBROUS WEBS FOR VASCULAR GRAFT STRUCTURES", which she prepared after fulfilling the requirements specified in the associated legislations, before the jury whose signatures are below.

Thesis Advisor :	**Assist. Prof. Dr. İpek YALÇIN ENİŞ** İstanbul Technical University	.....
Jury Members :	**Prof. Dr. Hale KARAKAŞ** Istanbul Technical University	.....
	Prof. Dr. Gülşah ÇEÇENER Bursa Uludağ University	.....

Date of Submission : 29 December 2021
Date of Defense : 10 January 2022

To my family and beloved ones,

FOREWORD

First of all, I would like to thank my advisor, İpek Yalçın Eniş, who has made a great effort in my entire academic life and thesis period, whose support I always felt, who made me feel my strength in my desperate times and always opened my horizons.

I would like to thank Prof. Dr. Gülşah Çeçener and Havva Tezcan Ünlü from Bursa Uludağ University, Faculty of Medicine for their consultancy and support on biological tests, which constitute an important part of the thesis.

I would like to thank Dr. Hande Sezgin, Handan Palak and Suzan Özdemir, who generously provided me with their knowledge and assistance throughout my graduate process.

I would like to thank my dear mother, father and brother, who always believed in me, trusted me, provided me with all kinds of financial and moral support in my whole life, and were the greatest partners of my success. Without their support, I would always be incomplete.

I would like to thank Kanşav Sezgin for his support and trust in me all along the way.

Due to their support and motivation throughout the whole process, I would like to thank Setenay Akman, Aslıhan Özkan, Bahar Gövdeli and Dinem Salı.

December 2021

Janset ÖZTEMUR
(Textile Engineer)

TABLE OF CONTENTS

Page

FOREWORD ..... **ix**
TABLE OF CONTENTS ..... **xi**
ABBREVIATIONS ..... **xiii**
SYMBOLS ..... **xv**
LIST OF TABLES ..... **xvii**
LIST OF FIGURES ..... **xix**
SUMMARY ..... **xxi**
ÖZET ..... **xxv**
1. INTRODUCTION **1**
1.1 Objective of the Study 1
1.2 Tissue Engineering and Regenerative Medicine 2
1.3 Tissue Engineering Applications 4
1.3.1 Transplantation 4
1.3.2 Mimicking target organs 5
1.4 Vascular Grafts 7
1.4.1 Vascular diseases 7
1.4.2 Structure of blood vessel 9
1.4.3 Imitiation of native artery 10
1.5 Biomaterials Used in Vascular Graft Applications 14
1.5.1 Natural biomaterials 15
1.5.2 Synthetic biomaterials 17
1.5.3 Hybrid biomaterials 20
1.6 Vascular Graft Fabrication Techniques 21
1.6.1 Electrospinning 22
1.6.1.1 Electrospinning production parameters 23
1.7 Recent Studies About Electrospun Vascular Grafts 27
1.8 Novelty of the Thesis 32
2. EXPERIMENTAL WORK **35**
2.1 Materials and Methods 35
2.1.1 Materials 35
2.1.2 Methods 36
2.1.2.1 Surface fabrication 36
2.1.2.2 Morphological characterization 39
2.1.2.3 Chemical characterization 42
2.1.2.4 Thermal characterization 43
2.1.2.5 Biological investigations 43
3. RESULTS AND DISCUSSION **49**
3.1 Morphological Characterization of Preliminary Study 49
3.1.1 SEM characterization 49
3.1.2 Fiber diameter analysis 51

ABBREVIATIONS

2D : Two Dimensional

3D : Three Dimensional

AA : Acetic Acid

AC : Acetone

AVG : Average

DCM : Dichlormethane dimethyl carbonate

DMC : Dimethyl Carbonate

DMEM : Dulbecco's Modified Eagle Medium

DMF : Dimethylformamide

DSC : Differential Scanning Calorimetry

ECM : Extracellular Matrix

ECs : Endothelial Cells

ePTFE : Expanded Polytetrafluorethylene

ETH : Ethanol

FDA : Food and Drug Administration

FTIR : Fourier Transform Infrared Spectroscopy

HUVECs : Human Umbilical Vessel Endothelial Cells

Mn : Number Average Molecular Weight

MSC : Mesenchymal Stem Cells

MTS : (3-(4,5-dimethylthiazol-2-yl)-5-(3-carboxymethoxyphenyl)-2-(4-sulfophenyl) -2H-tetrazolium)

MW : Molecular Weight

PBS : Phosphated Buffer Saline

PCL : Polycaprolactone

PET : Polyester

PGA : Poly glycolic acid

PLA : Polylactid acid

PLCL : Poly (L-lactide co-caprolactone)

PLGA : Poly (lactic-co-glycolic acid)

PLLA : Poly (L-lactide)

PU : Polyurethane

RM **:** Regenerative Medicine

SD **:** Standard Deviation

SEM **:** Scanning Electron Microscope

SMCs **:** Smooth Muscle Cells

TE **:** Tissue Engineering

TEVG **:** Tissue Engineered Vascular Graft

THF **:** Tetrahydrofuran

WCA **:** Water Contact Angle

SYMBOLS

°C	**:** Celcius
µm	**:** Micrometer
kV	**:** Kilovolt
m^2	**:** Meter Square
ml	**:** Mililiter
mmHg	**:** Burst Pressure
mPa	**:** Mega Pascal
N	**:** Newton
nm	**:** Nanometer

LIST OF TABLES

Page

Table 1.1: List of commercially available tissue engineering products for regenerative applications **8**
Table 1.2: Mechanical properties of native human blood vessels **12**
Table 1.3: Properties of PCL with different molecular weight (Mw) (Jiang & Zhang, 2013)..... **18**
Table 1.4: Physiochemical properties of PLA (Nampoothiri, Nair, & John, 2010) .. **19**
Table 1.5: Nanofiber production techniques for vascular graft applications (Zdraveva et al., 2017). **22**
Table 2.1: Solvent system components and their properties (Sigma Aldrich) **35**
Table 2.2: Sample codes and properties of the solvent systems..... **37**
Table 2.3: Sample codes and solvent details of the second study **38**
Table 2.4: Sample codes and the weight ratios of the polymer solutions **39**
Table 3.1: The average fiber diameters, and fiber morphology notes **52**
Table 3.2: The average fiber diameters, and fiber morphology notes **55**
Table 3.3: Pore analysis of the bead-free samples..... **58**
Table 3.4: Contact angle measurements of the fibrous webs **58**
Table 3.5: DSC analysis of fibrous surfaces **61**
Table 3.6: The average fiber diameters of the fibrous surfaces..... **65**
Table 3.7: Pore analysis of the bead-free samples..... **66**
Table 3.8: Contact angle measurements of the fibrous webs **67**
Table 3.9: DSC analysis of the samples during heating..... **72**
Table 3.10: Degredation rates (%) of the samples from 1 to month 4 ..... **74**

LIST OF FIGURES

Page

Figure 1.1 : Photograph of infamous mouse with tissue- engineered human ear (C. Vacanti, 2006). **3**
Figure 1.2 : The structure of a native artery. **10**
Figure 1.3 : Design parameters of a native artery. **10**
Figure 1.4 : Scanning electron microscope (SEM) images of a tubular vascular graft structure; before burst pressure testing (a), after testing (aneurysm part) (b). Aneurysm part of the scaffold (c) Reprinted from Yalcin Enis, Horakova, Gok Sadikoglu, Novak, & Lukas (2017). **13**
Figure 1.5 : Principle of the vascular tissue-engineering (inspired by the study of Sorrentino & Haller, 2011). **14**
Figure 1.6 : Synthesis of poly(ε-caprolactone) from ε-caprolactone or 6-hydroxyhexanoic acid (Bartnikowski et al., 2019). **17**
Figure 1.7 : Stereoforms of lactides. Reprinted from (Nampoothiri et al., 2010). **20**
Figure 1.8 : Components of electrospinning unit. **23**
Figure 1.9 : Schematic diagram of surface pore formation induced by breath figures mechanism. Reprinted from (C. Huang & Thomas, 2018). **26**
Figure 2.1 : Polymers used in thesis. Polycaprolactone with 45,000 Mn (a), poly (L-lactide) (b), polylactic acid (c), and polycaprolactone with 80,000 Mn (d). **35**
Figure 2.2 : Electrospinning apparatus (a) and fabricated surface on the collector (b). **36**
Figure 2.3 : Samples prepared for analysis (a), coating apparatus (b), and scanning electron microscope (SEM) (c). **40**
Figure 2.4 : Image J analysis. **40**
Figure 2.5 : Threshold of a SEM image. **41**
Figure 2.6 : 3G hz Porometer device. **41**
Figure 2.7 : KSV Attension Optical Contact Angle Meter. **42**
Figure 2.8 : FTIR device (UATR Two, Perkin Elmer) (a) and DSC device (DSC400, Perkin Elmer) (b). **42**
Figure 2.9 : Laminar flow cabinet for cell culture and UV sterilization processes. **44**
Figure 2.10 : Assay balance (a), biodegradation samples placed in 24 well plates (b), incubator (c). **45**
Figure 2.11 : 25cm^2 flasks (a), FibroGRO™-LS Complete Media Kit and DMEM-F12 medium (b), and samples in 6 well plates (c). **45**
Figure 3.1 : SEM images of (a) PCL100_16 at magnification of 5kx, (b) PCL100_18, and (c) PCL100_20 at magnification of 1kx. **50**
Figure 3.2 : SEM images of (a) PLA100_7, (b) PLA100_8, and (c) PLA100_9 at magnification of 5kx. **50**
Figure 3.3 : SEM images of (a) PLA75PCL25_12 and (b) PLA50PCL50_12 at magnification of 3kx. **51**
Figure 3.4 : SEM images at 1kx magnification of PCL samples at different concentrations (a) PCL100_6, (b) PCL100_8, and (c) PCL100_10. **53**

Figure 3.5 : SEM images at 1kx magnification of PLA samples at different concentrations (a) PLA100_6, (b) PLA100_8, and (c) PLA100_10. ..... **54**
Figure 3.6 : SEM images at 1kx magnification of PLA/PCL blend based samples at different concentrations (a) PLA50PCL50_6, (b) PLA50PCL50_8, and (c) PLA50PCL50_10. ..... **54**
Figure 3.7 : SEM images of the samples and their thresholdings (a) PCL100_10, (b) PLA100_8, (c) PLA100_10, (d) PLA50PCL50_8 and (e) PLA50PCL50_10. ..... **57**
Figure 3.8 : DSC analysis of PLA100 sample at two different heating/cooling rates. **60**
Figure 3.9 : DSC analysis of PCL100 sample at one heating/cooling stage. **61**
Figure 3.10 : DSC analysis of PLA50PCL50 blend samples at two different heating/cooling rates. **62**
Figure 3.11 : SEM images at 1000x magnification of the fibrous samples. a1, a2, and a3 represent PLA100, PLLA100, and PCL100, respectively. Group b1 to b5 are the SEM images of PLA10PCL90, PLA20PCL80, PLA30PCL70, PLA40PCL60, and PLA50PCL50, respectively while group c1 to c5 are the SEM images of PLLA10PCL90, PLLA20PCL80, PLLA30PCL70, PLLA40PCL60, and PLLA50PCL50, respectively. ... **64**
Figure 3.12 : FTIR curves of PCL100, PLA100, PLLA100, PLA50PCL50, and PLLA50PCL50 fibrous webs. **68**
Figure 3.13 : DSC curves of PLA100, PCL100, and PLA/PCL blends at heating stage. **70**
Figure 3.14 : DSC curves of PLA100, PCL100, and PLA/PCL blends at cooling... **71**
Figure 3.15 : DSC curves of PLLA100, PCL100, and PLLA/PCL blends at heating stage. **73**
Figure 3.16 : DSC curves of PLLA100, PCL100. and PLLA/PCL blends at cooling stage. **74**
Figure 3.17 : MTS analysis of the surfaces cultured with fibroblast cells on 3rd and 7th days. **76**
Figure 3.18 : MTS analysis of the surfaces cultured with HUVECs on 3rd and 7th days. **77**

FABRICATION AND CHARACTERIZATION OF BIODEGRADABLE FIBROUS WEBS FOR VASCULAR GRAFT STRUCTURES

SUMMARY

Cardiovascular diseases are among the most common types of non-infectious diseases, causing approximately 20 million deaths worldwide to date. Deaths caused by cardiovascular diseases, triggered by the increase in the stress level brought about by settling from rural to urban at the global level and the spread of unhealthy eating habits, increased by 21.1% between 2007 and 2017. According to the World Health Organization data, it is estimated that the annual incidence of cardiovascular disease-related mortality will increase to 23.6 million worldwide by 2030. On the other hand, while the Covid-19 pandemic, which affected the entire world, caused an unexpected increase in cardiovascular diseases, the fact that people with these types of diseases were among the ones defined as a high-risk group once again revealed the seriousness of the situation.

Mild cardiovascular diseases are treated with dietary modification, lifestyle changes, and medications, while treatment options for more damaged blood vessels usually consist of bypassing a part of the autologous vessel to replace the diseased part. The use of autologous vessels requires an additional clinical procedure such as vascular integration to the damaged area, as well as taking veins from certain parts of the body such as leg vein, forearm artery, and thoracic artery for this procedure. In addition to the aforementioned risks, dimensional incompatibilities may also occur in some cases. For this reason, the necessity of finding alternative solutions in order to overcome these problems experienced in autologous vessels is among the prominent issues in recent years. Although allografts taken from donors or cadavers and xenografts procured from animals are alternatives, they cannot fully meet this need due to the lack of donor/incompatibility and their short lifespan. Replacing the damaged vessel with a vascular graft in the treatment of cardiovascular diseases is one of the preferred methods of recent times, but problems such as infection formation, risk of thrombosis, incompatibility in radial elasticity, inadequacy in cell development, especially in small-caliber vessel changes, limit surgical success. At this point, the search for new materials and constructions has come to the fore, and the design of biodegradable scaffolds that can be replaced by an autograft produced by the body over time has taken its place among the priority research topics. Although important findings have been obtained in the research that has accelerated in the last 10 years, there is no small-caliber biodegradable vascular graft that has achieved commercial success yet. In order to meet the need, it is expected from the vascular graft to provide structural support and encourage cellular activity for the body to produce its vessel.

The most important step in approximating vascular grafts designs to native blood vessel structure is to optimize the surface morphology and develop a microenvironment in which cells can attach and proliferate. For this reason, the features of the graft surface should be well understood and morphological criteria should be determined.

Within this thesis, a detailed literature review is realized to understand the native artery structure and an experimental study is carried in three parts including the selection of biopolymers, optimization of solution and production parameters, and morphological, structural, thermal, and chemical analyses of the structures.

The first experimental part of the thesis is a preliminary study that includes the selection of biomaterials as well as optimization of solution parameters (polymer concentration and blend ratio) and production parameters (feed rate, voltage, and tip-collector distance). A literature review is performed for surfaces produced by electrospinning using low molecular weight polycaproclactone (PCL) and polylactic acid (PLA) polymers as part of this investigation. The affects of parameters like molecular weight, concentration, and blending ratio on surface morphology, smooth fiber production, and fiber diameter parameters are examined during the research work. Electrospinning parameters are systematically studied, and the influences of these parameters on fiber production are determined. Basic parameters such as voltage, feed rate, and tip-collector distance have been optimized in this context by considering the environment's temperature and humidity, as well as the characteristics of the polymer solution. In the first stage, PCL at 16, 18, and 20 % concentrations, PLA at 7, 8, and 9% concentrations and 12% concentration of PLA/PCL (25/75 and 50/50 ratios) are used for surface formation. In this context, a definite conclusion is reached about the polymers to be used in the thesis by evaluating the performances of the determined parameters in the fibrous surface formation process and the morphological properties analyzed by scanning electron microscopy (SEM); furthermore, polymer solution concentration ranges and blending ratio are determined. The results indicate that the spinnability of low molecular weight PCL (45,000 Mn) is insufficient since either bead formation or thick and discontinuous fiber-like forms are observed in all polymer concentrations while neat PLA and PLA/PCL blends have better spinnability, which allows smooth fiber production.

In the second part of the thesis, higher molecular weight PCL (80,000 Mn) is introduced to the fibrous webs in order to take the advantage of its better mechanical properties and spinnability. Similar to the preliminary part, PCL, PLA and PCL/PLA blends are studied, but polymer concentration ranges are kept constant as 6, 8, and 10% for all polymeric structures. The morphologies of the electrospun webs are observed by SEM, also fiber diameter and porosity values are measured. Thus, the polymer concentration at which smooth and fine fibers are obtained is determined for neat PLA and PCL in addition to PLA/PCL blends. The hydrophobicity of the surfaces is evaluated by water contact angle analysis (WCA). Differential scanning calorimetry (DSC) is used to observe the thermal behavior of the surfaces during heating and cooling to investigate the crystallinity of the surfaces that provide insights about biodegradability processes. Although it is not possible to obtain fibers at low polymer concentrations on all polymeric surfaces, 8%, and 10% polymer concentration allow continuous fiber formation; moreover, an expected relationship between fiber diameter and porosity ratio is detected. Surfaces with the finest fibers are those with the highest porosity. On the other hand, the thermal behavior of the surfaces is in line with the literature and the highest crystallinity is that of PCL with about 40%.

In the last and final part of the thesis, poly (L-lactide) (PLLA), a derivative of PLA, is also introduced in the study, and its effects on surface properties are investigated. Within the scope of developing the most suitable surface for vascular grafts, which is one of the major objectives of the study, different blending ratios for both PLA/PCL and PLLA/PCL are determined in detail. Similar to previous experimental parts, the

structures are mainly subjected to SEM, Fourier-transform infrared spectroscopy (FTIR), and DSC analyses, and the effects of blend ratios on morphological, thermal, and chemical properties are investigated in details. It has been observed that the fiber diameter increases with the increase of the ratio of PLA, which has a high molecular weight, in the PCL structure, but the increase in the ratio of PLLA, which has a lower molecular weight than PCL, in the PCL structure causes a decrease in fiber diameter. It has been determined that the polymer ratio is very effective on the fiber diameter depending on the molecular weight of the polymers, and during the thermal analysis, it determines the characteristic curves in the heating and cooling processes. Selected samples of PLA100, PCL100, PLA20PCL80, PLA50PCL50, PLLA20PCL80, and PLLA50PCL50 are subjected to biodegradability analysis at 1st, 3rd, and 5th months. All samples except PLA20PCL80 showed an increase in degradation rate in consecutive months. It is thought that this exception ocuurs in the PLA20PCL80 because of the measurement accuracy. As expected and as seen in the literature research, the degradation rate of PLA (14.29% and 40%, respectively) at the end of the 3rd and 5th months is considerably higher than that of PCL (2.17% and 3.70%, respectively). On the other hand, it is observed that 50% PLA ratio in the blend considerably increases the weight loss of the surface. Moreover, the addition of PLLA on surfaces is also found to accelerate biodegradation, similar to PLA. Cell analysis (MTS) consists of the proliferation of fibroblast and human umbilical vessel endothelial cells (HUVECs), which are one of the basic cells of the native vascular structure. In the content of MTS cellular analysis, affirmative outcomes are obtained in both fibroblast cells and HUVECs compared to control samples, and it is observed that each surface is a suitable environment for cells to live. Besides, PLA appears to have a positive effect on cell viability on PCL up to 20%, and the highest cell proliferation occurred in the PLA20PCL80 sample.

The findings of the experimental studies as detailed in the three stages above shed light on the best way to examine the morphological, chemical, thermal, and biological properties of a wide variety of surfaces produced from PLA, PLLA, and PCL polymers. Surfaces designed and fabricated according to the optimized parameters are promising for layered vascular graft structures. In the studies that will take place in the thesis' continuation, small-caliber vessel grafts will be designed and fabricated from these optimized surfaces with desired orientation levels, taking into account the mechanical properties of the vessels and advanced cell activities both *in-vitro* and *in-vivo*.

VASKÜLER GREFT YAPILARINA YÖNELİK BİYOBOZUNUR LİFLİ YÜZEYLERİN ÜRETİMİ VE KARAKTERİZASYONU

ÖZET

Kardiyovasküler hastalıklar, bulaşıcı olmayan en yaygın hastalık türleri arasında bulunup dünya çapında bugüne değin yaklaşık 20 milyon ölüme yol açmıştır. Küresel düzeyde kırsaldan kente yerleşmenin beraberinde getirdiği stres seviyesindeki artış ve sağlıksız beslenme alışkanlıklarının yaygınlaşması ile tetiklenen kardiyovasküler hastalıklardan kaynaklanan ölümler 2007-2017 yılları arasında %21,1 oranında artış göstermiştir. Dünya Sağlık Örgütü verilerine göre 2030 yılına kadar dünya genelinde yıllık kardiyovasküler hastalıklarla ilişkili mortalite insidansının 23,6 milyona çıkacağı tahmin edilmektedir. Öte yandan tüm dünyayı etkisi altına alan Covid-19 salgını, kalp ve damar hastalıklarının beklenmedik şekilde artmasına sebep olurken, yüksek risk grubu olarak tanımlanan kişiler arasında kalp-damar hastalıklarına sahip kişilerin yer alması, durumun ciddiyetini bir kez daha gözler önüne sermiştir.

Hafif seyreden kardiyovasküler hastalıklar diyet modifikasyonu, yaşam tarzı değişiklikleri ve ilaçlarla birlikte tedavi edilirken daha hasarlı kan damarları için tedavi seçenekleri genellikle baypas yöntemi ile otolog damarın bir bölümünün hastalıklı kısmın yerini almasından ibarettir. Otolog damarların kullanımı hasarlı bölgeye damar entegrasyonunun yanı sıra bu işlem için bacak toplardamarı, ön kol arteri, göğüs arteri gibi vücudun belirli bölgelerinden damar alma işlemi gibi fazladan bir klinik işlem gerektirmekte ve bu işlem şeker hastalığı, obezite ve benzer kronik rahatsızlıkları olan ve önceden kalp ameliyatı geçirmiş hastalar için büyük risk taşımaktadır. Bu risklerin yanı sıra bazı durumlarda boyutsal olarak uyumsuzluklar da yaşanabilmektedir. Bu sebeple otolog damarlarda yaşanan sıkıntıların üstesinden gelebilmek adına alternatif çözümler bulmanın gerekliliği son yıllarda öne çıkan konular arasındadır. Donör veya kadavradan alınan alogreftler ve hayvanlardan tedarik edilen ksenogreftler birer alternatif olmalarına rağmen donör eksikliği/uyuşmazlığı ve kısa ömürlü olmaları nedeni ile tam olarak bu ihtiyacı karşılayamamaktadır. Kardiyovasküler hastalıkların tedavisinde hasarlı damarın vasküler greftle değiştirilmesi ise son zamanların tercih edilen yöntemlerinden biri konumundadır ancak özellikle küçük çaplı damar değişimlerinde yaşanan enfeksiyon oluşumu, tromboz riski, radyal elastisitede uyumsuzluk, hücre gelişiminde yetersizlik gibi sorunlar, cerrahi başarıyı kısıtlamaktadır. Tam da bu noktada yeni malzeme ve konstrüksiyon arayışları gündeme gelmiş, biyobozunur özellikte olup zamanla yerini vücudun kendi ürettiği bir otogrefte bırakabilecek iskelelerinin tasarımı öncelikli araştırma konuları arasında yerini almıştır. Son 10 yılda hız kazanan araştırma konusunda önemli bulgular elde edilmiş olmasına rağmen, henüz ticari başarı elde edebilmiş küçük çaplı biyobozunur vasküler greft bulunmamaktadır. Bu noktada oluşan ihtiyacı giderme hususunda vasküler greftten vücudun kendi damarını üretebilmesi için geçecek süre boyunca yapısal destek sağlaması ve hücresel aktiviteyi teşvik etmesi beklenir.

Vasküler greftler tasarımlarını gerçek damar yapısına yaklaştırmadaki en önemli adım yüzey morfolojisini optimize etmek ve hücrelerin tutunup yaşayabileceği bir mikro-çevre geliştirmektir. Bu nedenle, greft yüzeyinin taşıması gereken özellikler etraflıca kavranmalı ve morfolojik kriterler belirlenmelidir.

Tez kapsamında, gerçek damar yapısı araştırılmış ve greft yüzeyinin sunması gereken yüzey özellikleri dikkate alınarak biyomalzeme, çözücü sistemi ve üretim yöntemi gibi temel parametrelerin optimizasyonu üzerine üç temel çalışma gerçekleştirilmiştir.

Tezin ilk çalışması bir ön çalışma niteliğinde olup biyomalzemelerin seçimi, konsantrasyon, moleküler ağırlık ve karışım oranı belirlenimi kriterlerini içermektedir. Bu çalışma kapsamında, elektrospinning yöntemi ile PCL ve PLA polimerleri kullanılarak üretilen yüzeyler için literatür araştırması yapılmıştır. Araştırma sürecinde moleküler ağırlık, konsantrasyon ve karışım oranı gibi parametrelerin yüzey morfolojisi, düzgün lif oluşumu ve lif çapı parametreleri üzerinde etkileri incelenmiştir. Diğer yandan, elektrospinning parametreleri de detaylıca araştırılmış ve bu parametrelerin lif üretimi üzerindeki etkileri tespit edilmiştir. Bu bağlamda ortamın sıcaklık ve nem değerleri ile birlikte polimer solüsyonunun özellikleri de göz önünde bulundurularak voltaj, besleme hızı ve uç-toplayıcı mesafesi gibi temel parametreler optimize edilmiştir. İlk etapta %16, 18 ve 20 konsantrasyonlarda PCL (45,000 g/mol moleküler ağırlık), %7, 8 ve 9 konsantrasyonlarda PLA ve %12 sabit konsantrasyonda PLA/PCL (25/75 ve 50/50 oranlarda), yüzey oluşumu için kullanılmıştır. Bu bağlamda, belirlenen parametrelerin fibröz yüzey oluşturma sürecindeki performansları değerlendirilmiş ardından tez kapsamında kullanılacak olan polimerler, polimer solüsyonu konsantrasyon aralıkları ve karışım oranı belirlenmiştir. Elde edilen sonuçlar doğrultusunda PCL'nin moleküler ağırlığının lif oluşumu noktasında yetersiz kaldığı ve konsantrasyon değerleri ile birlikte üretim şartlarının tekrar optimize edilmesi gerektiği kanısına varılmıştır. Bununla birlikte, daha karşılaştırılabilir sonuçlar için PLA polimerinin konsantrasyon aralıklarının daha geniş belirlenmesi gerektiğini ve %12'lik konsantrasyonda çalışılan 50/50 oranındaki PLA/PCL karışımının tatmin edici sonuçlar verdiği ilk çalışmanın çıktıları arasındadır.

Ön çalışma ışığında belirlenen özellikler neticesinde, ikinci çalışma kapsamında yüzeylerin en verimli düzeyde üretilebileceği konsantrasyon aralıkları incelenmiştir. Tüm polimer ve polimer karışımları için üç farklı konsantrasyon aralığı sabit tutulmuş ve yüzey özellikleri analiz edilmiştir. Yüzeyler öncelikler taramalı elektron mikroskopu (SEM) analizine tabi tutulup morfolojileri gözlemlenmiş ve sonrasında lif çapı ile gözeneklilik analizi gerçekleştirilmiştir. Lif çaplarının 2.5 μm'den az olduğu tespit edilmiş ve lif çapları ile gözeneklilik değerleri arasında tutarlı bir ilişki tespit edilmiştir. Lif çapının en ince olduğu yüzelerin gözeneklilik oranı en fazla olup hücresel çalışmalar için umut vaadetmektedir. Bu analizler sonucunda, düzgün ve ince lif eldesinin sağlandığı konsantrasyon PLA, PCL ve PLA/PCL bazlı yapılar için belirlenmiştir. Diğer bir morfolojik analiz olan su temas analizi ile üretilen yüzeylerin su emiciliği ve hidrofobik/hidrofilik karakteri test edilmiş, ayrıca literatür bilgilerinin sağlaması yapılmıştır. Literatür çalışmalarında da teyit edildiği üzere üretilen tüm yüzeylerin hidrofobik karakterde olduğu gözlemlenmiştir. Fourier Transform Kızılötesi Spektroskopisi (FTIR) analizi ile ise üretilen yüzeyler üzerinde çözücü kalıntısı kalıp kalmadığı üzerine yorumlar yapılmıştır. Yüzeylerde ana polimerlerin karakteristik pikleri hem saf polimerik yüzeylerde hem de karışım yüzeylerinde gözlemlenmiş ve yüzeylerde herhangi bir çözücü kalıntısı kalmadığı saptanmıştır. FTIR analizini yanı sıra, yüzeylerin ısıtma ve soğutma esnasındaki termal davranışlarının gözlemlenmesi adına Diferansiyel Taramalı Kalorimetre (DSC) cihazı

kullanılarak veriler elde edilmiştir. Termal analizler, yüzeylerin kristaliniteleri ile ilgili bilgiler sağlamış ve bu DSC analizi sonuçları doğrultusunda biyobozunurluk süreçleri ile ilgili öngörü edinimine yardımcı olmuştur. PLA100, PCL100 ve PLA50PCL50 olmak üzere üç numune üzerinde yapılan termal karakterizasyonlarda, polimerlerin kendilerine özgü erime ve kristalizasyon eğrileri tespit edilmiş ayrıca polimerlerin kristalinite değerleri de hesaplanmıştır. Beklendiği üzere, yaklaşık %40 ile en yüksek kristalinite değeri PCL polimerinde görülmüştür.

Son ve nihai çalışmada ise bir PLA türevi olan PLLA da çalışmaya dahil edilmiş ve yüzey özellikleri üzerindeki etkileri incelenmiştir. Çalışmanın ana amaçlarından biri olan vasküler greftlere en uygun karışım yüzeyinin geliştirilmesi kapsamında hem PLA/PCL hem de PLLA/PCL karışımları için farklı karışım oranları kullanılarak gözlemler yapılmıştır. Diğer çalışmalara benzer şekilde yüzeyler yüzey görüntülenmesi, lif çapı, gözeneklilik ve DSC analizlerine tabi tutulmuştur ve yapıdaki PLA, PLLA ve PCL oranının bu özellikler üzerindeki etkileri incelenmiştir. Yüksek moleküler ağırlığa sahip olan PLA'nın PCL yapısı içindeki oranının artmasıyla lif çapının arttığı fakat moleküler ağırlığı PCL'den daha düşük olan PLLA'nın PCL yapısındaki oranının artışının lif çapında bir azalmaya neden olduğu gözlemlenmiştir. Polimerlerin moleküler ağırlığına bağlı olarak lif çapı üzerinde polimer oranının oldukça etkili olduğu, termal analiz esnasında ise ısıtma ve soğutma süreçlerinde karakteristik eğrilerin belirginliğini belirlediği tespit edilmiştir. Öte yandan nihai çalışma kapsamında PLA100, PCL100, PLA20PCL80, PLA50PCL50, PLLA20PCL80 ve PLLA50PCL50 seçili yüzeyleri için biyobozunurluk ve hücre analizleri gerçekleştirilmiştir. Hücre analizleri, gerçek damar yapısının temel hücrelerinden olan fibroblast ve insan umbilikal damar endotel hücrelerinin (HUVEC) yüzeylere tutunma ve yayılma adımlarını içermektedir. PLA20PCL80 haricindeki tüm numunelerde, birbirini takip eden aylarda (1, 3 ve 5nci aylarda) bozunma oranında artış görülmüştür. PLA20PCL80'deki bu istisnanın ölçüm hassasiyetinden kaynaklı olduğu düşünülmektedir. Beklendiği ve literatür araştırmalarında görüldüğü üzere 3 ve 5nci ayların sonunda PLA'nın bozunma oranı (sırasıyla %14.29 ve %40), PCL'ninkinden (sırasıyla %2.17 ve %3.70) oldukça yüksektir. Diğer yandan, harman içindeki %50 PLA oranının yüzeyin kütle kaybını oldukça artırdığı gözlemlenir. Dahası, yüzeylerdeki PLLA eklentisinin de PLA'ya benzer şekilde biyobozunmayı hızlandırdığı tespit edilir. 12 ay boyunca devam edecek olan biyobozunurluk testinin gelecek çalışmalarda daha sağlıklı sonuçlar vereceği tahmin edilmektedir. Biyolojik gözlemleri kapsayan MTS hücresel analizi kapsamında, kontrol numunelerine kıyasla hem fibroblast hücrelerinde hem de HUVEClerde olumlu sonuçlar elde edilmiş, her bir yüzeyin hücrelerin yaşayabilmesi için uygun bir ortam olduğu gözlemlenmiştir. PLA'nın %20 orana kadar PCL üzerinde hücre yaşayabilirliği konusunda olumlu etkisinin olduğu görülmektedir ve en fazla hücre proliferasyonu PLA20PCL80 numunesinde meydana gelmiştir.

Sonuç olarak, tez kapsamındaki tamamlanan üç temel çalışma, tez konusunun yeni ve geliştirilebilir yönlerini göstermektedir. Optimize edilen parametreler doğrultusunda tasarlanan yüzeyler, devam eden bu çalışmanın hedef yapısı olan katmanlı vasküler greft konstrüksüyonları için umut vadetmektedir. Tezin devamında yapılacak olan çalışmalarda, damarın mekanik özellikleri de göz önünde bulundurularak oryante bir yapıya sahip, küçük çaplı vasküler greftler oluşturulacaktır. Ardından hem *in-vitro* hem de *in-vivo* ortamdaki hücresel aktivitelerinin yanı sıra vasküler grefften otolog kan damarı oluşum süreçleri gözlemlenecektir.

1. INTRODUCTION

1.1 Objective of the Study

The goal of this research is to develop electrospun fibrous scaffold surfaces for vascular graft applications using non-toxic solvent systems, biocompatible and biodegradable polymers.

The biopolymer selection is the most crucial stage in approaching the regenerated tissue since it designates the final physical, mechanical, and biological qualities of the vascular graft. The solvent system, on the other hand, has an impact on the physical properties of the polymer surface and should be taken into account when considering hazardous side of the organic solvents. High-hazard solution systems are employed to improve physical attributes like fiber diameter in many studies, but their impacts on nature and human are overlooked. One of the cornerstones of surface formation is choosing a simple and less troublesome production process that can meet both the specified qualities of the polymer solution and fibrous surface to be generated.

Within the scope of the thesis, PLA, PLLA, and PCL polymers with excellent biocompatibility and an ambitioned biodegradation time are chosen to match the needs of vascular graft surfaces. These biopolymers and their blends at different polmer ratios are electropun into fibrous web structures using solvent systems that have low toxicity and less influential on human health. The solution and production parameters are optimized during the surface fabrication phase to meet the standards for cell activity on the graft surface. The usability of surfaces that perform morphological, thermal, chemical and biological analyzes as small-caliber vascular graft material will be tested. It is thought that the findings of the thesis will offer an innovative material alternative for small-caliber vascular grafts, which is a very current and commercially unsuccessful study subject, and will shed light on the studies conducted in this direction.

1.2 Tissue Engineering and Regenerative Medicine

Today's growing human population and living conditions have resulted in a slew of health issues, with tissue and organ damage caused by disease, injury, and a lack of physical development becoming a serious problem. Although organ and tissue transplantation is one of the first alternatives for treating damaged tissue or organs, obstacles such as a huge waiting list for donors, logistical issues, and incompatibility of the transplanted tissue with the patient limit its applicability (Chandra, Soker, & Atala, 2020). There are 117,336 people on the organ donation waiting list in the United States alone, with about 80% of those on the list waiting for more than a year ("Organ Procurement and Transplantation Network," 2021).

Tissue engineering (TE) has emerged as a viable solution for addressing this crucial medical need. TE and regenerative medicine (RM) are multidisciplinary fields that merge knowledge and technologies from a variety of disciplines, including biology, chemistry, engineering, medicine, pharmaceuticals, and material science, to improve therapeutic approaches and products for the maintenance or replacement of damaged tissues and organs (Langer & Vacanti, 1993). Since accidents, diseases, and congenital malformations have long been a part of life, the urge to repair a damaged body part is a phenomenon even seen in myths such as Prometheus' perpetual liver regeneration. The systematic deciphering of biology's secrets was combined with a scientific understanding of disease and trauma. In addition to partial organ or tissue repair using artificial materials or prothesis, the replacement one tissue with another was generated as a therapeutic option (J. P. Vacanti & Vacanti, 2013).

Many investigations on tissue regeneration and treatment have been conducted in the scientific community for many years. Dr. Charles Vacanti and colleagues at the University of Massachusetts Medical Center accomplished the first real step in tissue engineering by growing human cartilage *in-vitro* on a biodegradable scaffold and then constructing a cartilage structure on the back of a nude mouse that looked like a human ear (C. Vacanti, 2006) (Figure 1.1). Despite tissue engineering has been studied for many years, developing a structure that can imitate the target tissue and provide the exact microenvironment for cells to generate new tissue remains a challenge. Since there are different properties that the surface should have, the pre-production,

production and post-production stages of the scaffold surface should be discussed in detail.

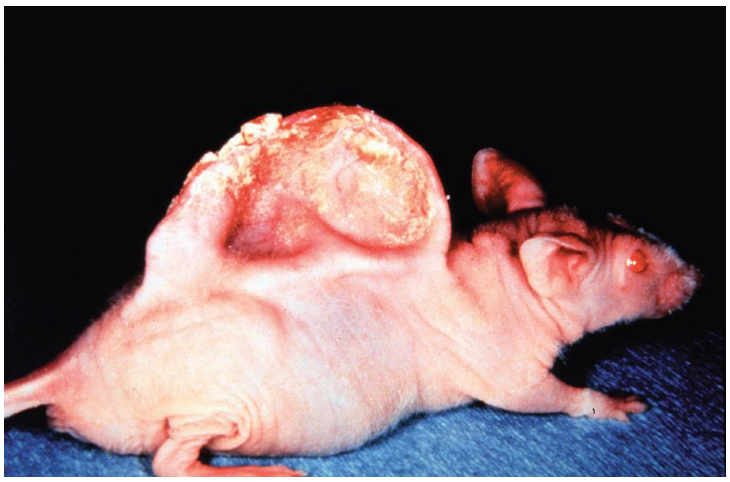

Figure 1.1 : Photograph of infamous mouse with tissue- engineered human ear (C. Vacanti, 2006).

Scaffolds provide adequate mechanical support as well as convenient survival conditions, optimal oxygen and nutrition levels, also efficient supplement and waste movement in the cell microenvironment (Dziki, Huleihel, Scarritt, & Badylak, 2017). Extracellular matrix (ECM), which is one of the most essential components in the cell microenvironment that provides mechanical reinforcement to preserve tissue/organ structure, and affects cell behaviour in many aspects such as cell viability, migration, proliferation, and differentiation (Barthes et al., 2014; Yi, Ding, Gong and Gu, 2017). To offer equivalent three dimensional (3D) microstructures for the damaged sites, the cells must build their own ECM simultaneously when the scaffold biodegrades (Mabrouk, Beherei, & Das, 2020). Therefore, a tissue-engineered scaffold should be a convenient structure that imitates the regulatory role of the natural ECM and leads the way in tissue regeneration (Luo, 2020). On the other hand, there are morphological features that a scaffold should possess, such as high surface to volume ratio (Adhikari, Tucker, and Thomas, 2019), adequate pore architecture and porosity (Loh and Choong, 2013), optimum fiber diameter at nano/microscale and desired fiber orientation (Li et al., 2018). Also, pore size and fiber diameter have a proportional relationship; pore size increases as the fiber diameter increases (Han et al., 2019). Pore size is an essential parameter as it affects mass transfer such as water and nutrient diffusion into the scaffold, also assists cell behaviours like cell attachment, viability, and proliferation (Luo, 2020). In addition to the importance of the biological and morphological

properties of tissue-engineered scaffolds, the mechanical features are also undeniably substantial. While numerous tissues, including the cardiac muscle, heart valves, and blood vessels have distinctly elastomeric properties, tensile modulus and strength are of vital significance for tendons and ligaments (Ma, 2008).

1.3 Tissue Engineering Applications

1.3.1 Transplantation

Cells with tissue-specific mechanisms of action have a powerful therapeutic effect, making cell-based therapies viable options for treating a wide range of injuries and disorders. Scaffold-based tissue engineering attempts to establish effective cell proliferation and development strategies as well as addresses the limits of direct cell injection therapies by producing 3D tissue constructs (De Pieri, Rochev, & Zeugolis, 2021). These constructs are classified as cell-free or cell-laden in today's scaffold-based tissue engineering studies.

Cell-Laden Scaffolds: Cells are seeded onto scaffolds in cell-based bioengineering, giving biological and anatomical functions such as cell microenvironment, cell proliferation, and tissue integration to the scaffold constructions (Kim, Atala, & Yoo, 2020). Cell development can also be performed through bio-printing (Akentjew et al., 2019; Patrício et al., 2014; Pereira et al., 2017) and co-electrospinning (Feng et al., 2020; Khanmodahammadi, Zolfagharzadeh, Bagher, Soltani, & Ai, 2020; Zussman, 2011) technologies to directly incorporate cells into the scaffold structure. This procedure often permits cells to be incorporated into the scaffold's inner structure, reducing the requirement for cells to move on their own. Yeo et al. (2015) electrospun the cells by embedding them in an alginate-based bioink and combining them with the PCL-based construct to create a tissue regeneration scaffold. In another study, a cell-loaded methacryloyl gelatin-alginate hydrogel layer was combined with PCL sub-micron fibers to simulate the human coronary artery, resulting in a successful construction with the coronary artery's unique J-shape mechanical characteristics (Akentjew et al., 2019). The need for cell seeding is avoided with these strategies, and the problem of nonhomogeneous cell dispersion is addressed.

Cell-Free Scaffolds: Despite their potential benefits, cell-based scaffolds have several disadvantages, including a lack of autologous cells, time/cost-intensive cell growth

processes, a relatively low survival rate, and a significant risk of immunological rejection (Q. Li, Ma, & Gao, 2015). These issues have prompted scientists to develop cell-free scaffolds that stimulate endogenous cells in the body and successfully address possible tissue healing subjects (L. Li et al., 2019). In this approach, a cell-free designed scaffold is implanted where host stem cells or tissue-specific cells are gathered in the damaged tissue area, and the treatment is provided by utilizing the body's own biological resources and its reparative ability (Aibibu, Hild, Wöltje, & Cherif, 2016). In a study of Jin et al., poly (L-lactic acid-co-caprolactone) (PLCL) and silk are used to produce a heparinized cell-free vascular graft via electrospinning and conduct an *in-vivo* research on a rabbit model. As a result of this research, it has been stated that a structure with sufficient mechanical characteristics is generated, allowing cell proliferation and native tissue synthesis.

The surface developed within the scope of the thesis is also designed as cell-free, no cell type is encapsulated on the fibrous surface.

1.3.2 Mimicking target organs

The field of tissue engineering applications is expanding as therapeutic applications evolve. Researchers are exploring on tissue engineering applications for all components of the biological system that can be biologically replaced or regenerated.

Kidney and Genitourinary System: One of the biggest global health challenges is kidney disease, which includes acute kidney injury, chronic kidney and end-stage renal disease (N. B. lai. Johnson, Hayes, Brown, Hoo, & Ethier, 2014). Dialysis for the rest of one's life and kidney transplantation are two of the current therapeutic options for renal disease. Although dialysis can substitute renal filtration by eliminating toxins through extracorporeal blood purification, it can't take care of other vital renal processes (Kim et al., 2020). Another urinary system part is the bladder and urethra. Genetic abnormalities, cancer, trauma, inflammation, and other ailments of the bladder and urethra can impair the anatomical tissue structure of the bladder and urethra, resulting in full loss of function (Y. Zhang, Yoo, & Atala, 2020). Tissue engineering becomes a promising option using natural and synthetic biomaterials for the treatment of damaged areas in the urinary system.

Skin: The skin, which covers the biggest surface of the human body, performs a critical function in protecting the body from different external stimuli. It is made up of three

layers: epidermis, dermis, and hypodermis (H. M. Wang et al., 2013). Furthermore, the skin is one of the most injured organs, and numerous acute and chronic wounds such as burning, abrasion, lesion, or leg ulcer pose a significant threat to dermal tissues (Chaudhari et al., 2016). In skin injuries, the process includes recruiting immune cells to the damage site, fibroblasts building a new tissue matrix, keratinocyte re-epithelialization, and wound revascularization. This is a very complicated and progressive process involving a wide range of variables. Otherwise, the patient may die or the wound may become chronic (Groeber, Holeiter, Hampel, Hinderer, & Schenke-Layland, 2011). Although many therapies or donations can help with these issues, they are not always sufficient. Tissue engineering is used to study the growth and proliferation of skin cells as well as the therapy of damaged areas. Collagen, one of the most significant components of human connective tissues, has emerged as a promising therapy option, particularly for skin soft tissues (H. M. Wang et al., 2013). Other polymers commonly utilized in wound therapies include fibrin (Gsib, Egles, & Bencherif, 2017), hyaluronic acid (Hemshekhar et al., 2016), and poly(lactic-co-glycolide) (PLGA) (Caihong Zhu et al., 2018).

Muscoloskeletal System: The muscoloskeletal system is mostly made up of bone, cartilage, and tendon, and it is a major tissue engineering study area. Furthermore, there is a commercial market for cartilage (e.g., MACI [Verical], Maix [Matrical], and Hyalograft [Fidia Advanced Biopolymers]) and bone tissue (e.g., Bio4 [Osiris Therapeutics], Bond Apatite [Augma Biomaterials], and TruGraft [Osteobiologics]) (Belleghem, Mahadik, Snodderly, & Fisher, 2020). Bone damage is one of the most prevalent orthopedic disorders, and while it is an alternative to donor treatment, it is insufficient owing to a lack of bone supply, a high complication rate, disease transfer, and a variety of infections (L. Li et al., 2019). Cartilage problems, on the other hand, are rather prevalent and necessitate extensive clinical intervention. In the therapy of these disorders, mesenchymal stem cells (MSC) are used in the Microfracture and Autologous Chondrocyte Implantation approach. However, the post-operative microenvironment may fail to coordinate MSCs, resulting in inadequate native cartilage development (Guo et al., 2018). Bone and cartilage tissue engineering comes into play as a result of the scenarios outlined above, and it is hopeful for individuals suffering from these diseases.

Cardiovascular System: Cardiovascular disorders are among the leading diseases that cause death worldwide (Ghiasi, Zendehboudi, & Mohsenipour, 2020). The absence of regeneration following myocardial injury is one of the major constraints in the therapy of cardiovascular disease (Y. Zhao, Eng, Lee, Radisic, & Vunjak-Novakovic, 2020). The cardiovascular system is the system that pumps critical blood fluid, also cardiac, heart valve, and vascular graft tissue engineering researches are included. Because of its vital functions, the cardiovascular system is one of the tissue engineering applications with the most limits and challenges. As a result, all components should be analysed critically, and the product should be created accordingly. Despite the fact that there are numerous promising research in this subject (Yalcin Enis, Sadikoglu, Horakova, & Lukas, 2018; Gao et al., 2019; Horakova et al., 2018; Yalcin Enis, Horakova, Sadikoglu, Novak, & Lukas, 2017; F. Zhang et al., 2021), no product has yet been developed that achieves the desired outcome.

In this thesis, by targeting the native vascular structure, which is one of the most important elements of the cardiovascular system, studies are carried out on obtaining a biodegradable surface suitable for this target tissue.

In addition to the applications mentioned above, tissue engineering-based studies are also carried out on subjects such as the nervous system, retinal degeneration, dental applications, lung regeneration, and drug (Lanza, Langer, Vacanti, & Atala, 2020). In addition, some tissue engineering products commercially available in the market and their information are given in Table 1.1 (Belleghem et al., 2020).

1.4 Vascular Grafts

1.4.1 Vascular diseases

Not included in the infectious diseases category, cardiovascular diseases (including coronary heart disease and stroke) are the most common disease worldwide and accounted for an estimated 17.8 million deaths in 2017. More than three-quarters of these deaths occurred in low-income and middle-income countries (Kaptoge et al., 2019). Deaths from cardiovascular diseases triggered by the increased stress level brought about by rural to urban resettlement and unhealthy eating habits increased by 21,1% between 2007 and 2017 (Fuster, 2014; Kaptoge et al., 2019). According to the data of the World Health Organization, it is estimated that the annual incidence of

deaths due to cardiovascular diseases worldwide will reach 23,6 million by 2030 (World Health Organization, 2020).

Table 1.1: List of commercially available tissue engineering products for regenerative applications.

Tissue	Commercial Name	Scaffold Material	Cells	Manufacturer
Skin	Dermagraft	PGA and PLA fibers and silicon film	Fibroblasts	Advanced Biohealing, USA
	Apligraf	Bovine collagen	Keratinocytes and fibroblasts	Organogenesis, USA
	Orcel	Bovine collagen sponge	Keratinocytes and fibroblasts	Ortec International, USA
	TissueTech	Hyaluronic Acid	Keratinocytes and fibroblasts	Fidia Advanced, Biopolymers, Italy
	Matriderm	Human acellular dermis	Keratinocytes and fibroblasts	Dr. Suwelack Skin & Health Care, Germany
	Alloderm	Human acellular dermis	none	LifeCell, USA
Bone	Osteocel	Demineralized human allograft bone	Human mesenchymal stem cells	NuVasive, USA
	AlloStem	Demineralized human allograft bone	Allograft stem cells from human adipose tissue	AlloSource, USA
	Trinity/Trinity Evolution	Demineralized human allograft bone	Human mesenchymal stem cells and osteoprogenitor cells	Orthofix, USA
Cartilage	MACI	Porcine collagen membrane	Autologous cultured chondrocytes	Vericel, USA
	Carticel	none	Autologous cultured chondrocytes directly injected into defect with Dulbecco's Modified Eagles Medium (DMEM)	Vericel, USA
	ChondroCelect	none	Autologous cultured chondrocytes cell suspension	TiGenix, Belgium
	BioSeed-C	Bioresorbable two component gel-polymer scaffold	Autologous cultured chondrocytes	BioTissue, Switzerland
	DeNovoNT	Human particulated juvenile cartilage	Allogeneic chondrocytes	Zimmer, USA
Eye	Prokera	Amniotic membrane tissue	none	BioTissue, USA

While mild cardiovascular diseases are treated with modification of dietary, lifestyle changes, and medications, treatment options for more damaged blood vessels usually consist of replacing the diseased part with a portion of the autologous vessel via bypass method (Pashneh-Tala, MacNeil, & Claeyssens, 2016). Although autologous vessels are considered to be a quite good candidate for cardiovascular diseases, reasons such as alteration of the vascular structure (atherosclerosis), dimensional incompatibility of the autologous vessel, donor morbidity and the patient's previous vascular change or other diseases pose a risk (Liu et al., 2020; Zamani et al., 2017). On the other hand, saphenous vein, which is the most preferred autologous vein in bypass procedures, carries the risk of structural deterioration when exposed to blood pressure as well as vascular occlusion (Bos, Poot, Beugeling, Van Aken, & Feijen, 1998; Eschenhagen, Reichenspurner, & Zimmermann, 2013). Therefore, the necessity of finding alternative solutions to overcome the problems experienced in autologous vessels has been among the prominent issues in recent years. However, allografts taken from donors or cadavers, and xenografts obtained from animals are alternatives, they cannot fully meet this need due to the lack/incompatibility of donors and their short life (Hasan et al., 2014). For all these reasons, grafts, which offer more risk-free and easier application, promise for patients who need vascular replacement.

1.4.2 Structure of blood vessel

The native artery has a highly complex, multi-layered structure, and in a replacement vascular graft design each layer is expected to be imitated by considering the physical, mechanical, histological and topographic features of each layer of the native vessel (Adhikari et al., 2019). The vascular structure consists of three main layers: tunica intima, tunica media and tunica adventitia (Figure 1.2). *Tunica intima*, the innermost part of the three concentric layers closest to the blood flow, consists mainly of a simple but regular single endothelial cell (EC) layer containing connective tissues, and is directly connected to the basement membrane. Also, biological signaling events, orientation of ECs, intracellular protein expression, cytoskeleton construction, anti-platelet aggregation, and cell-cell interactions can be regulated in this layer (Jia, Li, Weng, Gu, & Chen, 2020). *Tunica media* is the habitat of spindle-shaped smooth muscle cells (SMC). Having low tensile strength in the middle layer, elastin functions as a relaxant stress behavior and distributes stress evenly across the wall of the vessel to the stronger collagen fibers (Goins, Webb, & Allen, 2019). *Tunica adventitia*, the

outermost layer of fibroblast cells, consists of an extracellular collagen matrix which contains perivascular nerve cells, and is responsible for preventing vasodilation and deformation under physiological stress (Goins et al., 2019; Yalcin Enis & Gok Sadikoglu, 2018). The goal of this thesis is to develop linear surfaces that best match target tissue and can be used in layers with different properties before vascular graft formation.

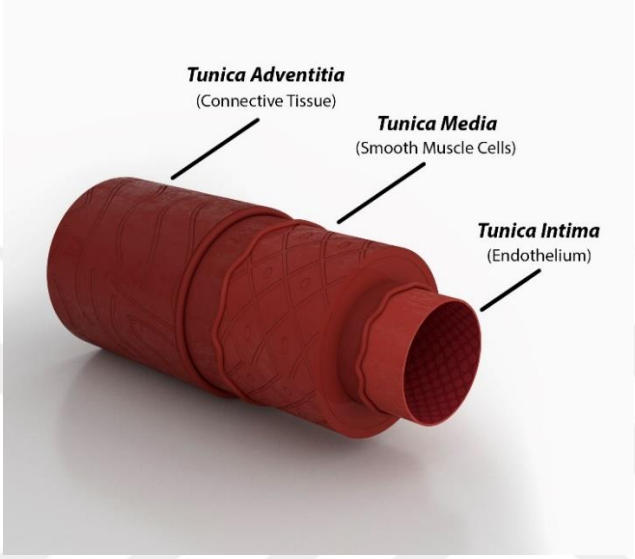

Figure 1.2 : The structure of a native artery.

1.4.3 Imitiation of native artery

In order to mimic the target tissue, vascular grafts must meet certain structural requirements, just like other tissue engineering applications. These characteristics can be divided into three categories: structural, mechanical, and biological (Figure 1.3).

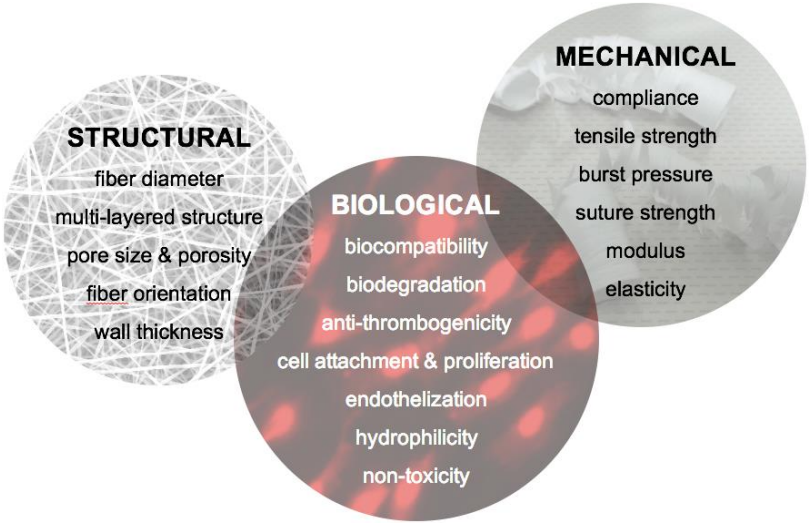

Figure 1.3 : Design parameters of a native artery.

Each layer of the arterial construction has different characteristics and serves different functions. Therefore, the morphological, mechanical, and biological properties of each layer should be unique. The innermost layer is expected to have low porosity that allows the proliferation of ECs but also prevents blood leakage, while the middle and outer layers are expected to have a larger porosity suitable for SMCs diffusion (J. Wu et al., 2018). Considering these qualifications, the pore properties of each vascular graft layer surface can be optimized by adjusting the fiber diameter, which is directly proportional to the pore size and porosity (Soliman et al., 2011). In addition to the specified morphological parameters such as fiber diameter and pore size, the wall thickness of the scaffold, as a dimensional feature, also determines the mechanical and biological properties of vascular grafts (Yalcin Enis & Gok Sadikoglu, 2018). Yalcin et al. (2016) performed histological analysis of the native vessel and measured the lumen thickness in the range of 400-1000 μm. Additionally, varying research in the literature, investigates vascular graft architectures with various wall thicknesses, both single-layer and multi-layer, and the effects of these values on the vessel's compliance value (Abdal-hay, Bartnikowski, Hamlet, & Ivanovski, 2018; Devan Ohst, 2015; R. Johnson, Ding, Nagiah, Monnet, & Tan, 2019). It is possible to deduce that thin wall thickness enhances the compliance properties in line with the findings obtained from these researches that emphasize the importance of wall thickness.

Dynamic-mechanical compliance between the native artery and the vascular graft is highly crucial; otherwise, flow separation and low wall shear stress may arise as well as the failure of blood flow and intimal hyperplasia (Montini-Ballarin et al., 2017). The graft structure should match the mechanical characteristics of the native human blood vessels (Table 1.2) as closely as feasible in order to endure the numerous mechanical loads that the vascular graft is exposed to and to achieve a successful construction. The vascular structure shows low modulus response at low strain first due to low modulus elastin, while at higher tensions it shows stiffening behavior by straightening elastin and high modulus collagen fibers; furthermore, this mechanical behavior is called the J-shaped structure (Zhalmuratova et al., 2019). Imitation of this structure in accordance with mechanical needs affects the elastic behaviors such as the formation of the J-shape structure, which is an extremely critical feature (Montini-Ballarin et al., 2016). The researchers aim to design vascular grafts that behave as a J-

shaped structure under pressure in their studies by utilizing both natural (Akentjew et al., 2019) and synthetic polymers (Rapoport et al., 2012; Yang et al., 2016).

Table 1.2: Mechanical properties of native human blood vessels.

Typeof Blood Vessel	Elastic Modulus (MPa) Circ./Long.*	Ultimate Stress (MPa) Circ./Long.	Strain at Failure (%) Circ./Long.	Burst Pressure (mmHg)	Suture Retention (N)	Compliance (%/100mmHg)	Ref.
Saphenous vein	42.62 ±27.76 /130.2 ±56.36	3.01 ±1.91 /13.22 ±5.73	NA	NA	NA	NA	(Donovan, Schmidt, Townshend, Njus, & Sharp, 1990)
	NA	NA	11±5/17±10	1599±877	1.76-2.45	0.7-2.6	(Konig et al., 2009; Zamani et al., 2017)
Internal mammary artery	8 /16.8	4.1/4.3	134/59	NA	NA	NA	(Hasan et al., 2014)
	NA	NA	NA	3196±1264	1.35±4.5	11.5±3.9	(Konig et al., 2009)

Arteries whose constituent components are collagen and elastin are constantly exposed to pressure and shear stress due to the flow of blood with a velocity of 1,2 cm/s and a pressure of 87 mmHg, continuously. This biomechanical stretch and un-stretch cycles cause momentary dimensional changes in artery diameter (Hoskins et al., 2017). Therefore, a tissue-engineered vascular graft (TEVG) should be resistant to blood pressure and stretching cycle. Moreover, TEVGs should have a mechanical strength similar to native vessels, with a burst pressure of approximately 2000 mmHg to prevent aneurysmal expansion (Seifu, Purnama, Mequanint, & Mantovani, 2013). The aneurysm problem for vascular graft designs is also discussed by Yalcin Enis et al. (2017), not in terms of the compliance difference between the scaffold and the native vessel but the difference through the length of the fibrous scaffold because of nonhomogeneous fiber distribution obtained (Figure 1.4). The vascular scaffolds should also have sufficient suture retention when surgically sutured with the native artery (Zamani et al., 2017).

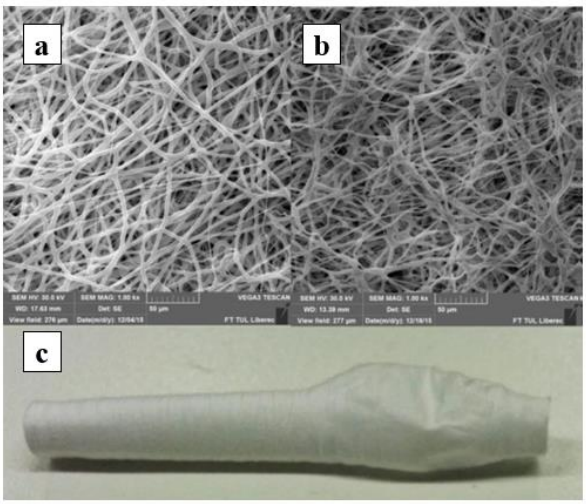

Figure 1.4 : Scanning electron microscope (SEM) images of a tubular vascular graft structure; before burst pressure testing (a), after testing (aneurysm part) (b). Aneurysm part of the scaffold (c) Reprinted from Yalcin Enis, Horakova, Gok Sadikoglu, Novak, & Lukas (2017).

The biological activity of vascular graft surfaces, in addition to structural and mechanical qualities, ensures vital information on the graft's applicability. Vascular graft structure must be biocompatible for the cells to survive and matrix deposition, besides to not causing any incompatibility in the body (Ratcliffe, 2000; Yalcin et al., 2016). Besides, blood-graft contact can promote blood coagulation by activating platelets, or biomaterial degradation can cause blood clot formation, hence the vascular graft structure must be hemocompatible (Mulinti, Brooks, Lervick, Pullan, & Brooks, 2018; Rizwan et al., 2020).

The extracellular microenvironment contains biochemicals that enable the biological activity of growth factors such as proteoglycan, collagen, elastin, glycosaminoglycans and structureless matrixcellular proteins (Petreaca & Martins-Green, 2013). Cell adhesion, filtration, and proliferation on the vessel surface are all signs that the cell is capable of forming its own ECM. Furthermore, the biodegradation of the scaffold when the cells produce the self-ECM is a significant criterion for vascular graft researches. Otherwise, the non-biodegradable polymer-based surface may have deleterious effects on living things and harm them (Rizwan et al., 2020). Together with being biodegradable, having sufficient biodegradability time offers the stability for cells to synthesize structural proteins and form autologous tissue (Hiob, She, Muiznieks, & Weiss, 2017; J. Wu et al., 2018). Before clinical investigations, *in-vitro* testing are critical for analyzing cell adhesion, proliferation, viability, and

morphology, as well as the graft's degradation over time. A suitable vascular graft should provide adequate anti-thrombogenicity to the structure to prevent coagulation or stenosis after implantation and promoting proper endothelialization (Joshi et al., 2020). Moreover, the production principle of the vascular grafts can bee seen in the Figure 1.5.

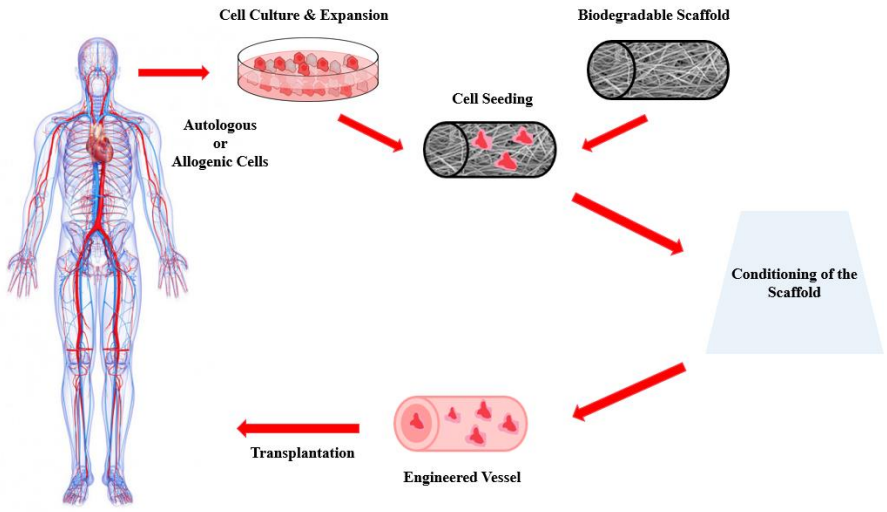

Figure 1.5 : Principle of the vascular tissue-engineering (inspired by the study of Sorrentino & Haller, 2011).

The scaffold material has a big role in the success of graft designs and the achievement of the above-mentioned attributes, along with the additional parameters such as solvent system and production method. Determining the appropriate biomaterial by considering the structural, mechanical and biological properties of the native vessel is vital for vascular graft designs. The main research focus of this thesis is on the structural and biological features of vascular grafts.

1.5 Biomaterials Used in Vascular Graft Applications

The selection of biomaterials is crucial for enhancing an effective regenerated vascular structure similarly in all tissue engineering strategies, as it affects long- and short-term mechanical properties, cell-cell and cell-matrix interactions, biocompatibility, biodegradability, toxicity, manufacturability, and shape of the final scaffold, in addition to providing the basic structure for cell growth (Chesterman, Zhang, Ortiz, Goyal, & Kohn, 2020; Suwantong, 2016; Thomas, Lekshmi, & Nair, 2013). Although it is highly preferred in large diameter grafts, the use of polymers such as polyethylene terephthalate (PET), polytetrafluoroethylene (ePTFE), and polyurethane (PU) in small

diameter grafts is limited due to incomplete endothelialization and intimal hyperplasia caused by the long stay of these polymers in the body (Hiob et al., 2017). Moreover, the use of the aforementioned polymers in small-caliber vessels, in addition to having properties such as inadequate structural porosity, insufficient cell adhesion, and proliferation, low elasticity level, also causes restenosis (narrowing of the vessel and thus the restriction of the blood) and various infections (Liu et al., 2020; Spadaccio et al., 2016). Thus, small-caliber graft designs, biodegradable synthetic polymers or natural/structural proteins are favored since they provide the qualities required to fulfil the goal of establishing an autologous blood vessel after implantation (Oztemur & Yalcin Enis, 2020). Polymers that can be degraded in the biological environment and do not show toxic effects in this process are also very advantageous materials because there is no need for a second operation to remove the graft from the body (Kai, Liow, & Loh, 2015; Xue & Greisler, 2003). Hence, biodegradable polymers have become promising materials for vascular grafting applications.

The biodegradable polymers can be divided into three groups as natural, synthetic, and hybrid. The natural biodegradable polymers are very successful in biocompatibility and cell activities, while synthetic ones have properties such as high strength and controllable degradation (Thomas et al., 2013). Even though natural and synthetic biomaterials can be used in neat form, their blend or copolymer versions with other biopolymers are also preferable due to compensate for the deficient sides of the polymers or to add extra superior properties to the scaffold.

1.5.1 Natural biomaterials

Biopolymers that are derived from natural sources are widely used in biomedical applications as they are highly biocompatible and offers opportunity to enhanced cell activities such as cell adhesion, growing, proliferation, and cell to cell signalling (Shojaee & Bashur, 2017).

Collagen: Collagen is the main protein in the ECM structure (Zhou, Cao, Ma, & Lin, 2010). There are two major types of collagens: fibrillar and non-fibrillar. For most animal tissues, fibrillar collagen forms (collagen type I, II, III, VI and XI) elongated fibril structures, which are recognised for their structural function in mechanical support. Collagen type I is one of the most commonly used collagen types in tissue engineering applications. Moreover, non-fibrillary collagens can be classified into sub-

categories including the network-forming collagens (collagen types IV and VII), fibril-associated collagens (collagen types IX and XII), and membrane-associated triple helix collagens (Copes, Pien, Van Vlierberghe, Boccafoschi, & Mantovani, 2019). Even though collagen has excellent biocompatibility and weak antigenicity, it suffers from the mechanical properties (Lee, Singla, & Lee, 2001).

Elastin: Elastin is also one of the core components of the extracellular vascular matrix that provides elasticity and strength (Koens et al., 2010). In addition to its desirable mechanical properties, elastin serves as a major promoter for vascular cells, prohibiting for smooth muscle cell migration and proliferation, and improving EC attachment and proliferation (Wise et al., 2011).

Gelatin: Gelatin is a type of protein that includes 19 aminoacids in its structure (Vroman & Tighzert, 2009). It is derived from skin, bone or connective tissues by hydrolysis of collagen. Although gelatin is preferred owing to its fluid loss prevention feature, it is generally used in a mixture of other biopolymers due to the insufficient mechanical and degredation features (Gu et al., 2016).

Silk Fibroin: Silk fibroin is a protein based polymer which is derived from animal sources (Catto et al., 2015). It is composed of highly repeated primary sequence, which results in great homogeneity in the secondary ß-sheet structure, a high crystalline characteristics and impressive mechanical features. As silk is an attractive biodegradable material in terms of not only its mechanical properties but also suitability for cell activities and biocompatibility, it has a great place in small vascular graft studies (Marelli et al., 2012). Moreover, it can be conveniently processed into a number of structures including hydrogels, films, porous scaffolds, and micro/nano particles (Chan et al., 2019).

Chitosan: Chitosan is a biocompatible, biodegradable, nontoxic, and non-antigenic biopolymer sourced from crustaceans such as crabs and shrimps (Chenhui et al., 2009). Further, it has a rigid and crystalline structure due to the strong intermolecular hydrogen bonds in the structure (Vroman & Tighzert, 2009). For this reason, it is mostly used in a blend of softer polymers in order to be used in tissue engineering applications.

1.5.2 Synthetic biomaterials

Synthetic polymers are widely used to acquire scaffolds with sufficient mechanical properties, which keep their strength for relatively long periods and allow the regeneration of new tissues. The mechanical properties of synthetic polymers can be managed effectively compared to natural polymers, so they allow the development of tissue engineering structures with improved mechanical properties (Song, Feijen, Grijpma, & Poot, 2011).

Poly (glycolic acid) (PGA): As a synthetic aliphatic polyester, PGA is one of the most commonly used biomaterials in tissue engineering applications (Matsuzaki, John, Shoji, & Shinoka, 2019). Despite its high mechanical strength and biocompatibility, its hard structure limits the use of PGA (Dehnavi, Parivar, Goodarzi, Salimi, & Nourani, 2019). For this reason, it is used as a copolymer or blended with other biopolymers that shows high elongation at breakage values.

Poly (ε-caprolactone) (PCL): PCL is a semicrystalline, aliphatic polyester that is biocompatible, rubbery and non-toxic (Ren et al., 2015). Moreover, PCL is synthesized at a suitable temperature (>120 ° C) by ring-opening polymerization of metal aloxides, metal carboxylates, and caprolactone monomer, in which tin or tin salts act as initiators (Bartnikowski, Dargaville, Ivanovski, & Hutmacher, 2019) (Figure 1.6). Despite the fact that ring-opening is the most common process for producing PCL, polycondensation of 6-hydroxyhexanoic acid can result in PCL of inferior quality and molecular weight (usually 10,000 g/mol and below). The ring-opening approach has also a drawback that requiring a catalyst for synthesis. Although many metal catalysts have a detrimental effect and require additional maintenance, calcium and magnesium-based catalysts are very popular because they do not cause any toxic effects and do not require an extra step (Labet & Thielemans, 2009).

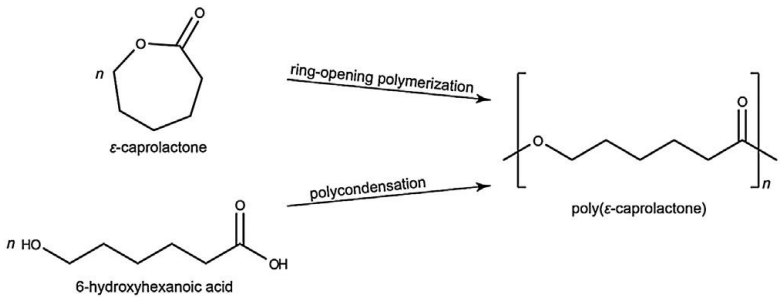

Figure 1.6 : Synthesis of poly(ε-caprolactone) from ε-caprolactone or 6-hydroxyhexanoic acid (Bartnikowski et al., 2019).

The molecular weight of polymers has a substantial impact on their ultimate product qualities, mostly for mechanical strength (Pant et al., 2011). PCL can be manufactured at a variety of molecular weights that results in a variety of features. PCL with a molecular weight of 15,000 g/mol is brittle, while 50,000 g/mol is more ductile (Deshmukh et al., 2017). In addition, Table 1.3 shows the properties of PCL with different molecular weights. High molecular weight PCL, on the other hand, has a high mechanical strength and oxygen permeability. Although it is not ideal for oxygen barrier products due to this property, it is beneficial for long-term implants and drug delivery systems (Cheung, Lau, Lu, & Hui, 2007).

Table 1.3: Properties of PCL with different molecular weight (Mw) (Jiang & Zhang, 2013).

Properties	PCL-low Mw	PCL-mid Mw	PCL-high Mw
Molecular Weight	37,000	50,000	80,000
Melting Point (°C)	58-60	58-60	60-62
Tensile Stress (kg/cm^2)	140	360	580
Elongation at break (%)	660	800	900

As a member of biodegradable polymers, PCL's slow degradation time makes it a popular choice for many biomedical applications (Mclauchlin & Thomas, 2012). Because of the high mobility of the chain segments and intermolecular interactions, it exhibits a low glass transition (-60 °C) and melting temperature (60 °C). This biopolymer, which has a very stable thermal structure, has the properties of full enzymatic degradation and superior chain flexibility (Deshmukh et al., 2017).

Although PCL is resistant to solvents such as water, aliphatic hydrocarbons, alcohol, and glycol at room temperature, it is soluble in aromatic polar and chlorinated hydrocarbons such as toluene, benzene, chloroform (CHL), cyclohexanone, carbon tetrachloride, tetrahydrofuran (THF), dimethyl carbonate (DMC), dioxane, and dichloromethane (DCM). Furthermore, PCL is partly soluble in acetone (AC), ethyl acetate, dimethyl formamide (DMF), 2-butanone, and acetonitrile (Mondal, Griffith, & Venkatraman, 2016; Sinha, Bansal, Kaushik, Kumria, & Trehan, 2004).

PCL is chosen as the primary polymer in this thesis due to its better biocompatibility and mechanical strength, as well as the slow biodegradation rate, non-toxicity, and flexibility. Furthermore, despite the fact that there are many solvent system options,

chloroform is selected as the main solvent since it is less damaging to nature and human body.

Poly (lactic acid) (PLA): PLA is a commercially available bio-based polymer used in a variety of applications due to its high strength, modulus and biodegradability. It is formed by bacterial fermentation of biomass such as sugar or starch, or polymerization of lactic acid, which can be formed by chemical synthesis (Murariu & Dubois, 2016). At the same time, its bioabsorbable and biocompatible properties make PLA an extremely promising material for medical applications (Saini, Arora, & Kumar, 2016). Moreover, lactide has three stereoforms: L-lactide, D-lactide, and meso-lactide (Figure 1.7). By catalytic ring opening polymerization, pure L-lactide, D-lactide, DL-lactide (50/50 combination of L and D isomers), or meso-lactide monomer is transformed into the matching high-molecular weight polyester (Nampoothiri et. al., 2010). The L-lactide ratio is a factor that influences PLA's crystallinity and results in high melting temperature and brittleness. The crystallinity of PLA reduces when 15% meso lactide or D-lactide is introduced, and the material becomes amorphous. Pure PLA melts at 180°C and has a glass transition temperature of 60°C because it comprises L-lactide or D-lactide mesoforms in its structure (Nijenhuis, Grijpma, & Pennings, 1991).

Relatively low oxygen and water permeability, brittleness, high polarity, high density, and poor heat resistance limit the use of PLA (Deshmukh et al., 2017). Various methods have been developed, such as blending with biopolymers with ductile properties such as PCL, to make PLA more tough and reduce its brittleness rate (Jiang & Zhang, 2013). Moreover, physiochemical properties of PLA can be seen in Table 1.4.

Table 1.4: Physiochemical properties of PLA (Nampoothiri, Nair, & John, 2010).

Properties	**PLA**
Density	1.25 g/cm^3
Glass Transition Temperature, T_g	50-64 °C
Melting Point, T_m	145-186 °C
Tensile Strength	28-50 MPa
Young's Modulus	1.2-3 GPa
Elongation at Break	2-6%

On the other hand, PLA is soluble in chloroform, methylene chloride, dioxane, acetonitrile, 1,1,2-trichloroethane, dichloroacetic acid, toluene, acetone, ethylbenzene at room temperature, and soluble in tetrahydrofuran only when heated to boiling point.

Insoluble in water but it can dissolve in selective alcohols and alkanes (Saini, Arora, & Kumar, 2016).

Poly(l-lactide) (PLLA) is a popular enantiomer of PLA for biomedical applications due to its processability, outstanding mechanical behaviours, and thermal stability (Xiang et al., 2019). Furthermore, PLLA is a slow crystallizing material with higher mechanical strength (~60 MPa) and modulus (~3 GPa) than many synthetic polymers (Jiang & Zhang, 2013).

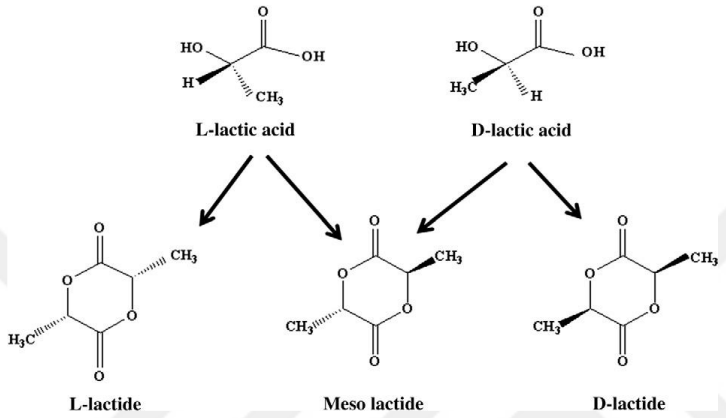

Figure 1.7 : Stereoforms of lactides. Reprinted from (Nampoothiri et al., 2010).

In this thesis, PLA and PLLA are chosen because of their favorable mechanical properties, biodegradability and biocompatibility. The aim is to examine the behavior of commercial PLA with different crystallinity and degradation rates and its L-lactide derivative, PLLA, blended with PCL and their effects on the mentioned parameters. On the other hand, the current thesis is one of the rare studies showing that PLLA polymer, which is rarely included in vascular graft studies in the literature, despite having an important commercial value, is a candidate for graft applications.

1.5.3 Hybrid biomaterials

Although natural and synthetic polymers can be employed in vascular graft architectures in their pure form, they may not be enough to meet certain of the qualities that grafts should have. Combining the strong mechanical aspects or outstanding structural characters of two or more synthetic materials (Abdal-hay et al., 2018; Oztemur & Yalcin-Enis, 2021; L. Zhao et al., 2021; N. Zhao, Lv, Ma, Zhu, & Li, 2019), as well as blending a natural biopolymer that provides advantages in terms of cellular activities and a synthetic biopolymer with high mechanical strength (Joshi et al., 2020; T. Wang et al., 2013; Y. Wu et al., 2018; L. Zhao et al., 2021) are all

examples that have been widely discussed in the literature. It is also a favored approach of combining the strong properties of biomaterials or compensating for their poor aspects by bringing them into copolymer form. Copolymers are made up of two or more monomeric substances joined together. Also, copolymers illustrate the various advantages of hybrid materials by combining the positive qualities of their monomeric species while eliminating their unfavourable properties, resulting in a synergistic copolymer final product (Astete & Sabliov, 2012). Many new biomaterials with tunable biophysical and biochemical characteristics have arisen from the copolymer method. Furthermore, the copolymerization approach is employed to provide good mechanical and electroactive qualities, as well as to enhance biodegradation (Francois, Dorcemus, & Nukavarapu, 2015; Ravi & Chaikof, 2010). As a result, biocompatible and biodegradable copolymers are becoming increasingly popular in vascular graft investigations (Agarwal et al., 2019; Braghirolli et al., 2017; Horakova et al., 2018; Shafiq et al., 2018).

PLA, PLLA, and PCL biopolymers are chosen for this study because of their high biocompatibility, biodegradability, mechanical strength, and flexibility. PLA/PCL and PLLA/PCL blends, in addition to their pure forms, have been throughly investigated for reasons of improved biocompatibility, brittleness, and mechanical strength. Although biopolymer selection is essential in vascular graft research, it is not a sufficient criterion for the formation of a desirable graft that closely resembles the native blood vessel. One of the complementary variables for the success of scaffold designs is the fabrication technique.

1.6 Vascular Graft Fabrication Techniques

There are a variety of production methods for fibrous surface formation that can be employed in vascular tissue engineering applications, including melt drwaing, particulate leaching, solvent casting, phase separation, freeze drying, self-assembly and 3D printing (Malik, Sundarrajan, & Hussain, 2020; Ong et al., 2017). Also, some of the nanofiber production methods and their properties that can be used for vascular graft applications are given in the Table 1.5. Although these approaches are effective in terms of producing fibous surfaces with effective porosity and permeability, which allow cell transport and proliferation, the scaffolds created by these methods have several drawbacks, such as uncontrollable fiber diameter and poor mechanical

behavior (Rogina, 2014). Electrospinning gains attention in recent decade, due to not only its versatility in spinning a wide range of polymeric fibers, but also the ability to produce fibers with uniform mechanical properties. Besides, this technique offers high surface-to-volume ratio during nanofiber production, customizable porosity, processability of fibers in a wide range of sizes and shapes, and the ability to manipulate nanofiber composition to obtain desired qualities and functionalities in the end product (Bhardwaj & Kundu, 2010). Moreover, by providing a 3D ECM structure, it is an excellent way for achieving cell adhesion and proliferation (Abruzzo et al., 2014). Because of the advantages it provides in terms of morphological, mechanical, and topographic features, as well as being easy and accessible, the electrospinning approach is favoured in surface development investigations for vascular graft applications within the scope of this thesis. For this reason, the electrospinning method, solution and production parameters are explained in detail in further sections.

Table 1.5: Nanofiber production techniques (Zdraveva et al., 2017).

Techniques	Principle	Diameter Range
Splitting of bicomponent fibers	Removal of one polymer out of islands-in-the-sea (or citrus pie)-spun fibers	>800 nm
Melt-blowing	Drawing polymer melt using hot air jet	>800 nm
Physical drawing	Physically drawing polymer solution	>50 nm
Flash-spinning	Simultaneous heating and pressurizing of polymer fluid	>200 nm
Phase separation	Formation of fibers by induced phase separation of solution	50-500 nm
Self-assembling	Self-organization of molecules in solution	<100 nm
Solvent dispersion	Shear-enhanced solvent precipitation in nonsolvent	~100 nm
Centrifugal spinning	Drawing spinning fluid using centrifugal force	>100 nm
Hydrothermal	Formation of fibers in hydrothermal solution	50-120 nm
Electrospinning	Stretching of solution by high electric field	10 nm to a few microns

1.6.1 Electrospinning

Electrospinning is an efficient method that encourages the innovation for manufacturing uniform and advanced fibers by using electric force. The main components of the electrospinning system are the feed pump, high voltage power supply, collector, and syringe (needle tip) as shown in Figure 1.8. The working

principle of the electrospinning method is based on the theory of exceeding the surface tension of the polymer solution and creating a jet by applying high voltage. The electric field generated between the tip and the collector causes the viscoelastic polymer solution transforming from spherical to conical shape (Taylor cone) to be repelled with a certain surface charge. When the electrostatic repulsive forces in the polymer solution exceed the surface tension of the polymer, the charged jet begins to detach from the Taylor cone and moves uniaxially from the electric field towards the grounded collector. Simultaneously, with the rapid spread of the jet, the solvents in the polymer solution evaporate and fibers in nano/micro scales begin to emerge. Further, the formed fibers are collected on the grounded collector and provide fibrous surface formation (Asmatulu and Khan, 2018).

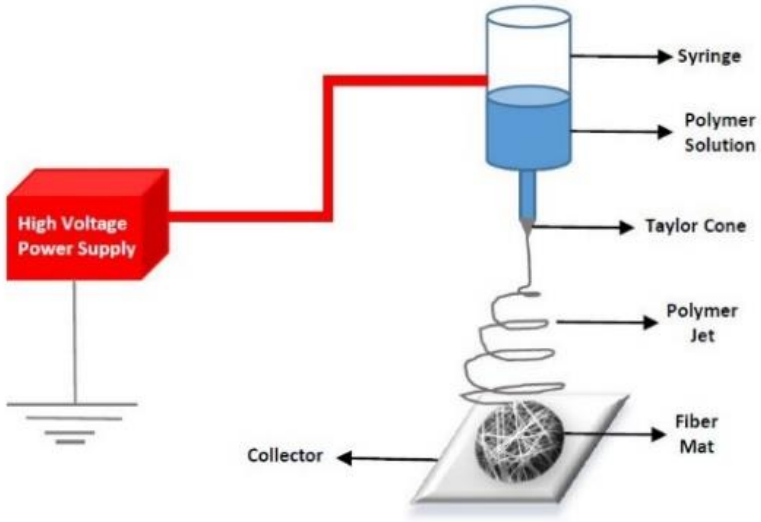

Figure 1.8 : Components of electrospinning unit.

The electrospinning technique is generally governed by parameters such as solution, production, and ambient factors. Each of these parameters significantly affects the morphology of the fiber; hence, the desired fiber morphology can be achieved by adjusting these parameters properly (Long et al., 2018).

1.6.1.1 Electrospinning production parameters

Solution Parameters

Solution properties such as concentration, molecular weight, viscosity, surface tension, and conductivity are the main parameters affecting fiber morphology.

Concentration

A minimum concentration of the solution is needed in the electrospinning enabling fiber formation to proceed. The solution concentration should be adjusted to an optimum value according to the properties of the materials used; otherwise, proper conditions will not be achieved and fiber with desired morphological propertied cannot be formed (Bhardwaj and Kundu, 2010). Studies in the literature show that very low solution concentration causes bead formation instead of fiber shape, whereas very high solution concentration prevents continuous fiber formation by causing difficulty in polymer flow from the nozzle (Ahmed, Lalia, and Hashaikeh, 2015). Moreover, concentration and fiber diameter are directly proportional, and the fiber diameter decreases as concentration decreases (Costa, Bretas, and Gregorio, 2010).

Molecular Weight and Viscosity

Molecular weight is one of the aspects that play a significant role in the production of the strong and highly oriented fibers while having a significant impact on rheological and electrical properties such as viscosity, surface tension, conductivity, and dielectric constant. Increased molecular weight can effectively reduce the defects in the molecular chain ends and enhance molecular strength. Moreover, the molecular weight of the polymer represents the number of entangled polymer chains in a solution, and so the solution viscosity (Bhardwaj and Kundu, 2010; Gupta and Kothari, 1997). Viscosity plays a crucial role in the determination of fiber diameter and morphology during the electrospinning process. The effect of viscosity occurs in the same way as concentration like while low viscosity causes droplet formation, with increasing viscosity, uniform and beadless fibers may occur. On the other hand, in cases where the viscosity is too high, the polymer solution dries at the needle tip before the jet formation and continuous fibers cannot be achieved (Pham, Sharma, and Mikos, 2006).

Surface Tension

To produce a fibrous web with an electrospinning technique, the polymer solution loaded with the effect of the electric field in the first place is expected to exceed the surface tension and form a jet. Determining the surface tension is an essential factor for electrospun web production since if a solution with a very high surface tension the

fiber formation cannot be obtained. However, the surface tension can be adjusted by changing the material used or adding surfactants to the solution (Rogina, 2014).

Conductivity (Surface charge density)

Since the electrospinning process is a system working with the effect of the electric field, the electrical conductivity of the solution that will provide the fiber formation has an important effect on the stable operation of the system. As experimental studies in the literature show that it is possible to attain uniform and thin fibers with increased electrical conductivity (Tan, Inai, Kotaki and Ramakrishna, 2005; Uyar and Besenbacher, 2008).

Production parameters

In addition to the solution parameters, production parameters mainly as voltage, feed rate, and tip to collector distance significantly affect the structure of the final fibrous web.

Voltage

The electric charge that triggers fiber formation from the polymer solution is directly related to the applied voltage. For this reason, adjusting the voltage is a determinant parameter that directly affects fiber production (Khajavi and Abbasipour, 2017). The increasing voltage will raise electrical efficiency, resulting in polymer build-up at the nozzle; depending on the viscosity and feed rate of the polymer; moreover, this situation may cause an advantage or a disadvantage. For this reason, the voltage setting should be considered together with these parameters (Subbiah, Bhat, Tock, Parameswaran and Ramkumar, 2005). While some research claim that high voltage hinders fiber production, others indicate that high voltage causes thick fibers to form due to the increasing potential difference, the solution comes to the collector with increasing acceleration (Bakar, Fonk, Eleyas and Nazeri, 2018; Deitzel, Kleinmeyer, Harris and Tan, 2001).

Feed Rate

Voltage and feed rate are interrelated production parameters; thus, the feed rate is a parameter that should be adjusted according to the components of the solution in addition to the voltage. The slow feed rate is generally a preferred option to allow the polymer solution to evaporate and form a jet (Bhardwaj and Kundu, 2010). At very

fast feed rates, the solution reaches the collector without evaporation and production results in pilling, wet fiber, or thick fiber formation (Khan and Kafiaha 2016; Rasouli, Pirsalami, and Zebarjad, 2019).

Tip to Collector Distance

The tip to collector distance can be optimized considering the voltage and feed rate parameters. A minimum distance from the tip to the collector is required to give the fibers sufficient time to dry before reaching the collector; otherwise, fiber irregularity or thicker fibers may occur at very close or far distances (Angel, Guo, Yan, Wang and Kong, 2020; Khan and Kafiaha, 2016).

Ambient parameters

Environmental factors affecting fiber morphology can be determined mainly as ambient temperature and relative humidity (RH). The effects of these factors on different polymer solutions are variable, so it is not correct to make a definite judgment even though it is known that they affect fiber morphology (Haider A., Haider S., and Kang, 2018). Existing studies have shown that high relative humidity particularly favors structural porosity. According to the outcomes of the studies, the pores in the fiber structure appear with increasing moisture due to the breath figure mechanism (Medeiros, Mattoso, Offeman, Wood and Orts, 2008; Megelski, Stephen, Chase and Rabolt, 2002). In many studies in the literature, it is seen that porous fibers are produced by electrospinning many polymers such as PLA in a humid environment with the effect of the breath figure mechanism (Huang and Thomas, 2018) (Figure 1.9). On the other hand, higher temperature allows a higher rate of vaporization of the solvent and decreases the viscosity of the polymer solution; hence, thinner fibers can be obtained (İçoğlu and Oğulata, 2017).

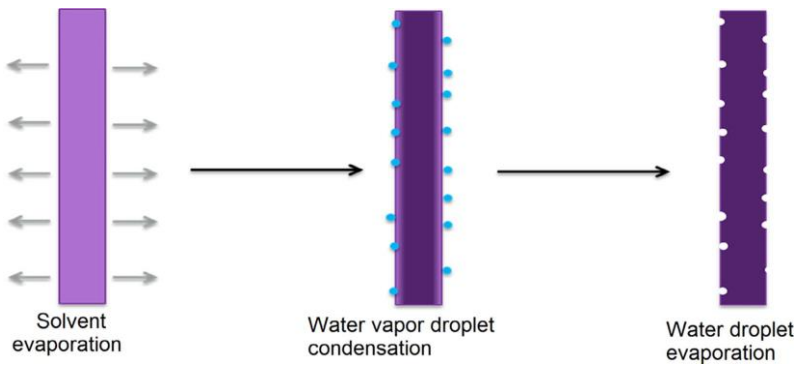

Figure 1.9 : Schematic diagram of surface pore formation induced by breath figures mechanism. Reprinted from (C. Huang & Thomas, 2018).

To obtain a suitable surface for vascular graft applications, the solution and production parameters of the electrospinning process mentioned above are optimized for each solution system separately within the content of the thesis.

1.7 Recent Studies About Electrospun Vascular Grafts

Natural polymers are preferred for vascular grafts due to aforementioned numerous advantages, but their insufficient mechanical properties limit their usage alone. Thus, they are mostly used in a blend form with other biomaterials. On the other hand, synthetic biopolymers can also be used alone, in a blend with other biopolymers or in the form of copolymers to meet the desired properties of vascular grafts. Considering the outstanding strengths of synthetic polymers, within the scope of this thesis, synthetic, biodegradable biopolymers PLA, PLLA and PCL are selected for fibrous web production. Moreover, a comprehensive literature review is conducted before the study, and some of the studies that guided for the thesis can be summarized as follow:

In fibrous surface development studies, the determination of materials and methods brings with it the necessity of some assesments such as morphological (including fiber diameter, porosity, and water contact angle), chemical, thermal and biological analysis. In this context, the morphological properties, chemical, thermal and biological behaviors of the target surfaces are examined from various literature studies during the thesis period. The mentioned properties are primarily examined based on PCL, which is the main polymer of the study. The impact of various solvent systems on the fibrous surface morphology is a subject that researchers have focused on. Yalcin-Enis et al. (2016) used a chloroform/ethanol (9/1) solvent system for PCL (45,000 Mn) at 14, 16, 18, and 20% polymer concentrations to develop fibrous surfaces. At the same time, they evaluated the effects of adding formic acid or acetic acid in various amounts (20, 40, 80, and 120 ml) to the PCL solution with an 18% polymer concentration. As a consequence of the research, it was seen that fiber diameter increases as the polymer concentration increases, however acid addition considerably reduces the fiber diameter of PCL. Qin and Wu (2012), to see the effect of different solvent systems such as DMF, 1-methyl-2-pyrrolidone (NMP), THF, DCM, AC, CHL, and dimethyl sulfoxide (DMSO) on PCL-based surfaces. Fibrous electrospun webs were fabricated and the morphological, chemical, and thermal characteristics of the surfaces were analysed. They observed that PCL dissolves most

rapidly in DCM and CHL, forming fibers with an average diameter of 4500 and 1600 nm, respectively; moreover, beaded structures or poor fiber dispersion have been noticed in other solvent systems. On the other hand, FTIR analysis of all surfaces gave the same result, and all solvents were removed from the surface during surface formation with the electric field effect. In the direction of thermal analysis, it has been determined that CHL forms a surface with relatively smaller T_g and T_m values due to its lower boiling point.

In addition to surface studies on PCL, extensive PCL-based scaffold investigations have also been carried out for vascular graft surfaces, which is the target tissue of the current thesis. Yalcin et al. (2016) presented a study in which the design parameters were determined to mimic the native vascular structure in morphological, mechanical, and biological aspects and to create a biodegradable small-caliber vascular graft structure. At a concentration of 18 w/v % solution was prepared by utilizing PCL (45,000 Mn) and CHL/ETH (9/1 v/v) solvent system. The tubular scaffolds were constructed with a diameter of 6 mm and a wall thickness of 250 µm. The scaffold surface consisted of homogeneous and bead-free fibers, and the diameter of the fibers was measured between 0.25-0.75 µm in the first peak and 1.75-2.25 µm in the second peak. While the porosity and the pore size were measured as 29-36.39% and 8.60-29 μm^2, respectively by a static software program, 49.7-93.83 μm^2 pore sizes were achieved by bubble method, which tests under dynamic conditions. Furthermore, the all samples showed sufficient biocompatibility for cell viability; moreover, in all cell cultures examined on the 1^{st}, 3^{rd}, 7^{th} and 14^{th} days, it was determined that the cells could survive and proliferate according to the MTT test using 3T3 fibroblasts.

In a later study of Yalcin et al. (2017), a 6 mm diameter bilayer vascular graft was fabricated using electrospinning method. PCL (45,000 and 80,000 Mn) and PLCL (70/30 molar ratio) were used as the main polymers. PCL (45,000 Mn) was dissolved in CHL/ETH, and PCL (80,000) and PLC were dissolved in CHL/ETH/acetic acid (AA). Bilayer structures were produced from combinations of each polymer types including randomly distributed inner layer (produced at 5,000 min^{-1}) and radially oriented (produced at 15, 000 min^{-1}) outer layer. Diameters of randomly distributed fibers were higher than that of oriented fibers for PCL (45,000 Mn) (4.02±1.22 µm for random fibers, and 3.47±0.88 µm for oriented fibers) and PCL (80,000Mn) samples (2.96±0.88 µm for random fibers and 2.50±0.85 µm for oriented fibers) which was

thought to be caused by mechanical stress. In contrast, due to the highly elastic behavior of PLCL, the randomly distributed fiber diameter was lower compared to the oriented fibers for PLCL surfaces (4.01±1.01 μm for random fibers and 4.59±1.42 μm for oriented fibers). The bilayer tubular structure with the highest ultimate tensile strength of 2.7 MPa belonged to PLCL+PCL_80 and its elongation at break was measured as 650%. Owing to the high elastic response, PLCL samples showed the highest burst resistance (1500 mmHg).

Jia et al. (2020), designed a biomimetic trilayer tubular vascular scaffolds from biodegradable polymers. They used PCL as an intima layer due to its super biocompatibility and low degradation rate, PLGA as a media layer, and PU for adventitia which is the outer layer because of its both biocompatibility and mechanical properties. The inner and outer layers were produced by electrospinning method while the media layer was produced via freeze-drying method due to macropore and high connectivity possibilities. The researchers obtained oriented PCL and PU nanofibers, and PLGA fibrous structure, which has significantly high porosity (83.73 ± 1.23 %) and large pore sizes (47.93 ± 18.73 μm). It was demonstrated that electrospun PCL and PU structures had higher degradation rate (24.86±7.29 % and 12.62±1.59 % at week 6, respectively) than PLGA scaffold (3.01±0.54 % at week 6) since ultrafine electrospun fibers have more interaction with lysozyme because of its high surface area. Consequently, a trilayer tubular biocompatible and biodegradable vascular graft was produced which has good endothelialization with restrained thrombosis and hyperplasia in the PCL intima layer, cell penetration due to large pore size in PLGA media layer, and high-level tensile strength in PU adventitia layer.

On the other hand, PLA is also in an interesting position in surface development studies for biomedical applications. For this reason, there are studies on optimizing the morphology of PLA and developing an appropriate solvent system. Huang and Thomas (2018) developed surfaces in a humid environment with 15% concentration of different solvent systems (AC, CHL, CHL/ETH, CHL/DMSO, and DMSO) to produce PLA-based scaffolds for biomedical applications. While the surface produced with the AC solvent system gave the smallest fiber diameter value, other solvent systems gave surfaces with a fiber diameter over 1 μm. On the other hand, due to the breath figure mechanism, structural pores have formed on the surfaces produced with solvent systems other than the surfaces produced with AC. Although all surfaces are

hydrophobic, the WCA values of surfaces are larger (>130 °) due to the high specific surface area.

Jahangir and Rumi (2017) examined the impact of different solvent systems on fiber morphology and diameter in electrospun PLA-based fibrous structures in a similar study. Surfaces were produced with single and binary solvent systems employing AC, 1-4-dioxane (DX), THF, DCM, CHL, DMF, and dimethylacetamide (DMAc) organic solvents while keeping a 10% polymer concentration constant. They discovered that surfaces produced with binary solvent systems containing single and binary acetone solution system have defect-free and nano-sized fibers. Further, more comprehensive studies on tissue engineering applications of PLA are also frequently found in the literature.

In a detailed study, Abudula et al. (2019) aimed to develop an electrospun cellulose nanofibril (CNF) reinforced vascular grafts structure using PLA and poly (butylene succinate) (PBS) biopolymers. CNF was chosen because of its nanoscale property that helps to achieve better orientation and strong adsorption ability of moisture useful for medical applications. PLA/PBS blend was used at different ratios (100/0, 75/25, 60/40, 50/50, 40/60, 35/65, 25/75 and 0/100), and the polymer blend was dissolved in CHL/AC (3/1) solvent system at a constant 6% concentration. For the CNF reinforced system, the ratios were kept as 50/50 for PLA/(PBS+CNF), and the CNF concentration was varied between 1-5%. With the addition of the PLA into the solution, the viscosity increased and the bead-free structures were obtained. On the other hand, the fiber diameter decreased with the CNF reinforcement (1019±75 nm for PLA, 409±51 nm for hybrid structure with 50/50 of PLA/PBS, 379±46 nm for composite fiber with 1% CNF, and 267±27 nm for composite fiber with 5% CNF). The optimal mechanical performance was obtained using PLA/PBS blend with a 50/50 ratio that has 112.5±1.5% elongation at break and 98.6±4.6 MPa elastic modulus in addition to highest tensile strength (2.77±0.23 MPa). Furthermore, the WCA value varied between 69 and 114.1°, and the angle decreased with CNF induction. In addition to the morphological and mechanical investigations, cell activity analysis displayed that PLA/PBS blends had better cell adhesion compared to the neat PLA and PBS. 7 and 14 days after the cell seeding, PLA/PBS (50/50) and CNT reinforced PLA/PBS scaffolds had higher cell proliferation than neat PLA and neat PBS.

Montini-Ballarin et al. (2016) actualised a study that points to the mechanical behaviors of an electrospun bilayer vascular grafts. In this study, a segmented poly (ester urethane) (SPEU) named PHD and poly(L-lactic acid) (PLLA) were used to imitate the mechanical features of elastin and collagen, respectively. While PHD was dissolved in 2,2,2-trifluoroethanol (TFE); DMF/DCM (40/60) mixture was used as a solvent for PLLA. Then, two types of polymer solutions were blended at 90/10 (for the outer layer) and 50/50 wt/wt (for inner layer) ratios to prepare PLLA/PHD blends. 5 mm diameter of vascular grafts were produced with different wall thicknesses. According to the uniaxial tensile test, the stress-strain curve of the PHD showed an elastic behavior like elastin, and the slope of the PLLA resembled collagen, which has a stiffer structure. Bilayer structure had Young's modulus values of 6.24±1.69 MPa in the circumferential direction and 29.54±5.85 MPa in the axial direction; moreover, with high strain values of bilayer scaffolds (142-233%), they exhibited more flexible structure than the rigid Dacron and Goretex commercial grafts. On the other hand, the compliance values of vascular grafts were between 1.59-1.72% (80-120mmHg), and although it was lower than the coronary artery, it showed J-shaped behavior like in the native blood vessel. Furthermore, the burst pressures were 1232-1775 mmHg (for axial elongation L/L_0=1) which is closer to human saphenous veins.

In addition to the singular properties of PLA, PLLA and PCL, the blend properties are also one of the main subjects of this study. In this context, the performance characteristics of electrospun structures produced at different PLA/PCL blend ratios (100/0, 50/50, 60/40, 70/30, 80/20, 90/10, 0/100) were evaluated by Sharma et al. (2019). The molecular weight of PLA used in the study is 116,000 g/mol, and that of PCL is 80,000 g/mol. Also, PLA and PCL are dissolved in chloroform/DMF (4/1 v/v), and fibrous webs produced with electrospinning technique. Morphological analysis revealed that fine fibers and beads were formed in structures with a PLA ratio of less than 70% in the structure due to the use of relatively lower molecular weight PCL. Depending on this situation, smooth fibers were formed in structures with higher PLA content and the fiber diameter increased as the PLA ratio increased. Moreover, the WCA values of all samples are found greater than 90° that indicates hydrophobicity of the surfaces. The melting points of both PLA and PCL are considerably visible in the DSC curves and as the PLA ratio in the blend structure rises, crystallinity of PLA increases from 16.1% to 21.5%, whereas crystallinity of PCL drops from 16.5% to 2%.

Zhai et al. (2013) designed a potential vascular graft for substitution of the femoral artery by using P(LLA-CL) block copolymer which has enhanced mechanical property, good degradation rate, and elastic property. Furhermore, heparin biomaterial was used to increase the proliferation of ECs and vascular SMCs. The scaffold was produced by a coaxial electrospinning method as to gain favor from both the strong properties of P(LLA-CL) and heparin. Heparin was utilized as a core component to be encapsulated while the P(LLA-CL) copolymer as the shell component. Besides the P(LLA-CL)/heparin blend, P(LLA-CL) scaffold was produced to determine the effect of heparin on the morphology and the cell activity. The results obtained in dry conditions showed that the tensile strength and strain values for P(LLA-CL) were 18.34 ± 0.18 MPa and 504 ± 21.62%, respectively, while for P(LLA-CL)/heparin it was 17.56 ± 0.43 MPa and 460 ± 33.14, respectively. The graft structure started to be covered in endothelial cells by the end of the 2nd week, and it was decided that the scaffold was a suitable candidate for vascular graft applications. Hence, at the end of the study, both P(LLA-CL) and P(LLA-CL)/heparin vascular grafts were implanted to Beagle dogs, and all of the scaffolds resulted in success. However, the P(LLA-CL)/heparin composite has been said to be a much better candidate for blood vessel repair, as it has a 100% patency rate in the early stage, 50% in the medium term, and 25% in the long term.

In the current thesis, biodegradable polymers are used; therefore, the degradation processes of polymers are among the research topics. Gaona et al. (2012) developed PLLA/PCL membrane constructions with various blend ratios to target cell attachment and proliferation convenience, and then analysed their biodegradability rates by hydrolytic degradation. They noticed that the rate of degradation increased as the PLLA ratio in the membrane content increased. It is among the outputs of the study that the crystallinity ratio increased as a result of the degradation in the amorphous region of the polymeric surface, but the PLLA crystallinity on the PLLA/PCL surfaces increased not only due to the hydrolysis of the amorphous region but also due to the recrystallization state of PLLA.

1.8 Novelty of the Thesis

Despite the effectiveness of materials like PET, ePTFE, and PU in large-diameter grafts, a satisfactory proportion of success has yet to be obtained for small-caliber

grafts. Researchers are still searching for biocompatible and biodegradable vascular graft designs that will provide solutions to these difficulties. Graft material, which provides the basic framework for cell proliferation, is critical in all tissue engineering applications for successful cell regeneration. Natural polymers such as collagen, fibrinogen, silk fibers, cellulose, chitosan, and gelatin are commonly used in vascular graft surface designs. These materials can fail in long-term vascular graft applications because to their poor mechanical strength, low processing capabilities, and rapid degredation. The material's sufficient biodegradation time provides the essential stability for cells to synthesize structural proteins and produce autologous tissue in addition to being biodegradable.

Within the scope of the current thesis, PLA, PLLA and PCL biopolymers and their blends at different ratios are selected for the development of vascular graft surfaces due to their biocompatibility, biodegradability, superior mechanical and thermal properties, convenience for cell activities, and non-toxic effects *in-vitro* and *in-vivo* studies. Many studies in the literature ignore the advantages of blending these polymers to achieve the desired properties of vascular grafts and do not make detailed comparisons of blend structures. In addition to the scaffold design, the impacts of blend ratios on morphological, chemical, thermal an biological properties are investigated in this research. Moreover, the properties of PLA and PLLA depending on their crystallinity are studied comparatively; and these findings are supported by biodegradability and cell analyses. This surface development phase prepares the infrastructure to promote the vascular graft studies that will take place in the continuation of the thesis.

2. EXPERIMENTAL WORK

2.1 Materials and Methods

2.1.1 Materials

PCL (Mn 45,000 and 80,000), PLA (Mn 230,000; Ingeo 2003 D with 4.3 mol% D-lactide content), PLLA (Mn 50,000), and the components of solvent systems (chloroform, ethanol, acetic acid, and acetone) are supplied from Sigma Aldrich. The images of the polymers can be seen in Figure 2.1. PCL, PLA, and PLLA are used in both neat and blend forms. Table 2.1 shows the components of solvent system and their properties.

Figure 2.1 : Polymers used in thesis. Polycaprolactone with 45,000 Mn (a), poly (L-lactide) (b), polylactic acid (c), and polycaprolactone with 80,000 Mn (d).

Table 2.1: Solvent system components and their properties (Sigma Aldrich).

Components	Chemical Formula	Molecular Weight (g/mol)	Boiling Point (°C)	Density (g/mL) at 25°C	Purity (%)
Chloroform	$CHCl_3$	119.38	60.5-61.5	1.480	99-99.4
Ethanol	CH_3CH_2OH	46.07	78	0.789	≥99
Acetic Acid	CH_3CO_2H	60.05	117-118	1.049	99.8-100.5
Acetone	C_3H_6O	58.08	56	0.791	≥99

For cell culture analysis, adult human primary dermal fibroblasts (PCS-201-012™) and human umbilical vein endothelial cells (HUV-EC-C) (ATCC CRL-1730) are used. Cells are cultured through FibroGRO™-LS Complete Media Kit (Millipore, MA, USA) and DMEM-F12 medium (Dulbecco's Modified Eagle Medium/Ham's F-12 Nutrient Mixture; Thermo Fisher Scientific). Further, main materials that are used in biological assessments and sterilzation processes of this thesis are glutaraldehyde solution, osmium tetraoxide (OsO_4) and dehydrated with amyl acetate that are supplied from Sigma Aldrich; ethanol (Merck KGaA, Darmstadt, Germany); phosphate-buffered saline (PBS), Trypan Blue and Trypsin-EDTA (0.025% trypsin/1mM EDTA) that are supplied from Gibco, Thermo Fisher Scientific, Grand Island.

2.1.2 Methods

2.1.2.1 Surface fabrication

Within the scope of this thesis, the surface fabrication procedure for vascular graft applications consists of two stages; solution preparation and electrospinning process. Polymers are dissolved in appropriate solvent sytem, and scaffold surfaces are fabricated using electrospinning set-up with horizontal feeding unit that supplied from Inovenso, Turkey (Nanospinner, Basic System) (Figure 2.2(a)). A grounded electrospinning device generates fiber at a specific feed rate and with an electric field effect. After the production phase, the fibrous web collected on the flat type of collector is allowed to dry for 24 hours at room temperature (Figure 2.2(b)).

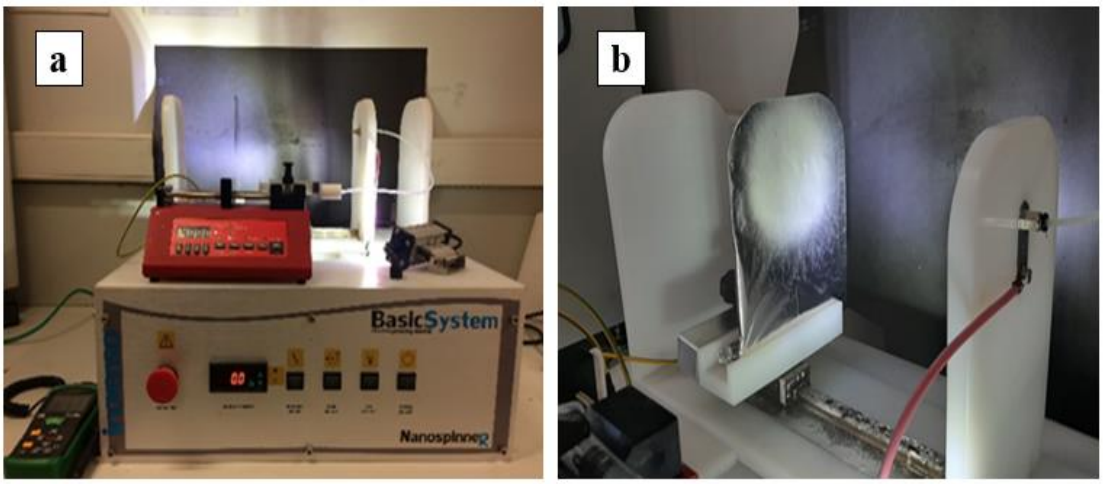

Figure 2.2 : Electrospinning apparatus (a) and fabricated surface on the collector (b).

The thesis study's experimental approach is divided into three stages:

i. Surface fabrication and optimization of PCL (45,000 Mw), PLA and their blends (a preliminary study): PCL (45,000 Mn) is dissolved in CHL/ETH (9/1 wt.) at the concentration of 16, 18 and 20% wt. whereas PLA is dissolved in CHL/AC (3/1 wt.) at the concentration of 7, 8 and 9% wt. In addition to neat PCL and PLA solutions, PLA/PCL blends are prepared in CHL/ETH/AA (8/1/1 wt.) solvent system at a concentration of 12% wt. Moreover, two different polymer blend ratios are introduced for PLA/PCL blend as 75/25 and 50/50. All solvents are stirred by magnetic stirrer for 2-3 hours, and then electrospun immediately. The PCL100 and PLA100 solutions are delivered by a 10 ml plastic syringe pump at the flow rate of 4-5 ml/h and 10±2 kV voltage is applied from 20 cm distance. For PLA/PCL solutions, the applied voltage, feed rate and the distance are adjusted to 15±1 kV, 5 ml/h and 23 cm, respectively. The productions are realized at 21±2°C temperature and 47±10% relative humidity. A blunt-ended 0.6 mm needle is clamped to the positive electrode of a high-voltage power supply generating of electric field and the flat collector is grounded. The polymer solutions are transformed to fibrous surfaces through the electric field. Solutions with sample codes and details are listed in Table 2.2.

Morphological characterizations are examined for the surfaces produced within the scope of this preliminary study.

Table 2.2: Sample codes and properties of the solvent systems.

Sample Codes	% Polymer Concentration	Weight Ratios					
		CHL	ETH	AA	AC	PLA	PCL
PCL100_16	16	9	1	-	-	-	100
PCL100_18	18	9	1	-	-	-	100
PCL100_20	20	9	1	-	-	-	100
PLA100_7	7	3	-	-	1	100	-
PLA100_8	8	3	-	-	1	100	-
PLA100_9	9	3	-	-	1	100	-
PLA75PCL25_12	12	8	1	1	-	75	25
PLA50PCL50_12	12	8	1	1	-	50	50

ii. Surface fabrication and optimization from PCL (80,000 Mn), PLA and their blends: Although PCL polymer with a molecular weight of 45,000 g/mol is used in the preliminary study, the desired smooth and continuous fiber formation could not be achieved. For this reason, the productions in the second stage continues with PCL with a molecular weight of 80,000 g/mol, which stands out with its better mechanical

properties and spinnability. PCL is dissolved in CHL/ETH/AA (8/1/1 wt.) at concentrations of 6, 8, and 10% wt. and PLA is dissolved in CHL/AC (3/1 wt.) at same concentrations. Moreover, following the findings of the previous study, it is decided to use the PLA/PCL blend in the second part of the study at 50/50 ratios, and the blend is coded as PLA50PCL50. Furthermore, PLA50PCL50 blends are prepared in CHL/ETH/AA (8/1/1 wt.) solvent system at concentrations of 6, 8, and 10% wt. All solvents are stirred by a magnetic stirrer for 2-3 hours to obtain homogenous solution and then electrospun immediately to prevent degradation. Optimum production parameters that allow continuous, smooth and bead-free fiber morphology are defined as 10±2 kV voltage, 3±1 ml/h feed rate, and 20 cm distance between the collector and needle tip. The temperature and relative humidity are measured as 18±1 °C and 40±6 %, respectively. Needle diameter is chosen as 0.6 mm. The sample codes and solvent details are listed in Table 2.3.

Morphological, chemical and thermal analysis are performed for the surfaces produced in the second part of this study.

Table 2.3: Sample codes and solvent details of the second part of the study.

Sample Codes	% Polymer Concentration	Weight Ratios					
		CHL	ETH	AA	AC	PLA	PCL
PCL100_6	6	8	1	1	-	-	100
PCL100_8	8	8	1	1	-	-	100
PCL100_10	10	8	1	1	-	-	100
PLA100_6	6	3	-	-	1	100	-
PLA100_8	8	3	-	-	1	100	-
PLA100_10	10	3	-	-	1	100	-
PLA50PCL50_6	6	8	1	1	-	50	50
PLA50PCL50_8	8	8	1	1	-	50	50
PLA50PCL50_10	10	8	1	1	-	50	50

iii. Investigation of pure and blended biopolymeric surfaces in the light of selected polymers and concentrations: Based on preliminary findings, an optimum polymer concentration of 8% is accepted and productions are carried out at this ratio. At this stage, due to its favorable qualities, PLLA is also included in this study. Thus, in addition to PLA, PCL and their blends, PLLA and its blends are also studied in this third part of the thesis. Blend ratios are selected as 10/90, 20/80, 30/70, 40/60, and 50/50 by weight for both PLA/PCL and PLLA/PCL. Each polymer solution system is stirred for 2 hours at room temperature. To produce continuous fibers, the voltage, feed rate, and tip-collector distances are kept constant at 14±1 kV, 4±1 ml/h, and 20 cm,

respectively. The average relative humidity is 66.38±8% and the temperature is 23.12±2°C. After the fabrication, fibrous surfaces on the aluminum foil are left to dry for 24 hours to remove residual organic solvents. Sample codes of the surfaces can be seen in the Table 2.4.

In the final part, morphological, chemical and thermal assesments of the surfaces as well as biodegradability and cell analysis are performed.

Table 2.4: Sample codes and the weight ratios of the polymer solutions.

Sample Code	Polymer Concentration (%)	Weight Ratios						
		CHL	ETH	AA	AC	PLA	PLLA	PCL
PLLA100	8	8	1	1	-	-	100	-
PLA100	8	3	-	-	1	100	-	-
PCL100	8	8	1	1	-	-	-	100
PLA10PCL90	8	8	1	1	-	10	-	90
PLA20PCL80	8	8	1	1	-	20	-	80
PLA30PCL70	8	8	1	1	-	30	-	70
PLA40PCL60	8	8	1	1	-	40	-	60
PLA50PCL50	8	8	1	1	-	50	-	50
PLLA10PCL90	8	8	1	1	-	-	10	90
PLLA20PCL80	8	8	1	1	-	-	20	80
PLLA30PCL70	8	8	1	1	-	-	30	70
PLLA40PCL60	8	8	1	1	-	-	40	60
PLLA50PCL50	8	8	1	1	-	-	50	50

2.1.2.2 Morphological characterization

Scanning electron microscope (SEM) analysis

SEM analysis is the first step in morphological characterization. Fiber diameter measurement, structural bead detection, and structural porosity analysis are all realized using SEM images. TESCAN VEGA3 scanning electron microscope is used to analysis the surface morphology of the fibrous surfaces. Before analysis under the electron beam, samples are coated with a thin layer of gold-palladium (Au-Pd) alloy at an operating voltage. 1kx, 3kx, and 5kx magnifications are used in SEM images of the surfaces. The fibrous samples for SEM analysis, coating apparatus, and SEM device can be seen in Figure 2.3.

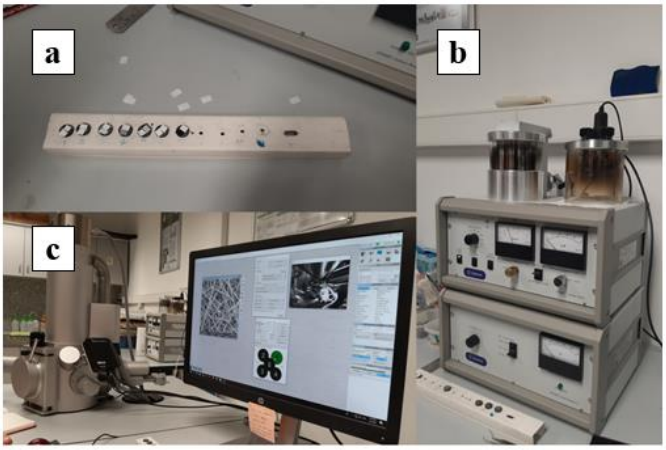

Figure 2.3 : Samples prepared for analysis (a), coating apparatus (b), and scanning electron microscope (SEM) (c).

Fiber diameter and pore analysis

Fiber diameter measurements are realized by Image J software (Figure 2.4) using SEM images for each scaffold surface. Average fiber diameters are calculated from at least 50 randomly selected fibers and results are given with standard deviations (SD).

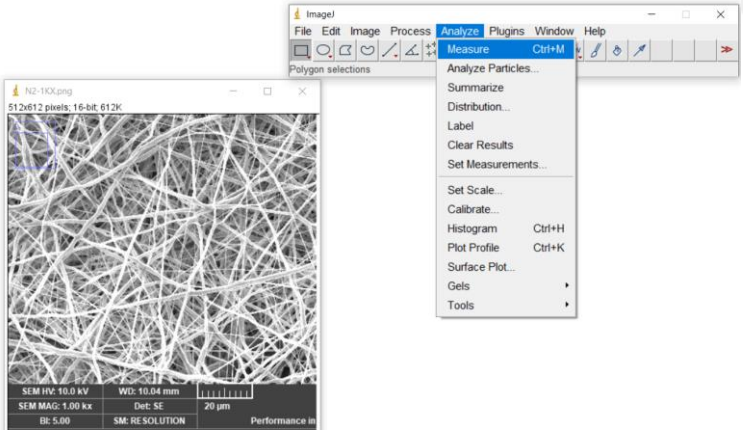

Figure 2.4 : Image J analysis.

Porosity (%) analysis in the thesis employed by thresholding method with Image J software.

Thresholding method with Image J software: Porosity are analysed from SEM images using the Image J software program based on a threshold technique that divides pixels within the target range of intensity values (Ferreira & Rasband, 2012). The measurement principle is two-dimensional and it is used to make comparisons between samples since data is obtained from SEM images (Figure 2.5). Pore size measurements are realized in a range of 1-10 μm^2.

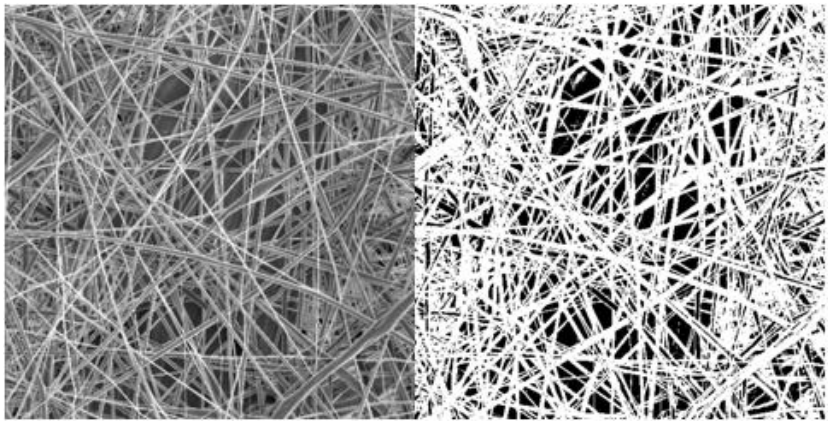

Figure 2.5 : Threshold of a SEM image.

Pore size analysis is carried out using 3G hz Porometer device (Quantachrome, Anton Paar) (Figure 2.6). Pore sizes of the selected surfaces (PLA100, PCL100, PLA20PCL80, PLLA50PCL50, PLLA20PCL80, and PLLA50PCL50) are measured using the air expulsion technique. The testing range is from 0.013 to 500 μm, and the pressure gradient from 0 to 0.35 bar. In order to analyse the pore sizes, the samples are cut with a diameter of 18 mm and wetted with a wetting agent to create surface tension. The wetting agent is immediately penetrated by the surfaces, after which the measurement is started on the device. Meanwhile, the device sends an air flow to the pores of the sample with the effect of pressure and 256 measurements are made at each bar pressure. After the wetting agent is completely evacuated from the pores, the pore sizes are determined by measuring with the dry state of the samples, and the data recorded via a software system.

Figure 2.6 : 3G hz Porometer device.

Water contact angle analysis

The water contact angles of scaffold surfaces are detected by KSV Attension Optical Contact Angle Meter (Figure 2.6) using sessile drop measurement method to analysis the hydrophilicity of surfaces. Mean values of the angles and SDs are given. Higher water contact angle indicates a more hydrophobic surface (Gu et al., 2016).

Figure 2.7 : KSV Attension Optical Contact Angle Meter.

2.1.2.3 Chemical characterization

Fourier transform infrared spectrocopy (FTIR) analysis

Chemical characteristics of the scaffolds are determined using FTIR device (UATR Two, Perkin Elmer) (Figure 2.7(a)) in Textile Technologies and Design Faculty, Enstrumental Analysis Laboratory. FTIR analysis is a method of determining the chemical structure of a material by displaying the polymer's distinctive peaks and identifying whether or not there is any solvent residue on the surface (Ipek Y. Enis, Vojtech, & Sadikoglu, 2017). With this analysis, while the presence of polymers in the blends is proven, it is tested whether residual solvent is left in the scaffold structure.

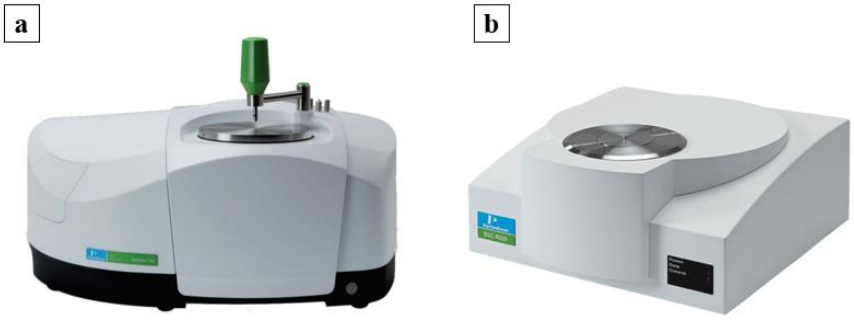

Figure 2.8 : FTIR device (UATR Two, Perkin Elmer) (a) and DSC device (DSC400, Perkin Elmer) (b).

2.1.2.4 Thermal characterization

Differential scanning calorimetry (DSC) analysis

DSC analysis is performed to recognize the thermal characteristics of polymer surfaces using Perkin Elmer DSC400 (Figure 2.7(b)) in Textile Technologies and Design Faculty, Enstrumental Analysis Laboratory. In a nitrogen atmosphere at atmospheric pressure, the melting behaviour of the samples is investigated. All webs are heated at a rate of 10 °C/min from -30 to 190 °C. There are two stages (heating and cooling) to the DSC analysis for PLA, PLLA, PLA/PCL and PLLA/PCL based samples. T_g values, crystallization, and melting points are all determined using these procedures. Furthermore, the behaviours of the samples under various heat settings are examined.

The area integration approach is used to calculate the crystallization and melting enthalpies using the Origin Software application. PLA, and PLLA are known to have 100% crystalline melting enthalpies (ΔH_0) of 93 J/g while PCL has 136 J/g melting enthalpy (Xiang et al., 2019; Zhai, Ko, Zhu, Wong, & Park, 2009). Equation 2.1 for PLA or PLLA, and equation 2.2 for PCL are also used to calculate crystallinity degrees (Simones, Viana, & Cunha, 2009; Xiang et al., 2019). In the equations, ΔH_m is the melting enthalpy, ΔH_{cc} is the cold crystallization enthalpy, and X_c is the percentage of crystallization value.

$$Xc, pla/plla\ (\%) = \left[\frac{\Delta Hm, pla/plla - \Delta Hcc, pla/plla}{\Delta H0, pla/plla\ Wpla/plla}\right] \times 100 \quad (2.1)$$

$$Xc, pcl\ (\%) = \left[\frac{\Delta Hm, pcl}{\Delta H0, pcl\ Wpcl}\right] \times 100 \quad (2.2)$$

$W_{pla/plla}$ and W_{pcl} are the weight fractions of PLA/PLLA and PCL, respectively (0.5 in the blend and 1 for the pure materials) (Herrero-Herrero, Gómez-Tejedor, & Vallés-Lluch, 2018).

2.1.2.5 Biological investigations

Following the morphological, chemical, and thermal analyses, it is decided to continue the biological analyses with PLA100, PCL100, PLA20PCL80, PLA50PCL50, PLLA20PCL80, and PLLA50PCL50 within the scope of the thesis. The determined surfaces are subjected to biodegradability testing and *in-vitro* cell cultivation. These analyses are carried out with the laboratory infrastructure facilities of Uludağ

University-Medical Biology Department, under the coordination of Prof. Dr. Gülşah Çeçener and with the support of Havva Tezcan Ünlü.

Scaffold Sterilization

PLA100, PCL100, PLA20PCL80, PLA50PCL50, PLLA20PCL80, and PLLA50PCL50 are sterilized by washing once in 70% ethanol, and rinsed three times in sterile phosphate buffer saline (PBS). After that, the fibrous webs are sanitized on both sides by exposing them to UV light for 30 minutes. Further, all cell culting and UV strelization processes are accomplished in the laminar flow cabinet (Figure 2.8).

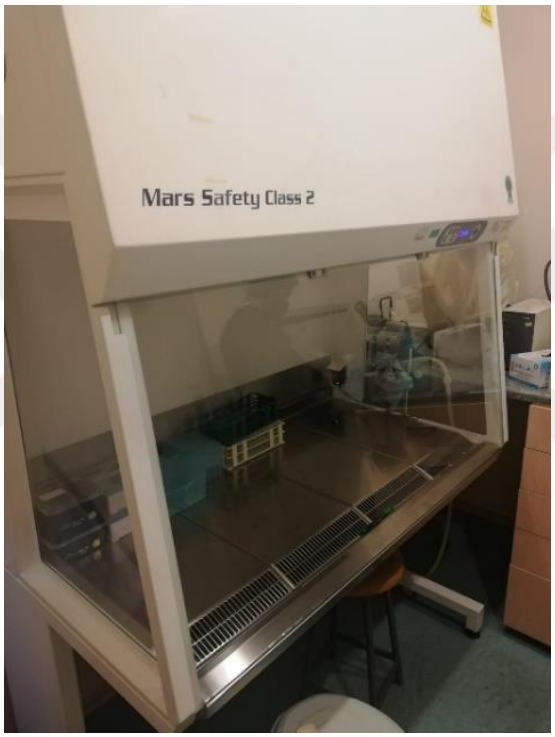

Figure 2.9 : Laminar flow cabinet for cell culture and UV sterilization processes.

Biodegradation Assay

Sterilized selected surfaces (PLA100, PCL100, PLA20PCL80, PLA50PCL50, PLLA20PCL80, and PLLA50PCL50) are cut into 1x1 cm pieces, allowing for one measurement per month for 5 months, and initial weights are measured with an assay balance (Figure 2.9 (a)). The webs are taken into the 24 well plates (Figure 2.9 (b)), and 300 µl of PBS is added on them, after that they are incubated at 37 °C in a 5% CO_2 incubator (Figure 2.9 (c)).

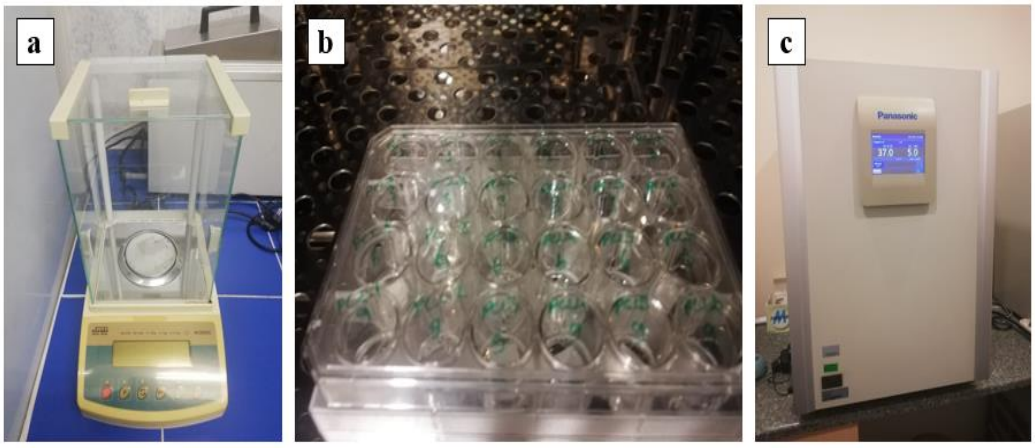

Figure 2.10 : Assay balance (a), biodegradation samples placed in 24 well plates (b), incubator (c).

***In-vitro* cell culture**

Selected surfaces (PLA100, PCL100, PLA20PCL80, PLA50PCL50, PLLA20PCL80, and PLLA50PCL50) are cultivated with both HUVECs and fibroblast cells. The cells stored in cryo tubes are transferred to the appropriate culture medium in 15 ml falcons, and then centrifuged at 1200 rpm for 5 minutes. After centrifugation, the supernatant is poured into 25cm^2 flasks (Figure 2.10 (a)) containing cell-specific growth medium (FibroGRO™-LS Complete Media Kit and DMEM-F12 medium) (Figure 2.10 (b)) and incubated at 37 °C in an incubator containing 5% CO_2 (Figure 2.9 (c)). After the cells reach 80% density in each flux, the cells are passaged into 75 cm^2 flasks, and every three days, the growth mediums are replaced. Moreover, the samples are placed into the 6 well plates (Figure 2.10 (d)).

Figure 2.11 : 25cm^2 flasks (a), FibroGRO™-LS Complete Media Kit and DMEM-F12 medium (b), and samples in 6 well plates (c).

Cell viability analysis

Cell count analysis, which is the determining factor for assay optimization, is performed using 4% Trypan blue to distinguish live and dead cells in the experiment. Trypan blue is a negatively charged dye and does not penetrate into cells whose cell membrane is not damaged. However, cells with damaged cell membranes (dead) absorb trypan blue and appear in blue color under the microscope. Thus, live and dead cells are counted on the thoma slide, allowing the desired amount of live cells to be cultivated.

In order to perform cytotoxic analysis, the cell lines in the flasks are washed once with PBS, then cells are treated with Trypsin-EDTA (0.025% trypsin/1mM EDTA) and incubated for 5 minutes at 37°C in a 5% CO_2 incubator. After incubation, the substances are taken into 15 ml falcons with an appropriate medium and centrifuged at 1200 rpm for 5 minutes at room temperature. The supernatant is removed and 1 ml of medium is added to the pellet after centrifugation. The cells are counted under the microscope for cytotoxic analyses after being prepared in 1.5 ml eppendorf with Trypan blue at a 1/1 ratio, ready for counting on the Thoma slide.

Cell proliferation (MTS) analysis

The proliferation of the HUVEC and fibroblast cell line on the biopolymer is determined by MTS technique. MTS is a spectrophotometric and colorimetric test that uses mitochondrial dehydrogenase to convert tetrazolium salts into formazan salts in living cells, and the measured absorbance value is proportional to the number of viable cells.

Proliferation measurements are taken on the 3^{rd} and 7^{th} days, in accordance with the cell growth rates. 1x1 cm sterile PLA100, PCL100, PLA20PCL80, PLA50PCL50, PLLA20PCL80, and PLLA50PCL50 scaffolds are inserted in 24 well plates in three repeats to assess the proliferation rate. In a CO_2 incubator, the scaffolds on which the medium is applied are incubated overnight at 37°C. Before cell cultivation, the medium in which the surfaces are incubated overnight is removed from the wells, and $1x10^5$ cells are seeded into each well. The previous medium on the cells is removed and serum-free medium is introduced before the MTS measurement. 100 µl of MTS reagent is added to the wells and incubated for 3 hours at 37°C in a 5% CO_2 incubator.

At the end of the determined time, 200 µl of sample is transferred into a 96 well plate through the medium with reagent added and analysed at the absorbance level of 490 nm in the Elisa Reder device. Results are expressed as the proliferation rates of experimental cells assuming 100% of control cell viability untreated with the compound.

3. RESULTS AND DISCUSSION

As in the experimental process, the results of the analysis of the surfaces produced within the scope of the thesis and the discussion of the results are carried out in three stages.

i. Surface fabrication and optimization of PCL (45,000 Mn), PLA and their blends (a preliminary study).

ii. Surface fabrication and optimization of PCL (80,000 Mn), PLA, and their blends.

iii. Investigation of pure and blended biopolymeric surfaces in the light of selected polymers (PLA, PLLA, and PCL) and concentrations.

i. Results of the Surface Fabrication and Optimization of PCL (45,000 Mn), PLA and Their Blends (a preliminary study)

3.1 Morphological Characterization of Preliminary Study

3.1.1 SEM characterization

SEM images of the PCL, PLA, and PLA/PCL fibrous structures at different concentrations are illustrated in the Figure 3.1, 3.2 and 3.3, respectively.

It is seen that even if beaded, fiber formation can be observed in PCL100_16. However, continuous fibers could not be achieved in PCL100_18 and PCL100_20 samples (Figure 3.1(a), 3.1(b), and 3.1(c)) due to the high solution viscosity. In cases of high viscosity, the solution may not allow jet formation and results in thick and discontinuous fibers on the collector (Pham et al., 2006). Although the 9/1 solvent system is previously studied in the literature (Ipek Y. Enis et al., 2017), the desired continuous and smooth fiber formation could not be obtained in this study. This situation is thought to be caused by instabilities in production parameters, especially moisture and temperature imbalance, which cannot be kept constant in production.

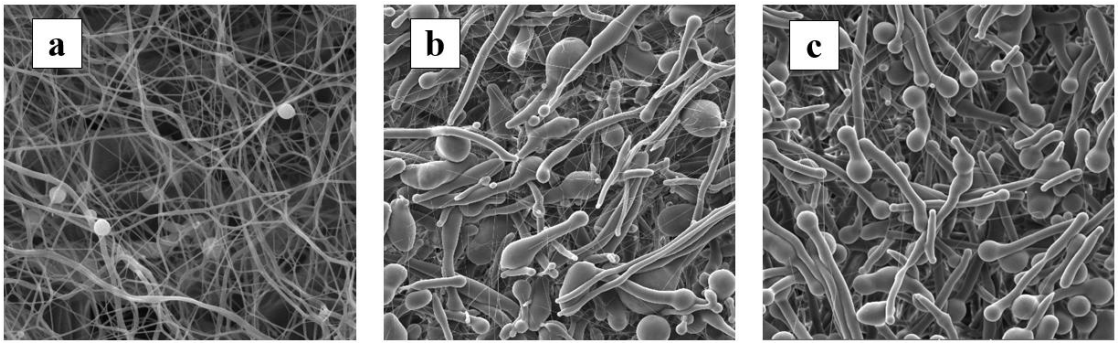

Figure 3.1 : SEM images of (a) PCL100_16 at magnification of 5kx, (b) PCL100_18, and (c) PCL100_20 at magnification of 1kx.

On the other hand, Figure 3.2 shows that PLA100_7, PLA100_8 and PLA100_9 have smooth and continuous fibers; moreover, all these three structures have many self-pores on the fiber surfaces. This may be due to the fact that acetone which is in the solvent partially dissolves the fiber surface as small spots even after electrospinning. This idea has also been supported by the literature and is called the breath figure mechanism, and the mechanism usually includes a water immiscible solvent and a hydrophobic polymer. During the electrospinning of the polymer in a humid environment (usually relative humidity is above 50%), water molecules in the air evaporate on the polymer surface and in this case the water molecules move to form circular traces. Thus, it evaporates and causes porous structure formation on the fiber (C. Huang & Thomas, 2018). Since the relative humidity RH is near 50% when these productions are performed, it is predicted that an identical breath figure mechanism appears.

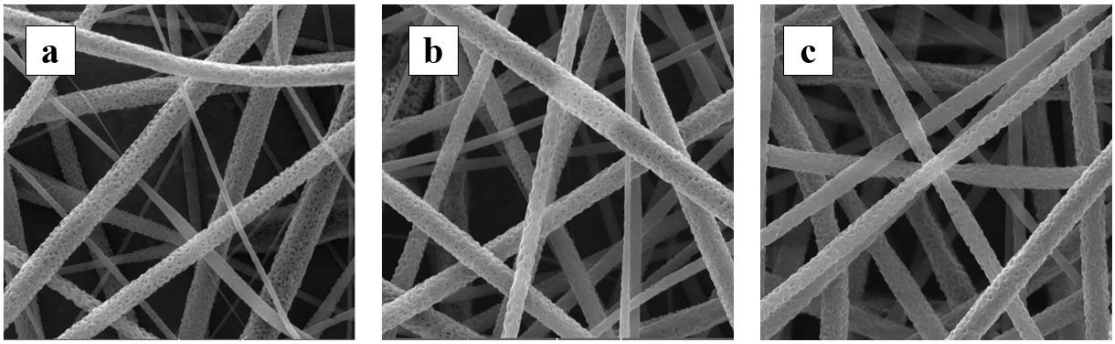

Figure 3.2 : SEM images of (a) PLA100_7, (b) PLA100_8, and (c) PLA100_9 at magnification of 5kx.

Furthermore, the PLA/PCL electrospun surfaces that can be seen in Figure 3.3 both have smooth structures including continuous fibers. These visual findings indicate that

PLA and PCL can homogeneously be blended at specified blending ratios with suitable solvent system (CHL/AC/AA 8/1/1) and electrospun without any problem.

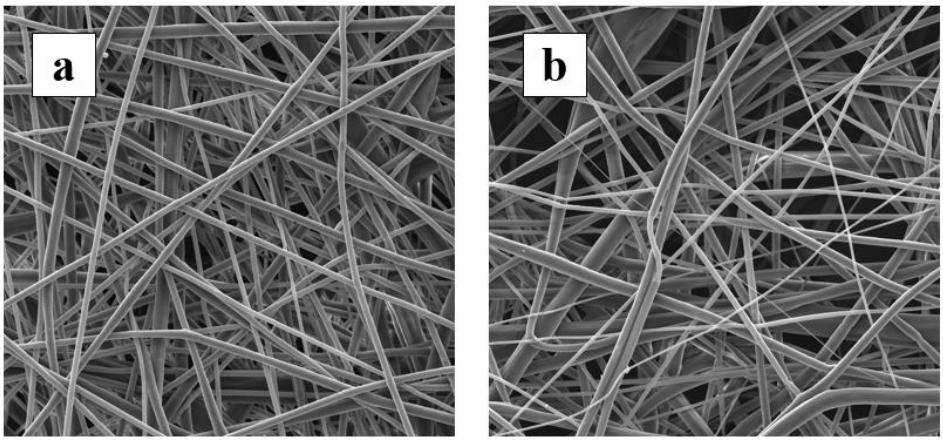

Figure 3.3 : SEM images of (a) PLA75PCL25_12 and (b) PLA50PCL50_12 at magnification of 3kx.

3.1.2 Fiber diameter analysis

Average fiber diameters with SDs, and fiber morphologies of the fibrous webs can be seen in the Table 3.1. Although no fibers are formed in PCL100_18 and PCL100_20, nanoscale fiber formation is achieved in the PCL100_16 sample. At polymer concentrations beyond 16%, the solution structure is assumed to be excessively viscous, and it sticks to the collector in the form of thick and discontinuous polymer strands rather than fibers. Excessive polymer concentration, which causes high viscosity, has a negative impact on the fiber formation process, in addition to insufficient polymer concentration. Fiber diameter analysis shows that the average fiber diameter slightly increases with increasing polymer concentration, although there is no big difference between PLA100_7, PLA100_8 and PLA100_9. This phenomenon is also included in the literature (Schueren et. al, 2011; Enis et. al., 2018). In order to understand the effect of using different polymer concentrations, wider polymer concentration ranges should be studied. When the fiber diameters of PLA75PCL25_12 and PLA50PCL50_12 (1.860 μm and 2.071 μm, respectively) are compared, it can be seen that there is a non-neglegible difference between them, and that the fiber diameter increases as the amount of PLA in the structure increases. The fact that PLA has a substantially larger molecular weight than PCL may explain this.

Table 3.1: The average fiber diameters, and fiber morphology notes.

Sample Codes	Avg. Fiber Diameter ± SD (μm)	Fiber Morphology
PCL100_16	0.273 ± 0.031	Beaded structure
PCL100_18	NA	Thick and discontinuous fiber-like structure
PCL100_20	NA	Thick and discontinuous fiber-like structure
PLA100_6	1.626 ± 0.369	Fiber formation
PLA100_7	1.637 ± 0.524	Fiber formation
PLA100_8	1.694 ± 0.343	Fiber formation
PLA75PCL25_12	2.071 ± 0.395	Fiber formation
PLA50PCL50_12	1.860 ± 0.541	Fiber formation

SEM analysis and fiber diameter measurements realized in the preliminary experimental part of this thesis show that PCL with a molecular weight of 45,000 g/mol is not successful in forming fibers at the concentrations studied. Low molecular weight PCL could not form sufficient molecular chains in its structure and successfully complete the fiber formation process. For this reason, further studies are continued with PCL with a molecular weight of 80,000 g/mol. In addition, PCL forms fibers at only 16% polymer concentration and contains beads on this surface, preventing a realistic fiber diameter determination. Low molecular weight of PCL100 causes low solution viscosity at 16 % polymer concentration, leading to beads rather than fiber formation while no contionuous fibers are observed at higher polymer concentrations (18 and 20 %). This situation is considered to be caused by instabilities in production parameters, which cannot be kept constant in production. On the other hand, continuous fibers are formed in PLA100 surfaces produced at 7, 8 and 9% polymer concentrations. However, structural pores are also formed which may be resulted from the breath figure mechanism regarding environmental conditions during the production. Since the concentration values studied for PLA100 are very close to each other, no differences in fiber diameters are detected. Lastly, uniform, smooth and continuous fiber formation is observed in both of the PLA/PCL blends (75/25 and 50/50) and these blends are found promising for further studies. However, the smaller diameter fibers generated in PLA50PCL50_12, makes this ratio more attractive.

ii. Results of the Surface Fabrication and Optimization of PCL (80,000 Mn), PLA, and Their Blends.

In the second part of the study, high molecular weight PCL (80,000 Mn) is used instead of low molecular weight PCL (45,000 Mn), which could not achieve the desired efficiency in the preliminary studies. Thus, it is aimed to benefit from the superior mechanical properties and spinability of PCL with 80,000g/mol, which is also supported by the literature (Hasan et al., 2018; Kakroodi, Kazemi, Rodrigue, & Park, 2018; Yalcin Enis & Gok Sadikoglu, 2018). In addition, PLA/PCL blends have also been re-optimized for high molecular weight PCL.

3.2 Morphological Characterization of Scond Part of The Study

3.2.1 SEM characterization

SEM images of the PCL, PLA, and PLA/PCL blend fibrous webs at different polymer concentrations (6-8-10%) are illustrated in Figure 3.4, 3.5, and 3.6, respectively.

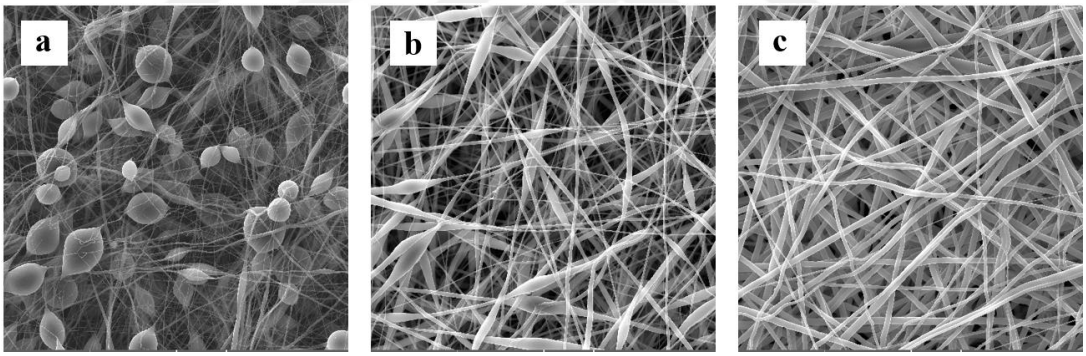

Figure 3.4 : SEM images at 1kx magnification of PCL samples at different concentrations (a) PCL100_6, (b) PCL100_8, and (c) PCL100_10.

According to the SEM image of PCL100_6 in Figure 3.4 (a), it is clear that bead formation rather than continuous fibers is predominantly observed. The SEM image of PCL100_8 (Figure 3.4 (b)) indicates that this sample has thicker regions along the length of the fibers, so it does not have a homogeneous fiber diameter. This situation is thought to be due to the beaded structure of PCL100_6 examined in the SEM image of Figure 3.4 (a), gradually elongating and turning into fiber. The SEM image of PCL100_10 in Figure 3.4 (c) shows that the structure contains beadless, continuous, and homogeneous fibers. When the morphologies of all three samples are evaluated, it is seen that the beaded structure decreases due to the increment of polymer

concentration from 6% to 10% for this sample group. This situation can be explained by the insufficient viscosity of the solution for lower polymer concentration, which is important for the entanglement of polymer in the molecular chains (Hossain, Gong, & Rigout,2016).

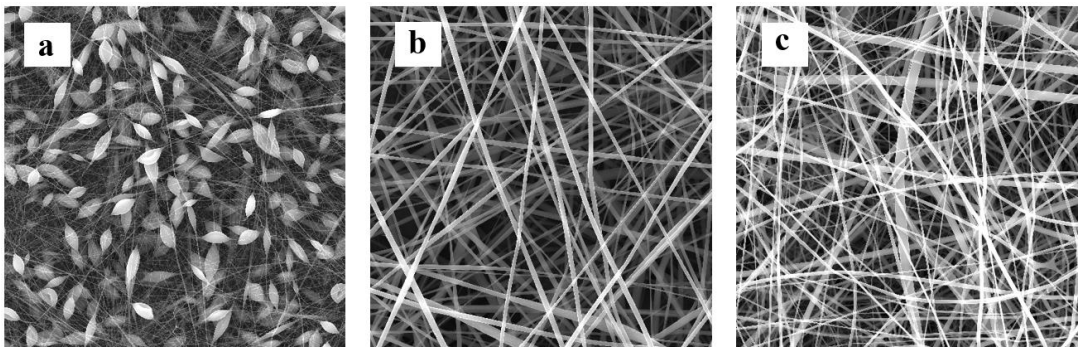

Figure 3.5 : SEM images at 1kx magnification of PLA samples at different concentrations (a) PLA100_6, (b) PLA100_8, and (c) PLA100_10.

Similar to the PCL100_6, beaded fibers are observed for PLA100_6 shown in Figure 3.5 (a) which is explained with the aforementioned low polymer concentration. When the polymer concentration increases to 8% or 10%, continuous fibers without beady structures are observed (Figure 3.5 (b) and (c)). Therefore, as supported in the literature, the beaded structure disappears with increasing concentration for PLA fibers (Jahangir, Rumi, Wahab, Rahman, & Sayed, 2017). In PLA_10 samples, it is sighted the thicker fibers started to form with increased polymer concentration.

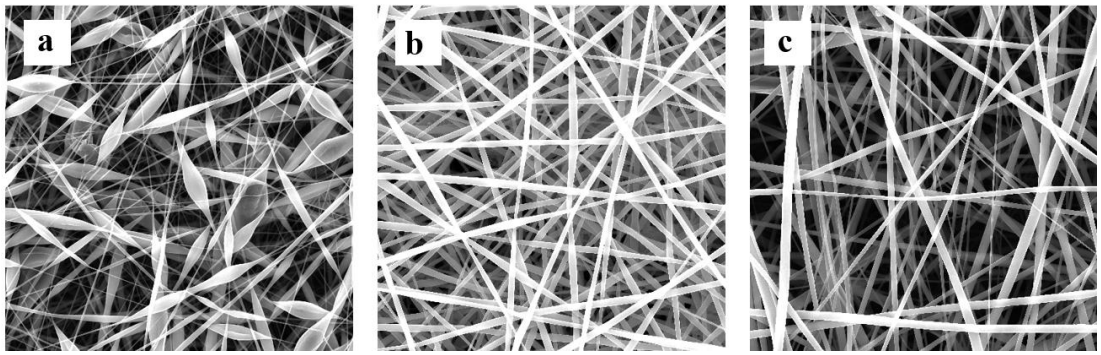

Figure 3.6 : SEM images at 1kx magnification of PLA/PCL blend based samples at different concentrations (a) PLA50PCL50_6, (b) PLA50PCL50_8, and (c) PLA50PCL50_10.

As expected, undesirable bead formation is observed for PLA50PCL50_6 (Figure 3.6 (a)), as in PCL100_6 and PLA100_6. The formation of a low concentration beaded structure is seen not only on neat polymer-based surfaces but also on surfaces obtained from blend polymer structures (Shao, Fang, Wang, & Lin, 2015). However, it is

possible to obtain continuous fibers without bead formation for PLA50PCL50_8 and PLA50PCL50_10 samples (Figure 3.6 (b) and (c)) with increasing polymer concentration as in neat polymers; PCL and PLA.

As a consequence of the morphological data obtained in the secondary part of the thesis, it is found that surfaces generated with 80,000 g/mol molecular weight PCL indicate promising outcomes. In addition, it is seen that the 6% polymer concentration is low for PCL, PLA and PLA/PCL blend and results in beads. On the other hand, uniform structures can only be obtained at higher concentrations.

3.2.2 Fiber diameter analysis

The average fiber diameters of PCL100 (80,000 Mn), PLA100 and PLA50PCL50 samples with changing polymer concentrations and the additional morphology notes can be seen in Table 3.2. Though the fiber diameters of PCL100_6, PLA100_6, and PLA50PCL50_6 are measured, the results are not reasonable due to their beady structures. The remaining samples have smooth and continuous fibers.

Table 3.2: The average fiber diameters, and fiber morphology notes.

Sample Codes	Avg. Fiber Diameter ± SD (µm)	Fiber Morphology
PCL100_6	0.668 ± 0.382	Beaded structure
PCL100_8	1.390 ± 0.575	Fiber formation *(nonhomogeneous fiber diameter through fiber length)*
PCL100_10	1.792 ± 0.654	Fiber formation
PLA100_6	0.454 ± 0.221	Beaded structure
PLA100_8	1.483 ± 0.527	Fiber formation
PLA100_10	1.798 ± 0.502	Fiber formation
PLA50PCL50_6	0.732± 0.515	Beaded structure
PLA50PCL50_8	1.687 ± 0.453	Fiber formation
PLA50PCL50_10	2.127 ± 0.617	Fiber formation

According to the fiber diameter measurements, as the concentration increases, the fiber diameter increases. This is an inevitable result proven by the literature (Haider et al., 2018; M. Herrero-Herrero et al., 2018; Maeda, Hagiwara, Yoshida, Hasebe & Hotta, 2014). In this context, the highest fiber diameters are achieved at 10% polymer concentrations for PLA100, PCL100 and PLA50PCL50 blends, while beaded

structures with nanoscale fibers are noticed in samples PCL100_6, PLA100_6 and PLA50PCL50_6 with low polymer concentrations. The diameters of nanofibers mainly depend on the size of the nozzle and the polymer content in the nozzle. The primary jet may break into several jets during the movement of a solution jet from the syringe to the metal collector, resulting in varying diameters of fibers. Unless there is any splitting, one of the most crucial parameters influencing fiber diameter is the solution viscosity. A larger fiber diameter results from the higher viscosity, and the solution viscosity is directly proportional to its concentration. In addition, solution viscosity and the solvent type have a relationship with each other, thus the fiber diameter can differ according to the solvent system. In a study conducted by Abel et al. (2019) PCL was used and it was determined that the fiber diameter is 0.81±0.38 μm when chloroform/methanol was used as a solvent at constant polymer concentration, and 1.04±0.65 μm when acetic acid was preferred. On the other hand, Kim et al. (2016) achieved PCL fibers with diameters of 0.11-1.69 μm, 0.42-0.78 μm, 1.63-2.50 μm, and 1.78-3.85 μm for formic acid, dichloromethane/dimethyl formamide, chloroform/dimethyl formamide, and dichloroethane solvent systems, respectively. Moreover, PLA fibers with an average diameter of 0.59±0.13 μm were produced with acetone whereas 3.06±3.20 μm PLA fiber diameter was achieved with chloroform. Using different ratios of chloroform/ethanol solvent system, PLA fibers in a diameter range of 1.49-3.12 μm were produced (Casasola, Thomas, Trybala, & Georgiadou, 2014). Thus, all measured fiber diameters for PCL samples (0.668-1.792 μm), and PLA samples (0.454-1.798 μm) are found in a range of literature, and although the solvent systems of PLA100 (3/1, CHL/AC) and PCL100 (8/1/1, CHL/AA/ETH) are different, their fiber diameters are not very far away from each other. However, despite the solvent system of the PLA50PCL50 blend is the same as that of PCL100 (8/1/1, CHL/AA/ETH), it results in a surface with a higher fiber diameter (in a range of 0.732-2.127 μm) than PLA100 and PCL100 samples. This situation can be caused by the PLA polymer content in PLA50PCL50 blend which is faced with different solvent types (8/1/1, CHL/AA/ETH). The effect of solvent type on PLA50PCL50 blends with similar outcomes is also studied by the researchers (Herrero-Herrero et al., 2018).

3.2.3 Porosity analysis

Thresholds are prepared using the Image J program, and combined with original SEM images used for the pore analyses (Figure 3.7).

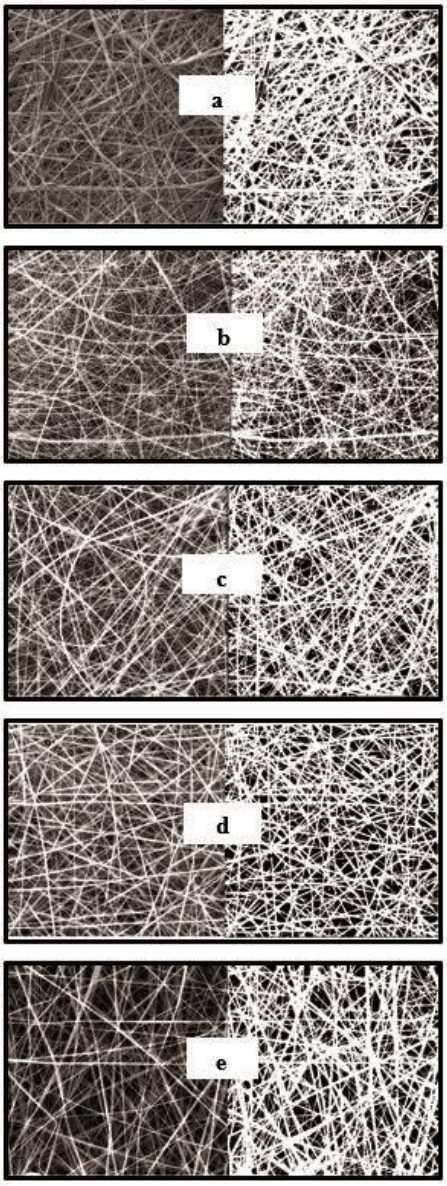

Figure 3.7 : SEM images of the samples and their thresholdings (a) PCL100_10, (b) PLA100_8, (c) PLA100_10, (d) PLA50PCL50_8 and (e) PLA50PCL50_10.

The pore analysis is conducted for only bead-free structures including PCL100_10, PLA100_8, PLA100_10, PLA50PCL50_8, and PLA50PCL50_10. The remaining samples are not tested because of undesired beady morphologies. Pore analysis of bead–free samples are listed in Table 3.3.

Table 3.3: Pore analysis of the bead-free samples.

Sample Codes	Porosity (%)
PCL100_10	18.23
PLA100_8	21.92
PLA100_10	17.95
PLA50PCL50_8	21.63
PLA50PCL50_10	14.55

When comparing all samples regardless of polymer type, it is possible to notice the effect of fiber diameter on porosity results. Current literature confirms the case that the average porosity increases with decreasing fiber diameter (Yalcin Enis & Gok Sadikoglu, 2018). As seen in Table 3.3, the highest porosity belongs to PLA100_8 and PLA50PCL50_8 with the lowest average fiber diameters as defect-free. On the other hand, it is determined that the porosity decreases with the increase in fiber diameter depending on the polymer concentration increase. The pore area should be at an optimal level that allows infiltration of cells and other biofactors, while not attenuate mechanical strength (Y.Z. Huang, Xie, & Li, 2020; Loh & Choong, 2013).

3.2.4 Water contact angle analysis

The hydrophilicity of the surface is a factor that influences the scaffold's wettability (Areias et al., 2012) and inversely related to the water contact angle in which the hydrophilic character diminishes as the contact angle increases (Haghjooy Javanmard, Anari, Zargar Kharazi, & Vatankhah, 2016; Moreno Raja et al., 2019). Tightly packed crystalline areas in the structure results in hydrophobic characteristic that prevent the water absorption of polymer surfaces (Areias et al., 2012; Korzhikov, Averianov, Litvinchuk, & Tennikova, 2016). Table 3.4 shows that the water contact angles of PCL, PLA and PLA/PCL blend samples.

Table 3.4: Contact angle measurements of the fibrous webs.

Samples	Contact Angle Mean [°]
PCL100_6	123.81±1.56
PCL100_8	120.18±0.97
PCL100_10	114.41±1.98
PLA100_6	117.79±1.89
PLA100_8	103.20±1.52
PLA100_10	114.08±5.05
PLA50PCL50_6	102.98±2.42
PLA50PCL50_8	120.79±0.54
PLA50PCL50_10	120.54±0.77

All samples exhibit hydrophobic behavior due to their large contact angles, which affects the wettability of the surfaces (Table 3.4). There is not much difference observed among the contact angles of the samples. Besides, the contact angle and hydrophilicity of the surfaces are not correlated with the polymer concentration and fiber diameter. Since the hydrophobic nature of PLA and PCL polymers which is a result of crystalline regions in their structures has been confirmed in the literature, it is an expected result that the contact angle values of the surfaces produced in this study are high (Moreno Raja et al., 2019).

The presence of tightly packed dense crystalline regions in polymer structures causes low water absorption, giving the structures a hydrophobic nature (Areias et al., 2012; Korzhikov et al., 2016). Metwally et al. found the water contact angle of the electrospun PCL surface to be between 126.9° and 129.3° for tissue engineering applications. Moreover, in a study conducted by Abudula et al., the water contact angle of PLA was determined to be approximately 114.1°. Since PLA50PCL50 blends have the characteristics of PLA and PCL biopolymers, PLA50PCL50 blend samples have also hydrophobic nature. On the other hand, the hydrophilic character improves the polarity and adhesiveness of the surface, which makes cell attachment and proliferation more possible (Shabani, Haddadi-Asl, Seyedjafari, Babaeijandaghi, & Soleimani, 2009). Previous studies have reported that cells favorably attach to surfaces with an average contact angle of 60-70 degrees (Amirian, Sultana, Joo, Park, & Lee, 2020). Therefore, various surface modification studies are carried out in the literature to improve the wettability and cell adhesion properties of PLA and PCL-based surfaces (Haddad et al., 2016; Oyane et al., 2005). However, although low water contact angle is an advantage, it is not the only one essential feature for cell adhesion, since many hydrophobic TE surfaces in the literature show sufficient cellular results (Scaffaro, Lopresti, & Botta, 2017; Yao et al., 2017).

3.3 Thermal Characterization

3.3.1 DSC analysis

DSC analysis is a fingerprint that defines the thermal and mechanical background of the polymers (Menczel & Prime, 2008). Thermal analyses performed as part of this thesis are completed in two stages (heating and cooling). PLA100_8, PCL100_8 and

PLA50PCL50_8 samples are selected for DSC analysis to observe the difference between the thermal behavior of biomaterials and analyses are carried out.

Thermal characterization for PLA is carried out in two different cycles. In the first cycle, the heating/cooling rate is determined as 20 °C/min, while in the second cycle it is 10 °C/min during heating and 5 °C/min during cooling. PLA100 has a cold crystallization and melting behavior at 96.3 °C and 149.5 °C, respectively. Moreover, two peaks are observed in the melting process. There is no peak during cooling since low crystallization PLA mainly crystallizes during heating (C. Li & Dou, 2014). The T_g peak (63 °C) of PLA100 is visible in Figure 3.8, and the crystallization is calculated as 21%. Also, these results are congruent with the literature (Sharma & Satapathy, 2019; R. T. Zhu et al., 2014).

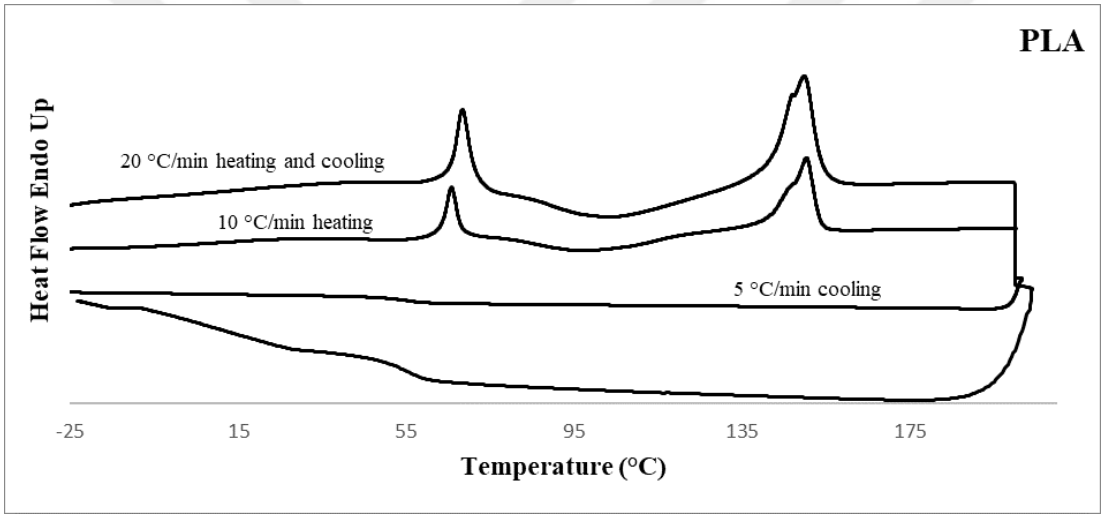

Figure 3.8 : DSC analysis of PLA100 sample at two different heating/cooling rates.

Unlike PLA100, a single heating/cooling rate is used for the thermal characterization of the PCL100. PCL is a semi-crystalline biopolymer that displays cooling crystallization around 24 °C (Figure 3.9). Despite the fact that it appears to melting behavior at roughly 62 °C after heating, the T_g value of PCL100 cannot be determined. This is because, according to the literature (Mohamed et al., 2008), the T_g of PCL is about -60 °C, and the beginning temperature in this investigation is not that low. Moreover, it has a high crystallinity percentage (56.7 %) as seen in Table 3.8 compared to PLA. These values regarding cooling crystallization and melting of PCL can be found in the literature (Lopez-Rodriguez, Lopez-Arraiza, Meaurio, & Sarasua, 2006).

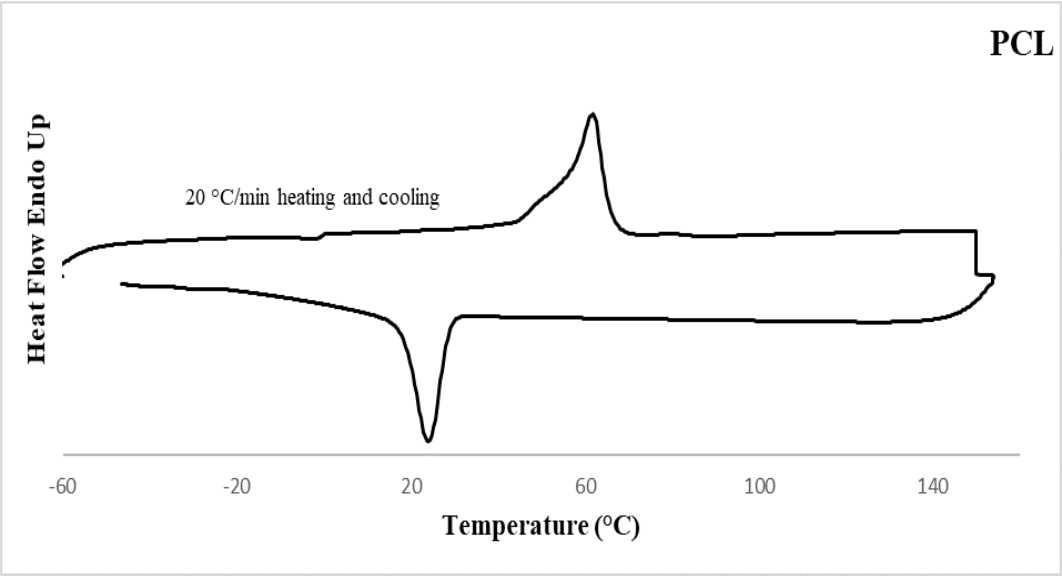

Figure 3.9 : DSC analysis of PCL100 sample at one heating/cooling stage.

Table 3.5: DSC analysis of fibrous surfaces.

Sample		PCL melting/crystallization		PLA cold crystallization		PLA melting/crystallization		X_c%	
		T_m (°C)	ΔH_m (J/g)	T_{cc} (°C)	ΔH_{cc} (J/g)	T_m (°C)	H_m (J/g)	PLA	PCL
PLA100	Heating	-	-	96.3	-3.1	149.5	20	21.5	-
	Cooling	-	-	-	-	-	-	-	-
PLA50PCL50	Heating	59.2	40.6	90.5	-2.2	149.7	8.4	5.7	14.5
	Cooling	32.5	-12.5	-	-	-	-	-	-
PCL100	Heating	55.8	79	-	-	-	-	-	56.7
	Cooling	24.0	-97.5	-	-	-	-	-	-

The thermal properties of both polymers can be seen in the blended webs too. The characteristic peaks can be observed in the DSC graph of PLA50PCL50 samples (Figure 3.10).

PLA is a semi-crystalline biopolymer that exhibits exothermic cold crystallization and endothermic melting behavior during heating (Lv et al., 2016). The difference between the heating and cooling rate in the second cycle of thermal analysis of PLA is realized to allow the material time required for the chains in the structure to transform into a crystalline form during heating or cooling. Otherwise, the material remains amorphous form before it can turn into this state (Gumus, Ozkoc, & Aytac, 2011). Thus, the peak calculations are accomplished according to the second stage. The multiple melting

activity emerged in PLA samples is because of the extensive rearrangement of the crystalline phase associated with crystallization at low temperatures (Di Lorenzo, 2006; Refaa, Boutaous, Xin, & Siginer, 2017).

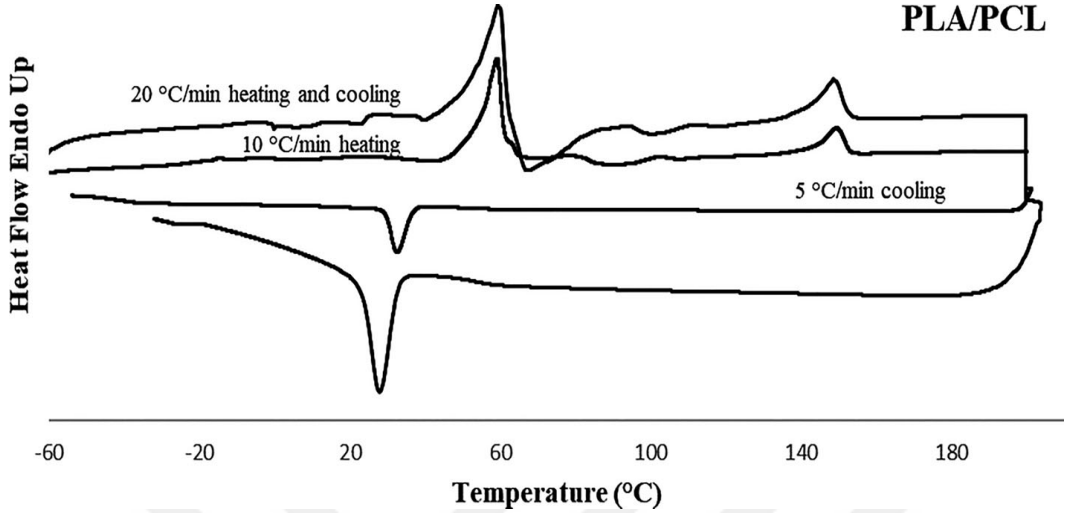

Figure 3.10 : DSC analysis of PLA50PCL50 blend samples at two different heating/cooling rates.

A single heating/cooling rate is utilized for the analysis of the PCL because the characteristic peaks can be clearly seen when this ratio is used. On the other hand, the characteristic peaks of PCL are found to be consistent with the studies in the literature (Lopez-Rodriguez et al., 2006). PLA/PCL surfaces are also analysed in two cycles due to the same reason with PLA. T_{cc} value of PLA in the PLA/PCL blend system is slightly lower than the neat PLA. With the integration of PLA which has more amorphous regions than PCL into the structure, the melting enthalpy of PCL decreases. Furthermore, PLA in PLA/PCL blend has peaks only during the heating process due to its low crystallinity like in neat PLA (Luyt & Gasmi, 2016). PCL in the PLA/PCL blend crystallizes at a higher temperature than neat PCL. This is thought to be caused by the solid PLA particles acting as substrate that facilitate the crystallization of PCL (D. Wu et al., 2011). It can be said that both polymers have an effect on each other's crystal formations. Moreover, the T_g of PLA cannot be examined, although more or less characteristic points of both polymers are visible on the curve of the PLA/PCL blend. This is due to the melting of the PCL in the structure when the glass transition temperature of PLA is reached (Patrício et al., 2014).

iii. Results of Pure and Blended Biopolymeric Surface Investigations in the Light of Selected Polymers (PLA, PLLA, and PCL) and Concentrations.

After the second part, it is concluded that the 8% polymer concentration is suitable for the PLA100, PCL100 and PLA50PCL50 structures for fiber formation and the experimental study continues with this polymer concentration. On the other hand, PLLA, a derivative of PLA, is included in this part to determine its suitability for tissue engineering applications. Therefore, the fiber formation is optimized both in pure form and in PCL blended form of PLLA. Main target of this experimental part is to find out the appropriate polymer blend for the target tissue in the light of experiences gained in previous parts. As a result, in addition to neat PLA, PLLA and PCL polymers, their blends at various blending ratios are investigated.

3.4 Morphological Characterization

3.4.1 SEM characterization

Morphologies of the surfaces produced from neat polymers (PLA100, PLLA100, and PCL100) and blends (PLA/PCL and PLLA/PCL) are seen in Figure 3.11. Smooth and continuous fibers are observed for neat PLA100 and PCL100 whereas PLLA100 shows beady structure. The low polymer concentration of PLLA100, which has a relatively lower molecular weight than PLA100 and PCL100, is likely to be the cause. Because of the formation of beaded structures on the collector during the transformation of the polymer solution to the fiber due to insufficient concentration (Ahmed, Lalia, & Hashaikeh, 2015).

PLA/PCL blends have continuous and smooth fibers and non-beady forms regardless of blend ratio although this is not the case for all PLLA/PCL blends. On the PLLA40PCL60 and PLLA50PCL50 surfaces, the polymer jet cannot be transformed to fiber completely and it turns into a beaded form in the structure, but on the surfaces of PLLA10PCL90, PLLA20PCL80, and PLLA30PCL70 continuous and reliable fibers can be noticed. It can be said that with the increase in the amount of PCL in the polymer solution, the polymer blend has a tendency to form fibers with the electric field effect.

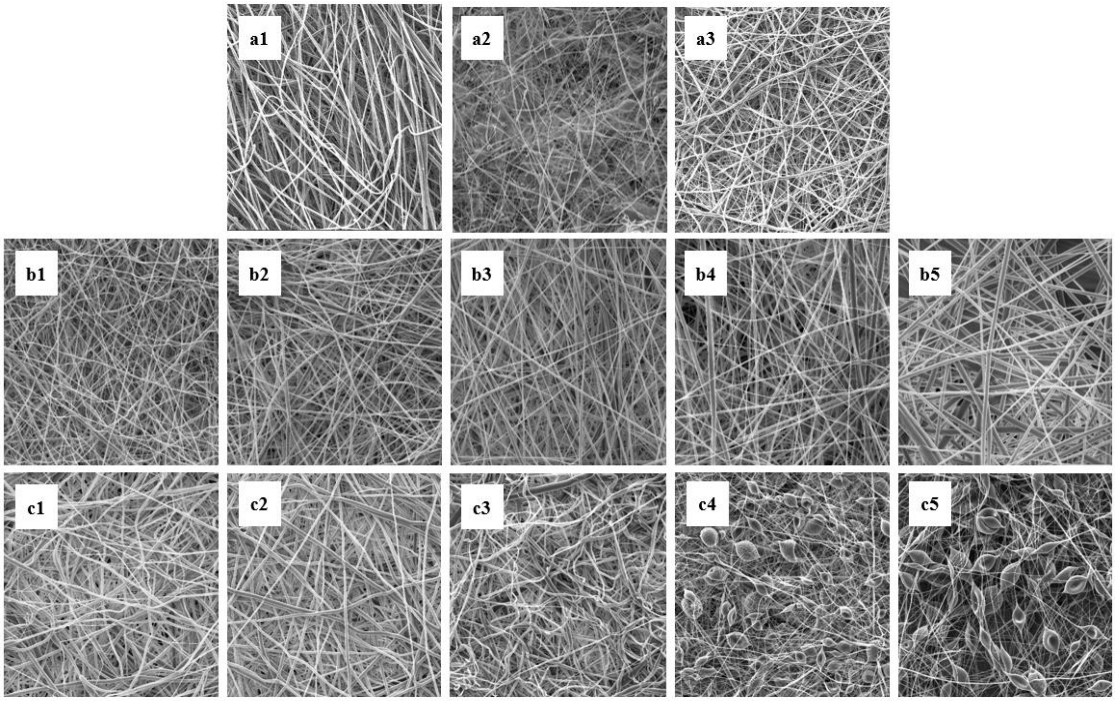

Figure 3.11 : SEM images at 1000x magnification of the fibrous samples. a1, a2, and a3 represent PLA100, PLLA100, and PCL100, respectively. Group b1 to b5 are the SEM images of PLA10PCL90, PLA20PCL80, PLA30PCL70, PLA40PCL60, and PLA50PCL50, respectively while group c1 to c5 are the SEM images of PLLA10PCL90, PLLA20PCL80, PLLA30PCL70, PLLA40PCL60, and PLLA50PCL50, respectively.

3.4.2 Fiber diameter analysis

Table 3.6 reveals that each fibrous surface has fibers within a diameter range of 0.962-1.733 μm except PLLA100, PLLA40PCL60 and PLLA50PCL50 due to the undesired beaded structures. Even tough, the polymer concentration of the PLA100 is same with the PCL100, the average fiber diameter is finer in the PCL100, similar to the outcomes of our previous part (Oztemur & Yalcin-Enis, 2021).

Similar fiber diameter ranges for PCL, PLA, and blends generated with different solvent systems may be found in the literature (Sharma & Satapathy, 2020; Vaz, van Tuijl, Bouten, & Baaijens, 2005; Vonbrunn et al., 2020). Moreover, PLLA100 surface has fibers in nano-size in its construction despite the beads on the surface. Although PLLA100 surfaces may be produced with continuous fibers without beads by optimizing solution parameters, this study does not focus on its neat form since it is so brittle to be used alone in tissue applications (W. Wang et al., 2015).

Table 3.6: The average fiber diameters of the fibrous surfaces.

Sample Codes	Average Fiber Diameter ± SD (μm)
PLA100	1.733±0.316
PLLA100	0.760±0.210
PCL100	0.968±0.401
PLA10PCL90	0.962±0.222
PLA20PCL80	1.047±0.365
PLA30PCL70	1.107±0.351
PLA40PCL60	1.155±0.685
PLA50PCL50	1.417±0.248
PLLA10PCL90	1.597±0.669
PLLA20PCL80	1.428±0.523
PLLA30PCL70	1.172±0.566
PLLA40PCL60	0.602±0.346
PLLA50PCL50	0.596±0.187

On blended surfaces, it has been demonstrated that blend ratios have an impact on fiber diameter. Whereas both all the PLA/PCL based samples have smooth fiber morphologies, the thicker fibers in PLA50PCL50's structure can be associated with increasing PLA ratio. Sharma et al. employed PLA, which has a higher molecular weight than PCL, and blended the two polymers in varied but limited proportions (30/70, 50/50, and 70/30) in a comparable study. They noticed that as the amount of PLA in the blend increases, the fiber diameter increases as well, and this is attributable to the polymers' molecular weights (Sharma & Satapathy, 2019). Aside from the influence of increasing PLA in the blends, the PLA100 has the greatest average diameter fiber. Furthermore, PLLA10PCL90, PLLA20PCL80, and PLLA30PCL70 blends exhibit organized networks of continuous fibers with an average diameter less than 1,6 μm, unlike PLLA40PCL60 and PLLA50PCL50 which are not totally composed of fibers. Since the low molecular weight PLLA (50,000Mn) is used in the study, it is thought that a high PLLA ratio (40 and 50% wt.) in the blend reduces fluid viscosity and causes undesired bead formation.

3.4.3 Porosity analysis

Following the polymer concentration impact, a further porosity analysis is conducted to investigate the influence of additional PLLA to the sturucture as well as the blend ratio on surface porosity. The phenomenon that the fiber diameters of the surfaces are

reflected in the pore properties is confirmed by the data given in Table 3.7. Only surfaces with beadless architecture are subjected to porosity analysis, so the porosity properties of PLLA100, PLLA50PCL50 and PLLA40PCL60 are not examined.

Table 3.7: Porosity analysis of the bead-free samples and pore size analysis for selected samples.

Sample Codes	Average Porosity (%)	Average Pore Size (µm)±SD
PLA100	19.83	5.36±2.98
PLLA100	NA	NA
PCL100	28.46	5.08±2.97
PLA10PCL90	29.54	NA
PLA20PCL80	25.94	6.55±2.96
PLA30PCL70	25.19	NA
PLA40PCL60	24.29	NA
PLA50PCL50	23.86	5.57±2.99
PLLA10PCL90	22.75	NA
PLLA20PCL80	23.42	23.97±6.81
PLLA30PCL70	23.93	NA
PLLA40PCL60	NA	NA
PLLA50PCL50	NA	4.83±1.38

PCL100 and PLA10PCL90 are the samples with the smallest fiber diameter and the highest porosity values (28.46% and 29.55%, respectively). Conversely, PLLA10PCL90 and PLA100, which have the largest fiber diameters, are the samples with the lowest porosity values. Similar correlation is observed in all samples. On the other hand, the average porosity of the constructions 24.72%, which is low when compared to some of other studies that Image J method is not used for porosity analysis in the literature (Antonova et al., 2018; Jia, Li, Weng, Gu, & Chen, 2020). Although these findings provide useful information about the effect of fiber diameter distribution on pore analysis, the values obtained may differ slightly from the actual porosity values. However, it is well known that the porosity values obtained on nano/micro fiber surfaces produced by electrospinning are substantially greater (Amirian et al., 2020). Image J software can only measure the pores of the surfaces as 2 dimensional (2D) without depth perception, which results in lower porosity values. Whereas this measurement may not provide accurate pore information, it allows the surfaces to be compared amongst themselves. As a result, it can be predicted that sufficient porosity values will be obtained when evaluated in 3D. When the pore sizes of the selected

surfaces are investigated, they are found to be 5-6 μm on average, with no variation on other surfaces except PLLA20PCL80. This variation in PLLA20PCL80 is assumed to be due to air pressure's effect on measurement accuracy. The acquired pore diameter results are consistent with those measured in the literature using various methodologies (De Valence et al., 2012; Rnjak-kovacina et al., 2011), as well as the desirable pore diameter range in vascular tissue engineering applications (Sankaran, Krishnan, & Sethuraman, 2014).

3.4.4 Water contact angle analysis

As also stated previously, PLA, PLLA and PCL exhibit hydrophobic behaviour due to the presence of highly crystalline regions in their structures (Haghjooy Javanmard et al., 2016; Moreno Raja et al., 2019). Table 3.8 lists the water contact angle measurements of the samples.

Table 3.8: Contact angle measurements of the fibrous webs.

Samples	Contact Angles ± SD [°]
PLA100	120.58±0.35
PLLA100	135.60±0.32
PCL100	127.77±0.87
PLA10PCL90	134.83±0.31
PLA20PCL80	119.14±0.46
PLA30PCL70	118.89±0.83
PLA40PCL60	128.79±0.26
PLA50PCL50	109.69±0.14
PLLA10PCL90	132.50±0.25
PLLA20PCL80	115.56±0.11
PLLA30PCL70	134.68±0.07
PLLA40PCL60	128.23±0.10
PLLA50PCL50	114.52±0.12

In some preliminary studies, cell adhesion is reported to occur on surfaces with water contact angles below 100° (Jia et al., 2020b). However, although the hydrophilic characteristic of the scaffold aids cell attachment to the surface in tissue engineering applications, certain investigations have shown that cells can hold and live on surfaces with high contact angles too (Behtaj, Karamali, Masaeli, G. Anissimov, & Rybachuk, 2021; Haghjooy Javanmard et al., 2016; Yao et al., 2017). With an average water contact angle of 135°, PLLA100 has the highest water contact angle among other samples. Despite the fact that both PLA100 and PCL100 surfaces are hydrophobic, PLA100 has a lower contact angle than PCL100 owing to the chemical structure

differences. The carbon backbones of PCL are devoid of numerous hydrophilic functional groups. When compared to PCL, which only contains a single carbonyl group and has its carboxyl groups deprotonated in an aqueous environment, PLA has a higher hydrophilicity owing to the existence of a carboxyl group (Sant, Hwang, Lee, & Khademhosseini, 2011). When the blend structures are analysed, it can be concluded that all surfaces have high water contact angles and hydrophobic properties as a result of their chemical stuructures.

3.5 Chemical Characterization

3.5.1 FTIR analysis

The FTIR spectrums of the surfaces composed of neat PCL100, PLA100 and PLLA100 in addition to selected blends (PLA50PCL50, and PLLA50PCL50) are shown in Figure 3.12.

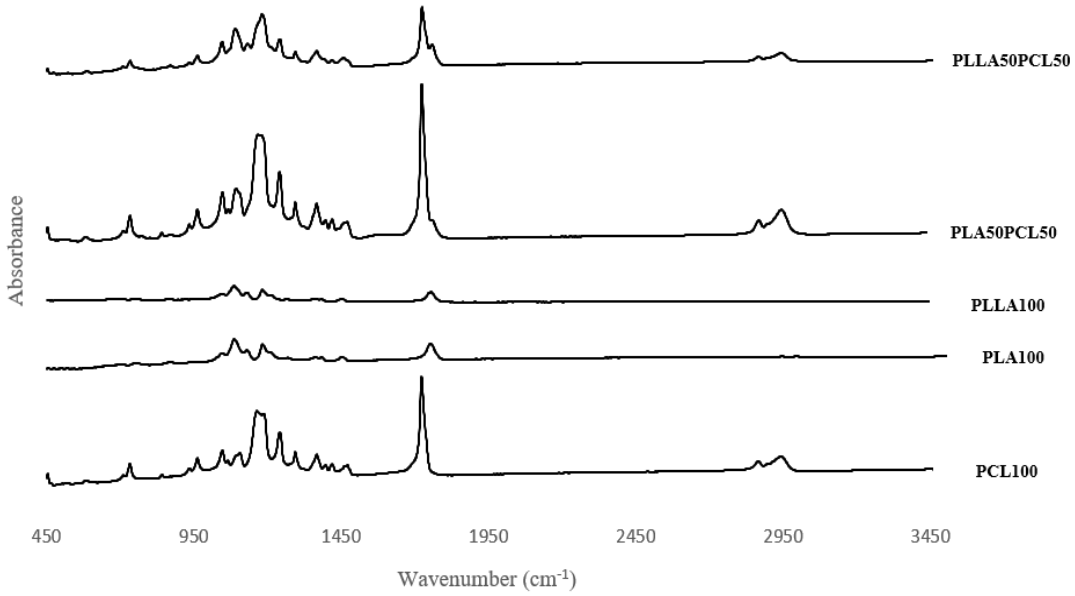

Figure 3.12 : FTIR curves of PCL100, PLA100, PLLA100, PLA50PCL50, and PLLA50PCL50 fibrous webs.

In PCL100, PLA50PCL50, and PLLA50PCL50 surfaces, peaks indicating skeletal vibration of CH_2 can be seen at 735 cm^{-1}, but not on the neat PLA100 and PLLA100 surfaces. This scenario is unique to PCL, and it is a peak that can be found in both PCL blends and neat PCL100 (Vilay, Mariatti, Ahmad, Pasomsouk, & Todo, 2010). At wavelengths of 1040 and 1190 cm^{-1}, vibration is detected in all samples, confirming the presence of substantial primary skeletal vibration (Behtaj et al., 2021). Another

notable peak is 1185 cm^{-1}, which corresponds to the axial strain band of the C-O-C bond in the PLLA/PCL blend and behaves similarly to the C-O-C complex of ethers with asymmetric axial deformation. At PCL's peak of 1243 cm^{-1}, the scenario is the same (Almeida, Cristina, Rodrigues, & Jr, 2018). When comparing neat PCL100 to neat PLA100 sample, the peak exhibits in all samples around 2950 cm^{-1} is more apparent in pure PCL. This peak shows the symmetrical stretch of CH_3 in PLA100, whereas it is a vibration that expresses the asymmetrical stretch of CH_2 in PCL100 (Vilay et al., 2010). In the light of these results, it has been proven that the characteristic peaks of neat polymers can be determined and the characteristic peaks of both polymers can be observed in the blend samples. Characteristic peaks of PLA100 and PLLA100 uttermost similar as PLLA is a derivative of PLA; also, the peaks of neat PLLA100 sample meet with the literature outcomes (Haghjooy Javanmard et al., 2016).

FTIR examination, on the other hand, determines the existence of solvent system residues on the surface. The peaks of the primary solvent chloroform, which cause CCl_3 stretch at 680 cm^{-1} and 774 cm^{-1}, and C-H stretch at 3034 cm^{-1} are absent on surfaces (Enis et. al., 2017). Apart from ethanol, which has a C-O stretch of 2055 cm^{-1} and a symmetrical C-H stretch of 2850 cm^{-1}, acetic acid has an O-H vibration of 1292 cm^{-1} and a C-H vibration of 1292 cm^{-1}, which are not detected in any FTIR characterization too (M. A. Hasan, Zaki, & Pasupulety, 2006; Iwasita & Pastor, 1994). The CH_2 stretch at 1363 cm^{-1}, CH_3 stretch at 1427 cm^{-1}, and C=O ketone stretch at 1717 cm^{-1}, which belong to characteristic peaks of acetone that utilised in PLA's solvent system, do not appear in PLA's distinctive peaks (M. Costa, Santos, & Diamantino, 2009).

3.6 Thermal Characterization

3.6.1 DSC analysis

The thermal characterization realized in the final part of the thesis entails detecting the effect of PLLA as well as the blend ratio on the thermal characteristic of the surfaces. The thermal characteristics of the surfaces with different blending ratios are observed under the same heating and cooling conditions.

Figures 3.13 and 3.14 illustrate the behaviour of PLA/PCL blend structures at various ratios, as well as neat PLA100, during heating and cooling; Figures 3.13 and 3.14 show the response of neat PLLA and PLLA/PCL blend structures during heating and cooling. Around 60 °C, PCL100 has a larger and longer curve than the other samples. The reason for this is that PLA, which is in the crystalline phase, is incorporated into the structure while PCL melts (B. Gupta, Geeta, & Ray, 2012).

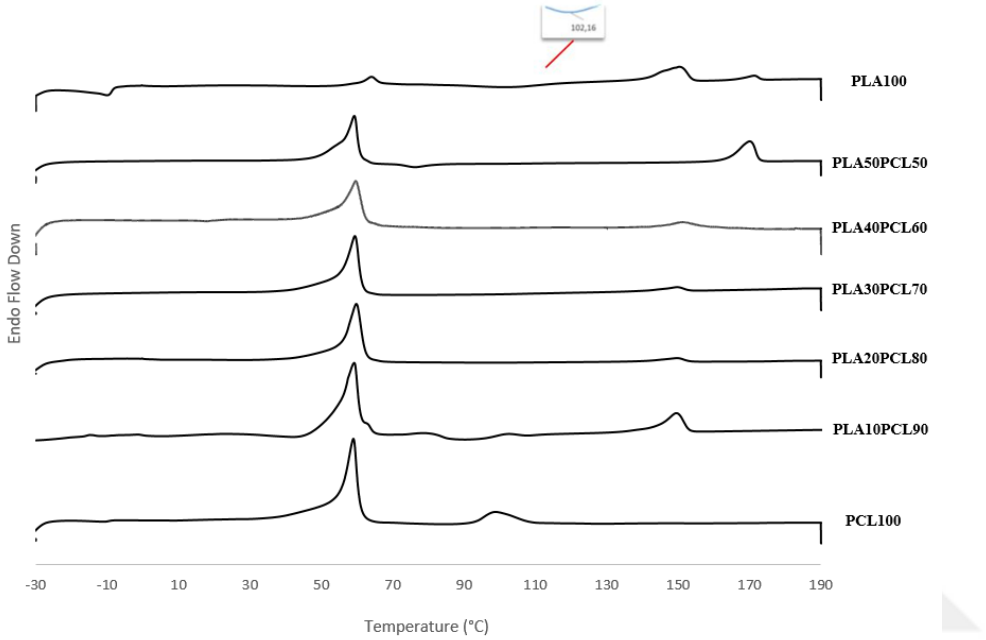

Figure 3.13 : DSC curves of PLA100, PCL100, and PLA/PCL blends at heating stage.

A polymer can melt only if it has a semi-crystalline structure, otherwise (if it is amorphous) it will not exhibit melting behaviour (Nofar, Sacligil, Carreau, Kamal, & Heuzey, 2019). Since all samples in the graph have melting properties, the polymers used in the study can be defined as semi-crystalline. Commercially used PLAs are considered amorphous only if their D-lactide content is greater than 10%. The ratio of D-lactide in the structure of PLA used within the scope of the study is 4.3%, and this ratio supports the semi-crystalline structure of the polymer (Nofar et al., 2019). As shown in the data, semi-crystalline PLA undergoes exothermic cold crystallization at around 102 °C (shown at higher magnification in Figure 3.13) and endothermic melting crystallization at around 150 °C, with a Tg value of 64 °C. The thermal characterization results of PLA published in the literature are likewise consistent with these findings (Q. Lv et al., 2016) as well as the second investigation results. Melt crystallization (T_c) occurs only in PLA100 and PLA50PCL50 samples during cooling;

moreover, PLA100's melt crystallization peak (around 107 °C) is shown at higher magnification as it is relatively small and not visible on the curve like heating section. This crystallization peak begins to diminish when the PCL ratio in the structure increases. On the other hand, the melting crystallization enthalpy curve of PCL begins to get smaller when the ratio of PLA which has a lower crystallinity in the PLA/PCL blends increases. Luyt and Gasmi (2016) investigated the thermal characteristics and crystallization behaviour of the PLA/PCL blend and stated similar findings. During heating, molten PCL affects the crystal formation of PLA, increasing its mobility and causing crystalline rearrangement (Luyt & Gasmi, 2016).

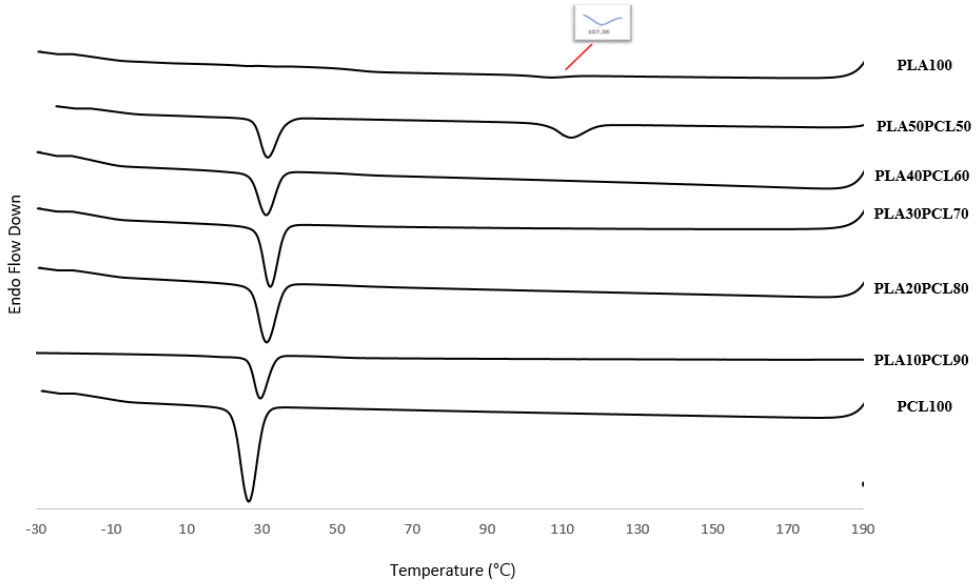

Figure 3.14 : DSC curves of PLA100, PCL100, and PLA/PCL blends at cooling.

Furthermore, the inclusion of PLA to the PCL structure results in the formation of a crystallization peak in the PLA50PCL50 sample, while having little effect on the melting temperature of PCL. This is because solid PLA particles act as an additional active substrate, promoting the structure's crystallization (D. Wu et al., 2011). However, the findings show that the structure must contain at least 50% PLA in order to demonstrate this activity. When Table 3.9 is reviewed, it is seen that PCL100 has higher crystallinity (37.32%) than PLA100 (17.85%), and that the crystallinity ratio rises as PCL in the blend structures increases. According to the DSC results of the second part of the study, higher crystallinity values can be seen for both neat PCL and PLA, which are 56.7% and 21.5%, respectively. It is thought that the the DSC analysis of the second part of the study is carried out a few months after the samples are

produced, and the amorphous regions in the structure are degraded, so the crystal regions have a higher percentage in the structure. In the third part of the study, the DSC analysis is performed shortly after production (comparably shorter than the second one), so the amorphous regions are not that much degraded and appear less in percentage.

Table 3.9: DSC analysis of the samples during heating.

Sample	PCL melting crystallization		PLA/PLLA cold crystallization[1]		PLA/PLLA melting crystallization[1]		X_c (%)	
	T_m	ΔH_m	T_{cc}	ΔH_{cc}	T_m	ΔH_m	PLA/PLLA	PCL
PLA	-	-	102.16	-3.28	151.58	19.88	17.85	-
PLA10PCL90	59.20	48.45	-	-	150.50	5.64	3.03	17.81
PLA20PCL80	60.55	40.28	-	-	149.79	2.34	1.26	14.81
PLA30PCL70	59.83	30.11	-	-	149.80	2.73	1.47	11.07
PLA40PCL60	60.02	25.01	-	-	151.46	5.00	2.69	9.19
PLA50PCL50	59.73	22.80	90.42	-2.23	151.31	9.93	4.14	8.38
PLLA	-	-	80.66	-20.75	143.70	65.48	48.10	-
PLLA10PCL90	60.16	72.43	-	-	171.00	10.85	5.83	26.63
PLLA20PCL80	60.10	54.27	-	-	171.16	11.56	6.22	19.95
PLLA30PCL70	59.69	46.57	-	-	170.93	16.04	8.62	17.12
PLLA40PCL60	58.97	37.13	79.67	-1.01	169.94	18.26	9.27	13.65
PLLA50PCL50	59.58	35.77	77.89	-2.88	170.51	26.82	12.87	13.15
PCL	59.03	50.75	-	-	-	-	-	37.32

Figures 3.15 and 3.16 show the attitude of PLLA and its blends during heating and cooling. PLA's crystallinity and melting temperature both increase as the ratio of D-lactide in the structure decreases, since more tightly packed structures improve molecular symmetry, which improves crystal formation. Furthermore, PLLA100 has

[1] Since PLLA is a derivative of PLA, the cold crystallization (Tcc), melt crystallization (Tm) and crystallinity (Xc) values of PLLA are given in the same column as PLA.

a highest crystallinity among other surfaces. As a result, the T_m of PLLA100 and its blends is around 170 °C, which is higher than PLA100 and its blends, as shown in Table 3.9. It can be said that the D-lactide content in PLA is 4,3% and the melting temperature is around 150-155 °C, and these findings are in line with the literature (Saeidlou, Huneault, Li, & Park, 2012).

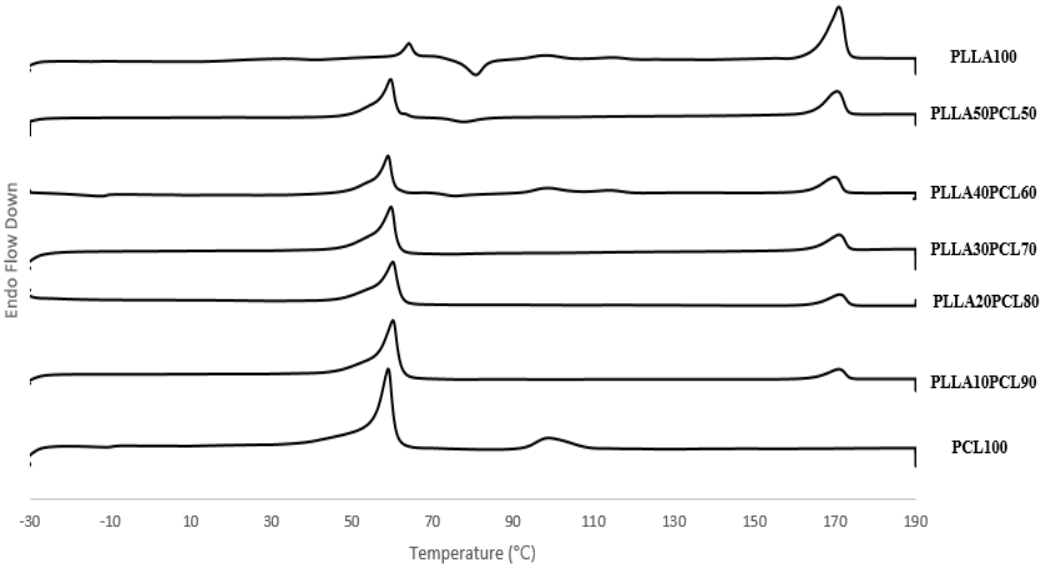

Figure 3.15 : DSC curves of PLLA100, PCL100, and PLLA/PCL blends at heating stage.

In comparison to PLA100, the proportion of crystallinity in PLLA100 is quite high. The consequences of incorporating PLLA into the structure are comparable to those of introducing PLA. For example, with increasing PLLA ratio, an increase in ΔH_{cc} and ΔH_m data is observed; moreover, a similar situation is also encountered in the DSC analysis of Can et. al.'s study (2011) in which PLLA/PCL (90/10, 80/20, 70/30) surfaces were produced at various blend ratios (Can, Udenir, Kanneci, Kose, & Bucak, 2011). Furthermore, despite the presence of multiple distinct peaks, the T_g values of PLA and PLLA are not discernable in the thermal examination of PLA/PCL and PLLA/PCL surfaces. It is thought that the reason of this situation is the melting behavior of the PCL at that temperature (Patrício et al., 2014).

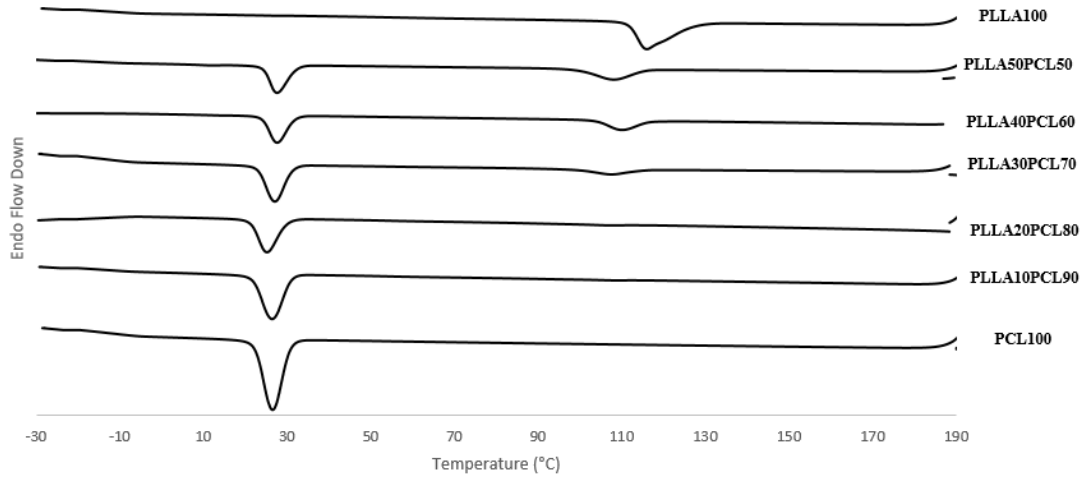

Figure 3.16 : DSC curves of PLLA100, PCL100. and PLLA/PCL blends at cooling stage.

3.7 Biodegradability Analysis

One of the reasons for using blended versions of the polymers as well as their neat forms in the thesis is to improve the surface degradation. Blending biodegradable polymers is a technique for changing desirable characteristics and adjusting degradability rates (Tokiwa, Calabia, Ugwu, & Aiba, 2009). Biodegradation rate is also one of the most essential parameters for generating surfaces suitable for the characteristic layer topologies of blood vessels.

Biodegration rates of the samples studied in this thesis are listed in Table 3.10.

Table 3.10: Degredation rates (%) of the samples from 1 to month 5

	1st Month	3rd Month	5th Month
PLA100	0.00	14.29	40.00
PCL100	0.00	2.17	3.70
PLA20PCL80	2.04	5.66	4.62
PLA50PCL50	0.00	5.00	13.33
PLLA20PCL80	2.86	5.56	8.82
PLLA50PCL50	0.00	3.85	7.69

The biodegradability test results prove the different biodegradability rates of the polymers used in the thesis. The biodegradation of PLA starts at the 3rd month (14.29 %) and is quite fast compare to PCL (2.17 %); furthermore, PLA degrades in the rate

of 40 % at the end of the 5th month while PCL reaches maximum 3.70 %. The biodegradation characteristics of PLA is also supported by litetarture (Nofar et al., 2019). When blends are evaluated, it is seen that the biodegradability rate of PCL increases by 4.62% with the addition of 20% PLA; when the PLA rate reaches 50%, this value increases and reaches 13.33%. Thus it can be said that 50% PLA in the 5th month considerably increases the degradation of the structure. This is thought to be due to the fact that PLA has more amorphous regions in its structure compared to PCL, as seen in the DSC analysis (Table 3.9). PLLA specimens could not be tested as it was not possible to obtain a specimen that retained its integrity to allow testing. However, PLLA blends have been tested for biodegradability. Although a clear effect of the percentage of PLLA on the rate of biodegradation has not been understood, it can be concluded that the addition of 20-50% of PLLA accelerates the rate of biodegradation of PCL. When PLA and PLLA are compared with each other, it can be seen that PLLA with a higher crystallinity (48.10%) has a slower degradation rate.

The unexpected degradation results that belong to PLA20PCL80 may be resulted from the accuracy of the measurements, as well as submitting the samples to various processes such as sterilizing and drying. The biodegradation processes of the surfaces continue within the scope of the study and it will be possible to make clearer inferences from the data that will be completed at the end of the 12-month period. On the other hand, hydrolytic degradation has been applied to surfaces, but when polymeric surfaces are subjected to enzymatic degradation, it may give different results than hydrolysis (Vieira et al., 2011). As a result, enzymatic degradation could be one of the research subjects in the future.

3.8 Biological Analysis

3.8.1 Cell proliferation (MTS) analysis

In cell seeding experiments with the scope of thesis, the control sample's cell proliferation value is set to 100, and the proliferation rates of the surfaces are compared accordingly (Figure 3.17 and Figure 3.18). When fibroblast cell proliferation values are investigated, it is clear that cell viability has improved on all surfaces since the 3rd day, and cell activation has increased on the 7th day compared to the 3rd day. The PLA ratio in the structure appears to boost cell survival by up to 20%, with the PLA20PCL80 surface having the highest proliferation value. However, if the PLA

ratio in the structure exceeds 20%, the viability values on the 3rd and 7th days are considered to be significantly impacted. PLA promotes cellular activity to a degree, but at high levels, it stiffens the structure, making cell attachment more difficult (Saunders & Hammer, 2010). On the other hand, the fact that the cells have more proliferation on fibrous surfaces compared to control samples with low surface area is an indication of the advantage that high surface area provides for cell activities (Park et al., 2007). PLLA20PCL80 and PLLA50PCL50 structures, on the other hand, exhibit behaviour similar to PLA/PCL blend surfaces. In a study by Sankaran et al. (2014), PLA and PCL were physically blended at 25/75 and 75/25 ratios, HUVEC was seeded on the surfaces, and MTS analysis was performed on the 1st, 3rd, and 7th days. Results exhibited that on the 1st day, there was little difference in cell proliferations compared to the control sample, but on the 3rd and 7th days, there was a significant increase; additionally, the cell proliferation of the surface with the ratio PLA/PCL (25/75) is relatively higher than that of PLA/PCL (75/25) due to the stiff structure of PLA (Sankaran, Krishnan, & Sethuraman, 2014).

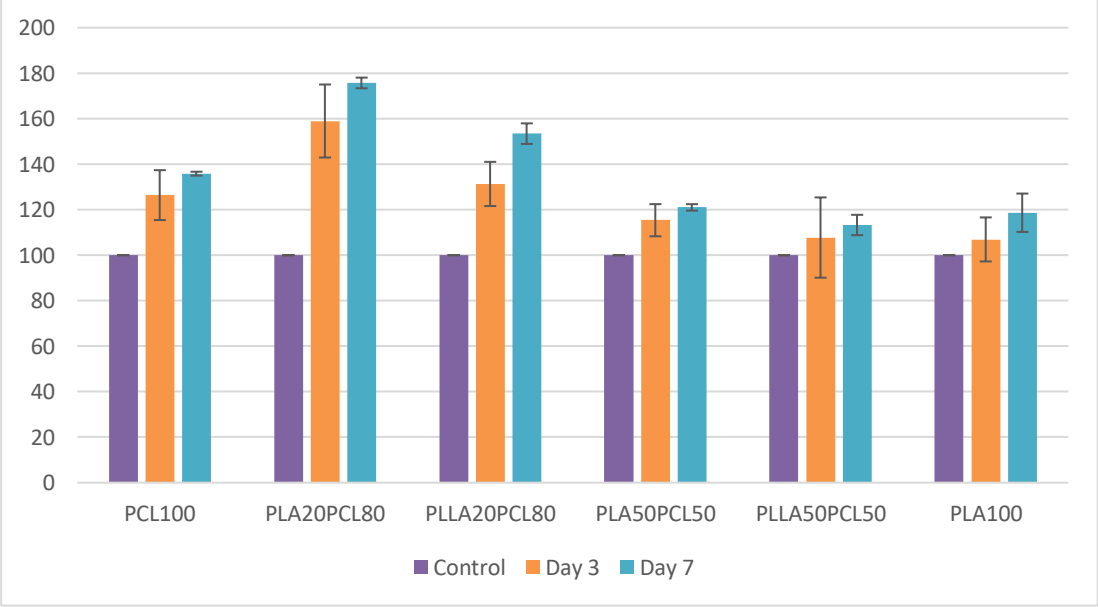

Figure 3.17 : MTS analysis of the surfaces cultured with fibroblast cells on 3rd and 7th days.

Similarly, while 20% PLLA supports the structure's cellular activity, increasing the rate to 50% has a negative impact on the situation. In a tissue engineering study conducted by Sadiasa et al. (2014), porous surfaces were created by pure leaching method using PCL/PLLA at different ratios (100/0, 90/10, 80/20 and 70/30). In both *in-vitro* and *in-vivo* cellular studies, it was determined that cell activities were higher

on blended surfaces. The output of this study is that PLLA, which increases the ratio of large pores on the surface, improves biocompatibility and bioactivity (Sadiasa, Nguyen, & Lee, 2014). Furthermore, the fact that PLLA/PCL blend structures have less cell proliferation than PLA/PCL blend structures could be due to PLLA having a more crystalline character than PLA resulting in undesired stiffer structures that limits cell activities.

The HUVECs exhibit similar cell activity likewise fibroblast cells on surfaces. According to the data obtained from MTS analysis (Figure 3.18), HUVECs grown on PLA20PCL80 has the highest cell proliferation value, and an increase in PLA ratio to 50% reduces cell proliferation from 137.4 to 106.9 on day 3 and from 168.3 to 114.7 on day 7. While cell viability decreased on the 3rd day compared to the control cells on PLLA20PCL80 and PLLA50PCL50, cell activities are regained on the 7th day.

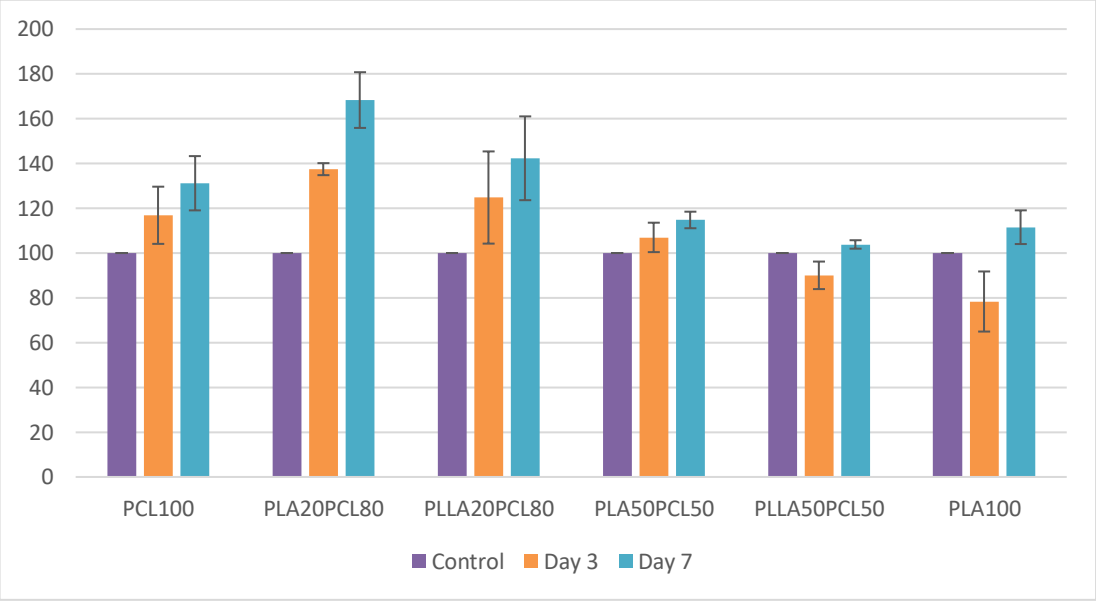

Figure 3.18 : MTS analysis of the surfaces cultured with HUVECs on 3rd and 7th days.

When the findings are evaluated from both cell lines, it can be clearly noticed that neat polymer surfaces (PLA100 and PCL100) have lower cellular activity than blend structures. Although cell viability varies according to the blending ratio, it is concluded that blend structures improve the proliferation of cells in any case. In a study by Herrero-Herrero et al. (2021), surfaces with the same fiber diameters were created from PLA, PCL and PLA/PCL blend, and the cellular activities of surfaces cultured with adipose tissue-derived mesenchymal stem cells (ASCs) were investigated. The cellular activity on the PLA/PCL surface is found to be quite high when compared to

pure PLA and PCL surfaces due to the strong synergistic effect of PLA and PCL (María Herrero-Herrero et al., 2021). Besides, various researchers have also discussed the strengths of PLA and PCL's synergistic effects (H. N. Kim et al., 2012; Z. Lv, Zhao, Wu, Zhu, & Li, 2018). In addition to biological features, the mechanical characteristics of the surfaces are considerably affected and improved by this synergetic impact too (Fortelny, Ujcic, Fambri, & Slouf, 2019). Scaffolds with greater mechanical properties help boost cell proliferation by allowing for better oxygen/nutrient exchange (Xu et al., 2018).

On the other hand, the survival rate of the fibroblast cell type is observed to be higher on all surfaces compared to HUVECs. This situation can be associated with the structures of the cells. Because HUVECs have a round shape while fibroblast cells have a more elongated shape, fibroblasts are easier to settle and attach to the surface pores (Biela, Su, Spatz, & Kemkemer, 2009). Briefly, both fibroblast cells and HUVECs can live and proliferate on the electrospun surfaces produced with the scope of this thesis; moreover, the proliferation rate increases from day 3 to day 7. Although many factors have an effect on the success rate of vascular graft surfaces, the viability of cells on surfaces is a promising indicator. Hence, it can be said that produced surfaces can be the effective candidates for vascular graft surface developments. In the light of this assessment, the cell proliferation data will be a step towards to *in-vivo* analysis.

4. CONCLUSIONS AND RECOMMENDATIONS

This thesis is composed of three supplementary studies. All these studies contribute to the knowledge with an innovative perspective by presenting new ideas for evaluating design criteria, developing suitable surfaces for vascular grafts, and researching and eliminating the shortcomings of the literature. In this context, the findings obtained during the study process are summarized.

The initial study focused on surface production utilizing PCL (45,000 Mn), PLA, and PLA/PCL (25/75 and 75/25), with an emphasis on optimizing production parameters

- Although three different polymer concentrations (16. 18. 20%) are used for PCL (45.000Mn) for CHL/ETH (9/1 wt.) solution. none of the samples are consisted of continuous and beadless fibers. Thus. PCL (45.000Mn) is excluded from the studies within the scope of the thesis and it has been decided to continue using PCL with a molecular weight of 80.000 Mw.
- Fiber formation with a diameter of approximately 1.6 μm and moisture-induced structural pores have been reported in PLA100_7, PLA100_8 and PLA100_9. Since the concentration values used for PLA are close to each other, the effects of the concentration on the surface cannot be discussed efficiently. Therefore, in order to determine the optimum polymer concentration, it is decided to prepare PLA-based polymer solutions with a wider concentration range.
- Surface productions are successfully obtained from PLA/PCL blends at 12% polymer concentration and under varying blend ratios. The average fiber diameters for the PLA75PCL25_12 and PLA50PCL50_12 sample groups are 2,071 μm and 1,860 μm, respectively. Although the desired fiber production could not be obtained from PCL polymer alone, it is observed that continuous and beadfree surfaces could be obtained when used in mixture with PLA, and it is thought that the optimizations of these blends will provide important findings for future studies.

The second investigation aims to optimize the manufacturing parameters of PLA, PCL (80,000Mn) and PLA/PCL (50/50) structures. All polymer solutions are kept at a constant concentration of 6%, 8%, and 10% for the period of this experimental part.

- Since 6% polymer concentration could not provide sufficient solution viscosity for all neat polymers and their blends produced, bead formation is observed on all fibrous surfaces (PLA100, PCL100 and PLA50PCL50).
- With increasing polymer concentration, smooth fibers with average fiber diameters of 1.390 μm and 1.792 are obtained in PCL100_8 and PCL100_10; 1.483 μm and 1.798 μm were obtained in PLA100_8 and PLA100_10; and 1.687 μm and 2.127 μm were achieved in PLA50PCL50_8 and PLA50PCL _10 samples, respectively. Optimum polymer concentration is determined as 8% for all sample groups.
- The results of the porosity investigation are likewise consistent with the fiber diameter measurements. PLA100_8 and PLA50PCL50_8, the surfaces with the smallest fiber diameter, also have the highest porosity (21.92% and 21.63%, respectively).
- WCA measurements for all sample groups yielded results above 100°, confirming that all surfaces are hydrophobic. In addition, it is concluded that the polymer concentration had no effect on the water absorbency character of the surfaces.
- DSC analysis performed to observe the behaviour of surfaces during heating and cooling and to calculate their crystallinity gives results consistent with the literature. In this context, the crystallinity of PLA100 is 21.5% and that of PCL100 is 56.7%. In PLA50PCL50 blend structure, PLA crystallinity is 5.7% and PCL crystallinity is 14%. The 50% incorporation of PLA into the PCL structure leads to a rather large decrease in the crystallinity of the PCL. Moreover, since the PLA in the blend acts as an additional active substrate, PCL melts in PLA50PCL50 at 59.2°C while neat PCL melts at 55.8°C.

In the third and last part of the study, in addition to PLA and PCL, PLLA polymer is also included in the production plan. A detailed study is carried out on PLA/PCL and PLLA/PCL blends by determining PCL as the main polymer. The polymer concentration is kept constant as 8% for all samples, and the effect of blend ratios on the final properties is focused.

- On all surfaces except PLLA40PCL60, PLLA50PCL50 and PLLA100 uniform fiber formation is achieved. It is thought that the reason for the incomplete fiber formation on these surfaces is the polymer viscosity that decreases with the increase in the ratio of low molecular weight PLLA.
- Fiber diameter measurements revealed that as the fraction of high molecular weight polymer in the blend ratio increases, fiber diameter increases. In PLA/PCL blends, the fiber diameter decreases from 0.962 μm to 1.417 μm (from PLA10PCL90 to PLA50PCL50) as the PLA increases in the structure, but this is different for PLLAPCL-based substrates because the molecular weight of PLLA is greater than PCL. Hence, the fiber diameter decreases from PLLA10PCL90 to PLLA50PCL50 (from 1.597 μm to 0.596 μm).
- Mean fiber diameters and porosity correlate similarly to the second part of the study, and porosity increases as fiber diameter decreases. PLA10PCL90, the surface with the lowest fiber diameter in this investigation (bead-free surfaces), has the maximum porosity of 29.54 %. However, one aspect should be noted: the porosity analysis is carried out using the Image J software system, which assesses the porosity of the surfaces in two dimensions. Therefore, it cannot be argued that it produces totally accurate results, although it does provide enough information to make basic comparisons.
- WCA analysis results confirmed the conclusion that all surfaces containing PLA, PLLA and PCL are hydrophobic. However, it is observed that PLA100 had a larger water contact angle value than PCL100, and this is explained by the chemical structure of the polymers. There are no hydrophilic functional groups in the carbon backbones of PCL. PLA has a higher hydrophilicity than PCL, which contains only a single carbonyl group and deprotonates the carboxyl groups in an aqueous medium due to the presence of a carboxyl group.
- FTIR analysis shows characteristic peaks of both PLA100, PLLA100, and PCL100 as well as all polymers on PLA/PCL and PLLA/PCL-based substrates. For example, the skeletal vibration of CH_2 seen in PCL100 at 735 cm^{-1} is invisible in PLA100 and PLLA100, but is clearly noticeable in PLA50PCL50 and PLLA50PCL50. In addition to the chemical characteristics of the polymers, this

analysis is performed to determine whether there is any solution left on the surface and it is seen that there is no residue of any solvent on any surface.

- DSC analysis indicates that the thermal properties of both constituent polymers are visible on blended surfaces. On PLA/PCL surfaces, there are melting peaks of PCL at roughly 60 °C, although the melting curve of PLA is at 150 °C. The same is true for surfaces made of PLLA/PCL. PCL crystallization increases as the ratio of PCL on PLA/PCL and PLLA/PCL based surfaces increases, while PLA and PLLA crystallization decreases. On the other hand, PLLA has the highest crystallinity ratio among all surfaces; this structure of PLLA is frequently mentioned in the literature.
- Biodegradability study is conducted on PLA100, PCL100, PLA20PCL80, PLA50PCL50, PLLA20PCL80, and PLLA50PCL50 samples at 1st, 3rd, and 5th months. With the exception of PLA20PCL80, all samples demonstrate an increase in degradation rate over time; moreover, this is assumed to be due to measurement precision in PLA20PCL80. The degradation rate of PLA (14.29% and 40%, respectively) at the end of the 3rd and 5th months is significantly higher than that of PCL (2.17% and 3.70%, respectively), as expected and as found in the literature research. On the other hand, it has been observed that 50% PLA ratio in the blend significantly increases surface weight loss. Furthermore, similar to PLA, the addition of PLLA to surfaces accelerates the biodegradation rate.
- The biological part of the study includes MTS cell culturing analysis with both fibroblast cells and HUVECs. Results show that on the 7th day of culturing, there is an increase in cell proliferation for all surfaces for both cell types. Moreover, the highest amount of cells for both cell types is seen on PLA20PCL80 sample on both days 3 and 7, while the rate of cell proliferation is found to decrease with increasing PLA ratio. Although PLA and PCL together provide a synergistic effect on surfaces, it has been observed that high amount of PLA hardens the structure and makes cell proliferation difficult. It is clear that all samples developed within the scope of this thesis are suitable candidates for vascular grafts despite the differences in cell proliferation values.

In summary, within the scope of the thesis, very detailed studies have been carried out, from material selection to production method, from the morphological, chemical and

thermal properties of the surfaces to their biological behavior in order to produce surfaces for vascular grafts. Accordingly, although it is concluded that the surfaces produced with PLA, PLLA and PCL are all good candidates for a microenvironment where cells can live and form their own ECMs for vascular graft designs, some samples have succeeded in coming to the fore with the advantages they offer. In this respect, PLA20PCL80 sample, in which PCL with high molecular weight (80,000Mn) is determined as the main polymer and containing 20% PLA addition, is found to be a candidate to be a preferred surface in vascular grafts when its homogeneous fiber distribution, stable production results and desired cellular analyses data were evaluated. Of course, the results need to be supported by mechanical and advanced cellular analysis. On the other hand, it is obvious that the detailed analysis results and comparisons obtained in the path spent until this final polymer selection will make an innovative contribution to the literature.

The research carried out within the scope of this thesis is part of a long-term project. Future studies will continue with the support of TUBITAK Project no 121M309. In this context, within the scope of future studies, it is foreseen that biodegradability tests will be followed for 12 months and even alternative methods will be tried. Comprehensive mechanical analyzes will be performed with the fabrication of tubular scaffolds from optimized solutions and the construction of layered vascular grafts. It is expected that the outputs of the project, whose preliminary studies have been carried out within the scope of this thesis and will be concluded with *in-vivo* studies, will lead to promising developments for small-caliber vessel grafts.

REFERENCES

Abdal-hay, A., Bartnikowski, M., Hamlet, S., & Ivanovski, S. (2018). Electrospun biphasic tubular scaffold with enhanced mechanical properties for vascular tissue engineering. *Materials Science and Engineering C*, *82*(July 2017), 10–18. https://doi.org/10.1016/j.msec.2017.08.041

Abruzzo, A., Fiorica, C., Palumbo, V. D., Altomare, R., Damiano, G., Gioviale, M. C., Lo Monte, A. I. (2014). Using polymeric scaffolds for vascular tissue engineering. *International Journal of Polymer Science*, *2014*. https://doi.org/10.1155/2014/689390

Adhikari, K. R., Tucker, B. S., & Thomas, V. (2019). Tissue engineering of small-diameter vascular grafts. *Biointegration of Medical Implant Materials*, *1957*, 79–100. https://doi.org/10.1016/B978-0-08-102680-9.00004-4

Agarwal, R., Blum, K. M., Musgrave, A., Onwuka, E. A., Yi, T., Reinhardt, J. W., Breuer, C. K. (2019). Degradation and in vivo evaluation of polycaprolactone, poly(ϵ-caprolactone-co-L-lactide), and poly-L-lactic acid as scaffold sealant polymers for murine tissue-engineered vascular grafts. *Regenerative Medicine*, *14*(7), 627–637. https://doi.org/10.2217/rme-2018-0069

Ahmed, F. E., Lalia, B. S., & Hashaikeh, R. (2015). A review on electrospinning for membrane fabrication: Challenges and applications. *Desalination*, *356*, 15–30. https://doi.org/10.1016/j.desal.2014.09.033

Aibibu, D., Hild, M., Wöltje, M., & Cherif, C. (2016). Textile cell-free scaffolds for in situ tissue engineering applications. *Journal of Materials Science: Materials in Medicine*, *27*(3), 1–20. https://doi.org/10.1007/s10856-015-5656-3

Akentjew, T. L., Terraza, C., Suazo, C., Maksimuck, J., Wilkens, C. A., Vargas, F., … Acevedo, J. P. (2019). Rapid fabrication of reinforced and cell-laden vascular grafts structurally inspired by human coronary arteries. *Nature Communications*, *10*(1), 1–15. https://doi.org/10.1038/s41467-019-11090-3

Amirian, J., Sultana, T., Joo, G. J., Park, C., & Lee, B. T. (2020). In vitro endothelial differentiation evaluation on polycaprolactone-methoxy polyethylene glycol electrospun membrane and fabrication of multilayered small-diameter hybrid vascular graft. *Journal of Biomaterials Applications*, *34*(10), 1395–1408. https://doi.org/10.1177/0885328220907775

Angel, N., Guo, L., Yan, F., Wang, H., & Kong, L. (2020). Effect of processing parameters on the electrospinning of cellulose acetate studied by response surface methodology. *Journal of Agriculture and Food Research*, *2*(November 2019), 100015. https://doi.org/10.1016/j.jafr.2019.100015

Antonova, L. V, Sevostyanova, V. V, Mironov, A. V, Krivkina, E. O., Velikanova, E. A., Matveeva, V. G., Barbarash, L. S. (2018). *EDITORIAL IN SITU VASCULAR*

TISSUE REMODELING USING BIODEGRADABLE TUBULAR SCAFFOLDS WITH INCORPORATED GROWTH FACTORS AND Methods. 25–36. https://doi.org/10.17802/2306-1278-2018-7-2-25-36

Areias, A. C., Ribeiro, C., Sencadas, V., Garcia-Giralt, N., Diez-Perez, A., Gómez Ribelles, J. L., & Lanceros-Méndez, S. (2012). Influence of crystallinity and fiber orientation on hydrophobicity and biological response of poly(l-lactide) electrospun mats. *Soft Matter*, *8*(21), 5818–5825. https://doi.org/10.1039/c2sm25557j

Asmatulu, R., & Khan, W. S. (Eds.). (2018). *Synthesis and Applications of Electrospun Nanofibers*. Elsevier. https://doi.org/10.1016/b978-0-12-813914-1.00014-6

Astete, C. E., & Sabliov, C. M. (2012). *Synthesis and characterization of PLGA nanoparticles*. *5063*. https://doi.org/10.1163/156856206775997322

Bakar, S. S. S., Fong, K. C., Eleyas, A., & Nazeri, M. F. M. (2018). Effect of Voltage and Flow Rate Electrospinning Parameters on Polyacrylonitrile Electrospun Fibers. *IOP Conference Series: Materials Science and Engineering*, *318*(1). https://doi.org/10.1088/1757-899X/318/1/012076

Barthes, J., Özçelik, H., Hindié, M., Ndreu-Halili, A., Hasan, A., & Vrana, N. E. (2014). Cell Microenvironment Engineering and Monitoring for Tissue Engineering and Regenerative Medicine: The Recent Advances. *BioMed Research International*, *2014*(i). https://doi.org/10.1155/2014/921905

Bartnikowski, M., Dargaville, T. R., Ivanovski, S., & Hutmacher, D. W. (2019). Degradation mechanisms of polycaprolactone in the context of chemistry, geometry and environment. *Progress in Polymer Science*, *96*, 1–20. https://doi.org/10.1016/j.progpolymsci.2019.05.004

Belleghem, S. M. Van, Mahadik, B., Snodderly, K. L., & Fisher, J. P. (2020). Overview of Tissue Engineering Concepts and Applications. In *Biomaterials Science* (Fourth Edi). Elsevier. https://doi.org/10.1016/b978-0-12-816137-1.00081-7

Bhardwaj, N., & Kundu, S. C. (2010). Electrospinning: A fascinating fiber fabrication technique. *Biotechnology Advances*, *28*(3), 325–347. https://doi.org/10.1016/j.biotechadv.2010.01.004

Bos, G. W., Poot, A. A., Beugeling, T., Van Aken, W. G., & Feijen, J. (1998). Small-diameter vascular graft prostheses: Current status. *Archives of Physiology and Biochemistry*, *106*(2), 100–115. https://doi.org/10.1076/apab.106.2.100.4384

Braghirolli, D. I., Helfer, V. E., Chagastelles, P. C., Dalberto, T. P., Gamba, D., & Pranke, P. (2017). Electrospun Scaffolds Functionalized with Heparin and VEGF Increase the Proliferation of Endothelial Progenitor Cells. *Biomedical Materials*, *12*(2). https://doi.org/https://doi.org/10.1088/1748-605x/aa5bbc

Casasola, R., Thomas, N. L., Trybala, A., & Georgiadou, S. (2014). Electrospun poly lactic acid (PLA) fi bres : Effect of different solvent systems on fi bre morphology and diameter. *Polymer*, *55*(18), 4728–4737. https://doi.org/10.1016/j.polymer.2014.06.032

Catto, V., Farè, S., Cattaneo, I., Figliuzzi, M., Alessandrino, A., Freddi, G., … Tanzi, M. C. (2015). Small diameter electrospun silk fibroin vascular grafts: Mechanical properties, in vitro biodegradability, and in vivo biocompatibility. *Materials*

Science and Engineering C, *54*, 101–111. https://doi.org/10.1016/j.msec.2015.05.003

Chan, A. H. P., Filipe, E. C., Tan, R. P., Santos, M., Yang, N., Hung, J., Wise, S. G. (2019). Altered processing enhances the efficacy of small-diameter silk fibroin vascular grafts. *Scientific Reports*, *9*(1), 1–14. https://doi.org/10.1038/s41598-019-53972-y

Chandra, P. K., Soker, S., & Atala, A. (2020). Tissue engineering: current status and future perspectives. In *Principles of Tissue Engineering*. INC. https://doi.org/10.1016/b978-0-12-818422-6.00004-6

Chaudhari, A. A., Vig, K., Baganizi, D. R., Sahu, R., Dixit, S., Dennis, V., … Pillai, S. R. (2016). Future prospects for scaffolding methods and biomaterials in skin tissue engineering: A review. *International Journal of Molecular Sciences*, *17*(12). https://doi.org/10.3390/ijms17121974

Chesterman, J., Zhang, Z., Ortiz, O., Goyal, R., & Kohn, J. (2020). Biodegradable polymers. In *Supramolecular Design for Biological Applications*. INC. https://doi.org/https://doi.org/10.1016/B978-0-12-818422-6.00019-8

Cheung, H. Y., Lau, K. T., Lu, T. P., & Hui, D. (2007). A critical review on polymer-based bio-engineered materials for scaffold development. *Composites Part B: Engineering*, *38*(3), 291–300. https://doi.org/10.1016/j.compositesb.2006.06.014

Copes, F., Pien, N., Van Vlierberghe, S., Boccafoschi, F., & Mantovani, D. (2019). Collagen-based tissue engineering strategies for vascular medicine. *Frontiers in Bioengineering and Biotechnology*, *7*(JUL), 1–15. https://doi.org/10.3389/fbioe.2019.00166

Costa, L. M. M., Bretas, R. E. S., & Gregorio, R. (2010). Effect of Solution Concentration on the Electrospray/Electrospinning Transition and on the Crystalline Phase of PVDF. *Materials Sciences and Applications*, *01*(04), 247–252. https://doi.org/10.4236/msa.2010.14036

De Pieri, A., Rochev, Y., & Zeugolis, D. I. (2021). Scaffold-free cell-based tissue engineering therapies: advances, shortfalls and forecast. *Npj Regenerative Medicine*, *6*(1). https://doi.org/10.1038/s41536-021-00133-3

De Valence, S., Tille, J. C., Giliberto, J. P., Mrowczynski, W., Gurny, R., Walpoth, B. H., & Möller, M. (2012). Advantages of bilayered vascular grafts for surgical applicability and tissue regeneration. *Acta Biomaterialia*, *8*(11), 3914–3920. https://doi.org/10.1016/j.actbio.2012.06.035

Dehnavi, N., Parivar, K., Goodarzi, V., Salimi, A., & Nourani, M. R. (2019). Systematically engineered electrospun conduit based on PGA/collagen/bioglass nanocomposites: The evaluation of morphological, mechanical, and bio-properties. *Polymers for Advanced Technologies*, *30*(9), 2192–2206. https://doi.org/10.1002/pat.4648

Deitzel, J. M., Kleinmeyer, J., Harris, D., & Beck Tan, N. C. (2001). The effect of processing variables on the morphology of electrospun. *Polymer*, *42*, 261–272.

Deshmukh, K., Basheer Ahamed, M., Deshmukh, R. R., Khadheer Pasha, S. K., Bhagat, P. R., & Chidambaram, K. (2017). Biopolymer Composites with High Dielectric Performance: Interface Engineering. In *Biopolymer Composites in Electronics*. Elsevier Inc. https://doi.org/10.1016/B978-0-12-809261-3.00003-6

Devan Ohst, J. J. (2015). Development of Novel, Bioresorbable, Small-Diameter Electrospun Vascular Grafts. *Journal of Tissue Science & Engineering*, *06*(02). https://doi.org/10.4172/2157-7552.1000151

Di Lorenzo, M. L. (2006). Calorimetric analysis of the multiple melting behavior of poly(L-lactic acid). *Journal of Applied Polymer Science*, *100*(4), 3145–3151. https://doi.org/10.1002/app.23136

Donovan, D. L., Schmidt, S. P., Townshend, S. P., Njus, G. O., & Sharp, W. V. (1990). Material and structural characterization of human saphenous vein. *Journal of Vascular Surgery*, *12*(5), 531–537. https://doi.org/10.1016/0741-5214(90)90005-U

Dziki, J. L., Huleihel, L., Scarritt, M. E., & Badylak, S. F. (2017). Extracellular Matrix Bioscaffolds as Immunomodulatory Biomaterials. *Tissue Engineering - Part A*, *23*(19–20), 1152–1159. https://doi.org/10.1089/ten.tea.2016.0538

Enis, Ipek Y., Vojtech, J., & Sadikoglu, T. G. (2017). Alternative solvent systems for polycaprolactone nanowebs via electrospinning. *Journal of Industrial Textiles*, *47*(1), 57–70. https://doi.org/10.1177/1528083716634032

Enis, Ipek Yalcin, Sadikoglu, T. G., Horakova, J., & Lukas, D. (2018). The post-morphological analysis of electrospun vascular grafts following mechanical testing. *Journal of Polymer Engineering*, *38*(6), 525–535. https://doi.org/10.1515/polyeng-2017-0157

Eschenhagen, T., Reichenspurner, H., & Zimmermann, W. H. (2013). Tissue-Engineered Cardiovascular Products. In *Principles of Tissue Engineering: Fourth Edition* (Fourth Edi). Elsevier. https://doi.org/10.1016/B978-0-12-398358-9.00084-7

Feng, K., Huang, R. meng, Wu, R. qing, Wei, Y. shan, Zong, M. hua, Linhardt, R. J., & Wu, H. (2020). A novel route for double-layered encapsulation of probiotics with improved viability under adverse conditions. *Food Chemistry*, *310*(December 2019), 125977. https://doi.org/10.1016/j.foodchem.2019.125977

Ferreira, T., & Rasband, W. (2012). ImageJ User Guide User Guide ImageJ. *Image J User Guide*, *1.46r*. https://doi.org/10.1038/nmeth.2019

Francois, E., Dorcemus, D., & Nukavarapu, S. (2015). *1 - Biomaterials and scaffolds for musculoskeletal tissue engineering*. 3–23. https://doi.org/10.1016/B978-1-78242-301-0.00001-X

Fuster, V. (2014). Global burden of cardiovascular disease: Time to implement feasible strategies and to monitor results. *Journal of the American College of Cardiology*, *64*(5), 520–522. https://doi.org/10.1016/j.jacc.2014.06.1151

Gao, J., Chen, S., Tang, D., Jiang, L., Shi, J., & Wang, S. (2019). Mechanical Properties and Degradability of Electrospun PCL/PLGA Blended Scaffolds as Vascular Grafts. *Transactions of Tianjin University*, *25*(2), 152–160. https://doi.org/10.1007/s12209-018-0152-8

Ghiasi, M. M., Zendehboudi, S., & Mohsenipour, A. A. (2020). Decision tree-based diagnosis of coronary artery disease: CART model. *Computer Methods and Programs in Biomedicine*, *192*, 105400. https://doi.org/10.1016/j.cmpb.2020.105400

Goins, A., Webb, A. R., & Allen, J. B. (2019). Multi-layer approaches to scaffold-

based small diameter vessel engineering: A review. *Materials Science and Engineering C*, *97*(November 2018), 896–912. https://doi.org/10.1016/j.msec.2018.12.067

Groeber, F., Holeiter, M., Hampel, M., Hinderer, S., & Schenke-Layland, K. (2011). Skin tissue engineering - In vivo and in vitro applications. *Advanced Drug Delivery Reviews*, *63*(4), 352–366. https://doi.org/10.1016/j.addr.2011.01.005

Gsib, O., Egles, C., & Bencherif, S. A. (2017). Fibrin : An Underrated Biopolymer for Skin Tissue Engineering iMedPub Journals Fibrin : An Underrated Biopolymer for Skin Tissue Engineering Abstract Fibrin and Its Key Role in Skin Wound Healing. *Journal of Molecular Biology and Biotechnology*, *2*(May), 1–4.

Gu, B. K., Park, S. J., Kim, M. S., Lee, Y. J., Kim, J. Il, & Kim, C. H. (2016). Gelatin blending and sonication of chitosan nanofiber mats produce synergistic effects on hemostatic functions. *International Journal of Biological Macromolecules*, *82*, 89–96. https://doi.org/10.1016/j.ijbiomac.2015.10.009

Gumus, S., Ozkoc, G., & Aytac, A. (2011). Plasticized and Unplasticized PLA/Organoclay Nanocomposites: Short- and Long-Term Thermal Properties, Morphology, and Nonisothermal Crystallization Behavior. *Journal of Applied Polymer Science*, 2837–2848. https://doi.org/10.1002/app

Guo, T., Noshin, M., Baker, H. B., Taskoy, E., Meredith, S. J., Tang, Q., Fisher, J. P. (2018). 3D printed biofunctionalized scaffolds for microfracture repair of cartilage defects. *Biomaterials*, *185*(August), 219–231. https://doi.org/10.1016/j.biomaterials.2018.09.022

Gupta, V. B., & Kothari, V. K. (1997). Manufactured Fibre Technology. In *Manufactured Fibre Technology*. https://doi.org/10.1007/978-94-011-5854-1

Haddad, T., Noel, S., Liberelle, B., El Ayoubi, R., Ajji, A., & De Crescenzo, G. (2016). Fabrication and surface modification of poly lactic acid (PLA) scaffolds with epidermal growth factor for neural tissue engineering. *Biomatter*, *6*(1), e1231276. https://doi.org/10.1080/21592535.2016.1231276

Haghjooy Javanmard, S., Anari, J., Zargar Kharazi, A., & Vatankhah, E. (2016). In vitro hemocompatibility and cytocompatibility of a three-layered vascular scaffold fabricated by sequential electrospinning of PCL, collagen, and PLLA nanofibers. *Journal of Biomaterials Applications*, *31*(3), 438–449. https://doi.org/10.1177/0885328216652068

Haider, A., Haider, S., & Kang, I. K. (2018). A comprehensive review summarizing the effect of electrospinning parameters and potential applications of nanofibers in biomedical and biotechnology. *Arabian Journal of Chemistry*, *11*(8), 1165–1188. https://doi.org/10.1016/j.arabjc.2015.11.015

Han, D. G., Ahn, C. B., Lee, J. H., Hwang, Y., Kim, J. H., Park, K. Y., Son, K. H. (2019). Optimization of electrospun poly(caprolactone) fiber diameter for vascular scaffolds to maximize smooth muscle cell infiltration and phenotype modulation. *Polymers*, *11*(4). https://doi.org/10.3390/polym11040643

Hasan, A., Memic, A., Annabi, N., Hossain, M., Paul, A., Dokmeci, M. R., … Khademhosseini, A. (2014). Electrospun scaffolds for tissue engineering of vascular grafts. *Acta Biomaterialia*, *10*(1), 11–25. https://doi.org/10.1016/j.actbio.2013.08.022

Hasan, A., Soliman, S., El Hajj, F., Tseng, Y. T., Yalcin, H. C., & Marei, H. E. (2018). Fabrication and in Vitro Characterization of a Tissue Engineered PCL-PLLA Heart Valve. *Scientific Reports*, *8*(1), 1–13. https://doi.org/10.1038/s41598-018-26452-y

Hemshekhar, M., Thushara, R. M., Chandranayaka, S., Sherman, L. S., Kemparaju, K., & Girish, K. S. (2016). Emerging roles of hyaluronic acid bioscaffolds in tissue engineering and regenerative medicine. *International Journal of Biological Macromolecules*, *86*, 917–928. https://doi.org/10.1016/j.ijbiomac.2016.02.032

Herrero-Herrero, M., Gómez-Tejedor, J. A., & Vallés-Lluch, A. (2018). PLA/PCL electrospun membranes of tailored fibres diameter as drug delivery systems. *European Polymer Journal*, *99*(December 2017), 445–455. https://doi.org/10.1016/j.eurpolymj.2017.12.045

Hiob, M. A., She, S., Muiznieks, L. D., & Weiss, A. S. (2017). Biomaterials and Modifications in the Development of Small-Diameter Vascular Grafts. *ACS Biomaterials Science and Engineering*, *3*(5), 712–723. https://doi.org/10.1021/acsbiomaterials.6b00220

Horakova, J., Mikes, P., Lukas, D., Saman, A., Jencova, V., Klapstova, A., Tonar, Z. (2018). Electrospun vascular grafts fabricated from poly(L-lactide-co-ε -caprolactone) used as a bypass for the rabbit carotid artery. *Biomedical Materials*, *13*(6). https://doi.org/https://doi.org/10.1088/1748-605X/aade9d

Hoskins, P. R., Lawford, P. V., Hardman, D., Hose, R., Narracott, A. J., Keevil, S. F., … Wilkinson, I. B. (2017). Cardiovascular Biomechanics. In P. R. Hoskins, P. V. Lawford, & B. J. Doyle (Eds.), *Cardiovascular Biomechanics*. Cham: Springer International Publishing. https://doi.org/10.1007/978-3-319-46407-7

Hossain, M. F., Gong, R. H., & Rigout, M. (2016). Effect of polymer concentration on electrospinning of hydroxypropyl-β-cyclodextrins/PEO nanofibres. *Journal of the Textile Institute*, *107*(12), 1511–1518. https://doi.org/10.1080/00405000.2015.1128714

Huang, C., & Thomas, N. L. (2018). Fabricating porous poly(lactic acid) fibres via electrospinning. *European Polymer Journal*, *99*(September 2017), 464–476. https://doi.org/10.1016/j.eurpolymj.2017.12.025

Huang, Y.-Z., Xie, H.-Q., & Li, X. (2020). Scaffolds in Bone Tissue Engineering: Research Progress and Current Applications. *Encyclopedia of Bone Biology*, 204–215. https://doi.org/10.1016/b978-0-12-801238-3.11205-x

İçoğlu, H. İ., & Oğulata, R. T. (2017). EFFECT OF AMBIENT PARAMETERS ON MORPHOLOGY OF ELECTROSPUN POLY (TRIMETHYLENE TEREPHTHALATE) (PTT) FIBERS. *Tekstil ve Konfeksiyon*, 215–223.

Jahangir, M. A., Rumi, T. M., Wahab, A., Rahman, M. A., & Sayed, Z. Bin. (2017). Poly Lactic Acid (PLA) Fibres: Different Solvent Systems and Their Effect on Fibre Morphology and Diameter. *American Journal of Chemistry*, *2017*(6), 177–186. https://doi.org/10.5923/j.chemistry.20170706.01

Jia, W., Li, M., Weng, H., Gu, G., & Chen, Z. (2020). Design and comprehensive assessment of a biomimetic tri-layer tubular scaffold via biodegradable polymers for vascular tissue engineering applications. *Materials Science and Engineering C*, *110*(February), 110717. https://doi.org/10.1016/j.msec.2020.110717

Jiang, L., & Zhang, J. (2013). Biodegradable Polymers and Polymer Blends. In *Handbook of Biopolymers and Biodegradable Plastics: Properties, Processing and Applications*. Elsevier. https://doi.org/10.1016/B978-1-4557-2834-3.00006-9

Johnson, N. B. lai., Hayes, L. D., Brown, K., Hoo, E. C., & Ethier, K. A. (2014). CDC National Health Report: leading causes of morbidity and mortality and associated behavioral risk and protective factors--United States, 2005-2013. *Morbidity and Mortality Weekly Report. Surveillance Summaries (Washington, D.C. : 2002)*, *63*(4), 3–27.

Johnson, R., Ding, Y., Nagiah, N., Monnet, E., & Tan, W. (2019). Coaxially-structured fibres with tailored material properties for vascular graft implant. *Materials Science and Engineering C*, *97*(October 2018), 1–11. https://doi.org/10.1016/j.msec.2018.11.036

Joshi, A., Xu, Z., Ikegami, Y., Yamane, S., Tsurashima, M., & Ijima, H. (2020). Co-culture of mesenchymal stem cells and human umbilical vein endothelial cells on heparinized polycaprolactone/gelatin co-spun nanofibers for improved endothelium remodeling. *International Journal of Biological Macromolecules*, *151*, 186–192. https://doi.org/10.1016/j.ijbiomac.2020.02.163

Kai, D., Liow, S. S., & Loh, X. J. (2015). Biodegradable polymers for electrospinning: Towards biomedical applications. *Materials Science and Engineering C*, *45*, 659–670. https://doi.org/10.1016/j.msec.2014.04.051

Kakroodi, A. R., Kazemi, Y., Rodrigue, D., & Park, C. B. (2018). Facile production of biodegradable PCL/PLA in situ nanofibrillar composites with unprecedented compatibility between the blend components. *Chemical Engineering Journal*, *351*(June), 976–984. https://doi.org/10.1016/j.cej.2018.06.152

Kaptoge, S., Pennells, L., De Bacquer, D., Cooney, M. T., Kavousi, M., Stevens, G., … Di Angelantonio, E. (2019). World Health Organization cardiovascular disease risk charts: revised models to estimate risk in 21 global regions. *The Lancet Global Health*, *7*(10), e1332–e1345. https://doi.org/10.1016/S2214-109X(19)30318-3

Khajavi, R., & Abbasipour, M. (2017). Controlling nanofiber morphology by the electrospinning process. In *Electrospun Nanofibers*. Elsevier Ltd. https://doi.org/10.1016/B978-0-08-100907-9.00005-2

Khan, Z., & Kafiaha, F. M. (2016). Preparation of polysulfone electrospun nanofibers : effect of electrospinning and solution parameters. *Membrane Technology for Water and Wastewater Treatment, Energy and Environment*, *2013*(Mst), 309–318. https://doi.org/10.13140/RG.2.1.4289.9681

Khanmodahammadi, M., Zolfagharzadeh, V., Bagher, Z., Soltani, H., & Ai, J. (2020). Cell Encapsulation in Core-Shell Microcapsulates Through Coaxial Electrospinning System and Horseradish Peroxidase-Catalyzed Crosslinking. *Biomedical Physics & Engineering Express*, *6*(1).

Kim, J. H., Atala, A., & Yoo, J. J. (2020). Tissue engineering of the kidney. In *Principles of Tissue Engineering* (pp. 825–843). INC. https://doi.org/10.1016/b978-0-12-818422-6.00047-2

Koens, M. J. W., Faraj, K. A., Wismans, R. G., Van Der Vliet, J. A., Krasznai, A. G.,

Cuijpers, V. M. J. I., … Van Kuppevelt, T. H. (2010). Controlled fabrication of triple layered and molecularly defined collagen/elastin vascular grafts resembling the native blood vessel. *Acta Biomaterialia*, *6*(12), 4666–4674. https://doi.org/10.1016/j.actbio.2010.06.038

Konig, G., McAllister, T. N., Dusserre, N., Garrido, S. A., Iyican, C., Marini, A., … L'Heureux, N. (2009). Mechanical properties of completely autologous human tissue engineered blood vessels compared to human saphenous vein and mammary artery. *Biomaterials*, *30*(8), 1542–1550. https://doi.org/10.1016/j.biomaterials.2008.11.011

Korzhikov, V., Averianov, I., Litvinchuk, E., & Tennikova, T. B. (2016). Polyester-based microparticles of different hydrophobicity: the patterns of lipophilic drug entrapment and release. *Journal of Microencapsulation*, *33*(3), 199–208. https://doi.org/10.3109/02652048.2016.1144818

Labet, M., & Thielemans, W. (2009). Synthesis of polycaprolactone: A review. *Chemical Society Reviews*, *38*(12), 3484–3504. https://doi.org/10.1039/b820162p

Langer, R., & Vacanti, J. (1993). Tissue Engineering. *Science*, *260*(5110), 920–926. https://doi.org/10.1126/science.8493529

Lanza, R., Langer, R., Vacanti, J. P., & Atala, A. (2020). Principles of Tissue Engineering. In R. Lanza, R. Langer, J. P. Vacanti, & A. Atala (Eds.), *Elsevier* (5th ed.). Elsevier.

Lee, C. H., Singla, A., & Lee, Y. (2001). Biomedical applications of collagen. *International Journal of Pharmaceutics*, *221*, 1–22. https://doi.org/https://doi.org/10.1016/S0378-5173(01)00691-3

Li, C., & Dou, Q. (2014). Non-isothermal crystallization kinetics and spherulitic morphology of nucleated poly(lactic acid): Effect of dilithium hexahydrophthalate as a novel nucleating agent. *Thermochimica Acta*. https://doi.org/10.1016/j.tca.2014.08.036

Li, L., Lu, H., Zhao, Y., Luo, J., Yang, L., Liu, W., & He, Q. (2019). Functionalized cell-free scaffolds for bone defect repair inspired by self-healing of bone fractures: A review and new perspectives. *Materials Science and Engineering C*, *98*(December 2018), 1241–1251. https://doi.org/10.1016/j.msec.2019.01.075

Li, Q., Ma, L., & Gao, C. (2015). Biomaterials for in situ tissue regeneration: Development and perspectives. *Journal of Materials Chemistry B*, *3*(46), 8921–8938. https://doi.org/10.1039/c5tb01863c

Li, X., Wang, X., Yao, D., Jiang, J., Guo, X., Gao, Y., Shen, C. (2018). Effects of aligned and random fibers with different diameter on cell behaviors. *Colloids and Surfaces B: Biointerfaces*, *171*(June), 461–467. https://doi.org/10.1016/j.colsurfb.2018.07.045

Liu, F., Liao, X., Liu, C., Li, M., Chen, Y., Shao, W., … He, J. (2020). Poly(l-lactide-co-caprolactone)/tussah silk fibroin nanofiber vascular scaffolds with small diameter fabricated by core-spun electrospinning technology. *Journal of Materials Science*, *55*(16), 7106–7119. https://doi.org/10.1007/s10853-020-04510-z

Loh, Q. L., & Choong, C. (2013). Three-dimensional scaffolds for tissue engineering

applications: Role of porosity and pore size. *Tissue Engineering - Part B: Reviews*, *19*(6), 485–502. https://doi.org/10.1089/ten.teb.2012.0437

Long, Y. Z., Yan, X., Wang, X. X., Zhang, J., & Yu, M. (2018). Electrospinning: The Setup and Procedure. In *Electrospinning: Nanofabrication and Applications* (pp. 21–52). Elsevier Inc. https://doi.org/10.1016/B978-0-323-51270-1.00002-9

Lopez-Rodriguez, N., Lopez-Arraiza, A., Meaurio, E., & Sarasua, J. R. (2006). Crystallization, Morphology, and Mechanical Behavior of Polylactide/Poly(caprolactone) Blends. *Polymer Engineering and Science*. https://doi.org/10.1002/pen.20609

Luo, Y. (2020). Three-dimensional scaffolds. In *Principles of Tissue Engineering* (pp. 343–360). INC. https://doi.org/10.1016/b978-0-12-818422-6.00020-4

Luyt, A. S., & Gasmi, S. (2016). Influence of blending and blend morphology on the thermal properties and crystallization behaviour of PLA and PCL in PLA/PCL blends. *Journal of Materials Science*, *51*(9), 4670–4681. https://doi.org/10.1007/s10853-016-9784-z

Lv, Q., Wu, D., Xie, H., Peng, S., Chen, Y., & Xu, C. (2016). Crystallization of poly(ϵ-caprolactone) in its immiscible blend with polylactide: Insight into the role of annealing histories. *RSC Advances*, *6*(44), 37721–37730. https://doi.org/10.1039/c6ra07752h

Ma, P. X. (2008). Biomimetic materials for tissue engineering. *Advanced Drug Delivery Reviews*, *60*(2), 184–198. https://doi.org/10.1016/j.addr.2007.08.041

Mabrouk, M., Beherei, H. H., & Das, D. B. (2020). Recent progress in the fabrication techniques of 3D scaffolds for tissue engineering. *Materials Science & Engineering C*, *110*(February), 110716. https://doi.org/10.1016/j.msec.2020.110716

Malik, S., Sundarrajan, S., & Hussain, T. (2020). Electrospun biomimetic polymer nanofibers as vascular grafts. *Materials Design and Process Communication*, (September), 1–21. https://doi.org/10.1002/mdp2.203

Marelli, B., Achilli, M., Alessandrino, A., Freddi, G., Tanzi, M. C., Farè, S., & Mantovani, D. (2012). Collagen-Reinforced Electrospun Silk Fibroin Tubular Construct as Small Calibre Vascular Graft. *Macromolecular Bioscience*, *12*(11), 1566–1574. https://doi.org/10.1002/mabi.201200195

Matsuzaki, Y., John, K., Shoji, T., & Shinoka, T. (2019). The evolution of tissue engineered vascular graft technologies: From preclinical trials to advancing patient care. *Applied Sciences (Switzerland)*, *9*(7). https://doi.org/10.3390/app9071274

Mclauchlin, A. R., & Thomas, N. L. (2012). Biodegradable polymer nanocomposites. *Advances in Polymer Nanocomposites: Types and Applications*, 398–430. https://doi.org/10.1533/9780857096241.2.398

Medeiros, E. S., Mattoso, L. H. C., Offeman, R. D., Wood, D. F., & Orts, W. J. (2008). Effect of relative humidity on the morphology of electrospun polymer fibers. *Canadian Journal of Chemistry*, *86*(6), 590–599. https://doi.org/10.1139/V08-029

Megelski, S., Stephens, J. S., Chase, D. B., & Rabolt, J. F. (2002). *Micro- and Nanostructured Surface Morphology on Electrospun Polymer Fibers*. 8456–

8466. https://doi.org/10.1021/ma020444a

Menczel, J. D., & Prime, R. B. (2008). Thermal Analysis of Polymers: Fundamentals and Applications. In *Thermal Analysis of Polymers: Fundamentals and Applications*. https://doi.org/10.1002/9780470423837

Mohamed, A., Finkenstadt, V. L., Gordon, S. H., Biresaw, G., Debra E., P., & Rayas-Duarte, P. (2008). Thermal Properties of PCL/Gluten Bioblends Characterized by TGA, DSC, SEM, and Infrared-PAS. *Journal of Applied Polymer Science*, *110*, 3256–3266. https://doi.org/10.1002/app.28914

Mondal, D., Griffith, M., & Venkatraman, S. S. (2016). International Journal of Polymeric Materials and Polycaprolactone-based biomaterials for tissue engineering and drug delivery : Current scenario and challenges. *GPOM*, *65*(5), 255–265. https://doi.org/10.1080/00914037.2015.1103241

Montini-Ballarin, F., Calvo, D., Caracciolo, P. C., Rojo, F., Frontini, P. M., Abraham, G. A., & V. Guinea, G. (2016). Mechanical behavior of bilayered small-diameter nanofibrous structures as biomimetic vascular grafts. *Journal of the Mechanical Behavior of Biomedical Materials*, *60*, 220–233. https://doi.org/10.1016/j.jmbbm.2016.01.025

Moreno Raja, M., Lim, P. Q., Wong, Y. S., Xiong, G. M., Zhang, Y., Venkatraman, S., & Huang, Y. (2019). Polymeric Nanomaterials. In *Nanocarriers for Drug Delivery*. Elsevier Inc. https://doi.org/10.1016/b978-0-12-814033-8.00018-7

Mulinti, P., Brooks, J. E., Lervick, B., Pullan, J. E., & Brooks, A. E. (2018). Strategies to improve the hemocompatibility of biodegradable biomaterials. In *Hemocompatibility of Biomaterials for Clinical Applications: Blood-Biomaterials Interactions*. Elsevier Ltd. https://doi.org/10.1016/B978-0-08-100497-5.00017-3

Nampoothiri, K. M., Nair, N. R., & John, R. P. (2010). An overview of the recent developments in polylactide (PLA) research. *Bioresource Technology*, *101*(22), 8493–8501. https://doi.org/10.1016/j.biortech.2010.05.092

Nijenhuis, A. J., Grijpma, D. W., & Pennings, A. J. (1991). Highly crystalline as-polymerized poly(L-lactide). *Polymer Bulletin*, *77*, 71–77.

Ong, C. S., Fukunishi, T., Liu, R. H., Nelson, K., Zhang, H., Wieczorek, E., … Hibino, N. (2017). Bilateral Arteriovenous Shunts as a Method for Evaluating Tissue-Engineered Vascular Grafts in Large Animal Models. *Tissue Engineering - Part C: Methods*, *23*(11), 728–735. https://doi.org/10.1089/ten.tec.2017.0217

Organ Procurement and Transplantation Network. (2021). Retrieved from US Department of Health and Human Services website: https://optn.transplant.hrsa.gov

Oyane, A., Uchida, M., Yokoyama, Y., Choong, C., Triffitt, J., & Ito, A. (2005). Simple surface modification of poly(ε-caprolactone) to induce its apatite-forming ability. *Journal of Biomedical Materials Research - Part A*, *75*(1), 138–145. https://doi.org/10.1002/jbm.a.30397

Oztemur, J., & Yalcin-Enis, I. (2021). Development of biodegradable webs of PLA/PCL blends prepared via electrospinning: Morphological, chemical, and thermal characterization. *Journal of Biomedical Materials Research - Part B Applied Biomaterials*, *109*(11), 1844–1856. https://doi.org/10.1002/jbm.b.34846

Oztemur, J., & Yalcin Enis, I. (2020). *The Role of Biopolymer Selection in the Design of Electrospun Small Caliber Vascular Grafts to Replace the Native Arterial Structure*.

Pant, H. R., Nam, K. T., Oh, H. J., Panthi, G., Kim, H. D., Kim, B. Il, & Kim, H. Y. (2011). Effect of polymer molecular weight on the fiber morphology of electrospun mats. *Journal of Colloid and Interface Science*, *364*(1), 107–111. https://doi.org/10.1016/j.jcis.2011.07.094

Pashneh-Tala, S., MacNeil, S., & Claeyssens, F. (2016). The tissue-engineered vascular graft - Past, present, and future. *Tissue Engineering - Part B: Reviews*, *22*(1), 68–100. https://doi.org/10.1089/ten.teb.2015.0100

Patrício, T., Domingos, M., Gloria, A., D'Amora, U., Coelho, J. F., & Bártolo, P. J. (2014). Fabrication and characterisation of PCL and PCL/PLA scaffolds for tissue engineering. *Rapid Prototyping Journal*, *20*(2), 145–156. https://doi.org/10.1108/RPJ-04-2012-0037

Pereira, R. F., Sousa, A., Barrias, C. C., Bayat, A., Granja, P. L., & Bártolo, P. J. (2017). Advances in bioprinted cell-laden hydrogels for skin tissue engineering. *Biomanufacturing Reviews*, *2*(1). https://doi.org/10.1007/s40898-017-0003-8

Petreaca, M., & Martins-Green, M. (2013). The Dynamics of Cell-ECM Interactions, with Implications for Tissue Engineering. In *Principles of Tissue Engineering: Fourth Edition* (Fourth Edi). Elsevier. https://doi.org/10.1016/B978-0-12-398358-9.00009-4

Pham, Q. P., Sharma, U., & Mikos, A. G. (2006). Electrospinning of Polymeric Nanofibers for Tissue Engineering Applications: A Review. *Tissue Engineering*, *12*(5), 1197–1211.

Rapoport, H. S., Fish, J., Basu, J., Campbell, J., Genheimer, C., Payne, R., & Jain, D. (2012). Construction of a tubular scaffold that mimics j-shaped stress/strain mechanics using an innovative electrospinning technique. *Tissue Engineering - Part C: Methods*, *18*(8), 567–574. https://doi.org/10.1089/ten.tec.2011.0286

Rasouli, M., Pirsalami, S., & Zebarjad, S. M. (2019). Optimizing the electrospinning conditions of polysulfone membranes for water microfiltration applications. *Polymer International*, *68*(9), 1610–1617. https://doi.org/10.1002/pi.5858

Ratcliffe, A. (2000). Tissue engineering of vascular grafts. *Matrix Biology*, *14*, 353–357. https://doi.org/10.1007/s10353-013-0224-x

Ravi, S., & Chaikof, E. L. (2010). *Biomaterials for vascular tissue engineering R eview. 5*, 107–120.

Refaa, Z., Boutaous, M., Xin, S., & Siginer, D. A. (2017). Thermophysical analysis and modeling of the crystallization and melting behavior of PLA with talc: Kinetics and crystalline structures. *Journal of Thermal Analysis and Calorimetry*, *128*(2), 687–698. https://doi.org/10.1007/s10973-016-5961-1

Ren, X., Feng, Y., Guo, J., Wang, H., Li, Q., Yang, J., Li, W. (2015). Surface modification and endothelialization of biomaterials as potential scaffolds for vascular tissue engineering applications. *Chemical Society Reviews*, *44*(15), 5680–5742. https://doi.org/10.1039/c4cs00483c

Rizwan, M., Yao, Y., Gorbet, M. B., Tse, J. W., Anderson, D. E. J., Hinds, M. T., & Yim, E. K. F. (2020). One-Pot Covalent Grafting of Gelatin on Poly(Vinyl

Alcohol) Hydrogel to Enhance Endothelialization and Hemocompatibility for Synthetic Vascular Graft Applications. *ACS Applied Bio Materials*, *3*(1), 693–703. https://doi.org/10.1021/acsabm.9b01026

Rnjak-kovacina, J., Wise, S. G., Li, Z., Maitz, P. K. M., Young, C. J., Wang, Y., & Weiss, A. S. (2011). *Tailoring the porosity and pore size of electrospun synthetic human elastin scaffolds for dermal tissue engineering*. *32*, 6729–6736. https://doi.org/10.1016/j.biomaterials.2011.05.065

Rogina, A. (2014). Electrospinning process: Versatile preparation method for biodegradable and natural polymers and biocomposite systems applied in tissue engineering and drug delivery. *Applied Surface Science*, *296*, 221–230. https://doi.org/10.1016/j.apsusc.2014.01.098

Saini, P., Arora, M., & Kumar, M. N. V. R. (2016). Poly(lactic acid) blends in biomedical applications. *Advanced Drug Delivery Reviews*, *107*, 47–59. https://doi.org/10.1016/j.addr.2016.06.014

Sankaran, K. K., Krishnan, U. M., & Sethuraman, S. (2014). Axially aligned 3D nanofibrous grafts of PLA-PCL for small diameter cardiovascular applications. *Journal of Biomaterials Science, Polymer Edition*, *25*(16), 1791–1812. https://doi.org/10.1080/09205063.2014.950505

Scaffaro, R., Lopresti, F., & Botta, L. (2017). Preparation, characterization and hydrolytic degradation of PLA/PCL co-mingled nanofibrous mats prepared via dual-jet electrospinning. *European Polymer Journal*, *96*(September), 266–277. https://doi.org/10.1016/j.eurpolymj.2017.09.016

Seifu, D. G., Purnama, A., Mequanint, K., & Mantovani, D. (2013). Small-diameter vascular tissue engineering. *Nature Reviews Cardiology*, *10*(7), 410–421. https://doi.org/10.1038/nrcardio.2013.77

Shabani, I., Haddadi-Asl, V., Seyedjafari, E., Babaeijandaghi, F., & Soleimani, M. (2009). Improved infiltration of stem cells on electrospun nanofibers. *Biochemical and Biophysical Research Communications*, *382*(1), 129–133. https://doi.org/10.1016/j.bbrc.2009.02.150

Shafiq, M., Wang, L., Zhi, D., Zhang, Q., Wang, K., Wang, L., Kim, S. H. (2018). In situ blood vessel regeneration using neuropeptide substance P-conjugated small-diameter vascular grafts. *Journal of Biomaterial Research Part B*, *107B*, 1669–1683. https://doi.org/10.1002/jbm.b.34260

Shao, H., Fang, J., Wang, H., & Lin, T. (2015). Effect of electrospinning parameters and polymer concentrations on mechanical-to-electrical energy conversion of randomly-oriented electrospun poly(vinylidene fluoride) nanofiber mats. *RSC Advances*, *5*(19), 14345–14350. https://doi.org/10.1039/c4ra16360e

Sharma, D., & Satapathy, B. K. (2019). Performance evaluation of electrospun nanofibrous mats of polylactic acid (PLA)/poly (e-caprolactone) (PCL) blends. *Materials Today: Proceedings*, *19*, 188–195. https://doi.org/10.1016/j.matpr.2019.06.698

Sharma, D., & Satapathy, B. K. (2020). Optimization and physical performance evaluation of electrospun nanofibrous mats of PLA, PCL and their blends. *Journal of Industrial Textiles*. https://doi.org/10.1177/1528083720944502

Shojaee, M., & Bashur, C. A. (2017). Compositions Including Synthetic and Natural

Blends for Integration and Structural Integrity: Engineered for Different Vascular Graft Applications. *Advanced Healthcare Materials*, *6*(12), 1–14. https://doi.org/10.1002/adhm.201700001

Simones, C. L., Viana, J. C., & Cunha, A. M. (2009). Mechanical Properties of Poly(e-caprolactone) and Poly(lactic acid) Blends. *Journal of Applied Polymer Science*, *112*, 345–352. https://doi.org/10.1002/app

Sinha, V. R., Bansal, K., Kaushik, R., Kumria, R., & Trehan, A. (2004). Poly-ε-caprolactone microspheres and nanospheres: An overview. *International Journal of Pharmaceutics*, *278*(1), 1–23. https://doi.org/10.1016/j.ijpharm.2004.01.044

Soliman, S., Sant, S., Nichol, J. W., Khabiry, M., Traversa, E., & Khademhosseini, A. (2011). Controlling the porosity of fibrous scaffolds by modulating the fiber diameter and packing density. *Journal of Biomedical Materials Research - Part A*, *96 A*(3), 566–574. https://doi.org/10.1002/jbm.a.33010

Song, Y., Feijen, J., Grijpma, D. W., & Poot, A. A. (2011). Tissue engineering of small-diameter vascular grafts: A literature review. *Clinical Hemorheology and Microcirculation*, *49*(1–4), 357–374. https://doi.org/10.3233/CH-2011-1486

Sorrentino, S., & Haller, H. (2011). Tissue engineering of Blood Vessels: How to Make a Graft. In N. Pallua & C. V. Suscheck (Eds.), *Tissue Engineering: From Lab to Clinic* (Vol. 9783642028, pp. 1–634). Springer, Berlin, Heidelberg. https://doi.org/https://doi.org/10.1007/978-3-642-02824-3_14

Spadaccio, C., Nappi, F., De Marco, F., Sedati, P., Sutherland, F. W. H., Chello, M., Rainer, A. (2016). Preliminary in vivo evaluation of a hybrid armored vascular graft combining electrospinning and additive manufacturing techniques. *Drug Target Insights*, *10*, 1–7. https://doi.org/10.4137/DTI.s35202

Subbiah, T., Bhat, G. S., Tock, R. W., Parameswaran, S., & Ramkumar, S. S. (2005). Electrospinning of nanofibers. *Journal of Applied Polymer Science*, *96*(2), 557–569. https://doi.org/10.1002/app.21481

Suwantong, O. (2016). Biomedical applications of electrospun polycaprolactone fiber mats. *Polymers for Advanced Technologies*, *27*(10), 1264–1273. https://doi.org/10.1002/pat.3876

Tan, S. H., Inai, R., Kotaki, M., & Ramakrishna, S. (2005). Systematic parameter study for ultra-fine fiber fabrication via electrospinning process. *Polymer*, *46*(16), 6128–6134. https://doi.org/10.1016/j.polymer.2005.05.068

Thomas, L. V., Lekshmi, V., & Nair, P. D. (2013). Tissue engineered vascular grafts - Preclinical aspects. *International Journal of Cardiology*, *167*(4), 1091–1100. https://doi.org/10.1016/j.ijcard.2012.09.069

Tomoki Maeda, Katsuya Hagiwara, Soki Yoshida, T. H. and A. H. (2014). Preparation and Characterization of 2-Methacryloyloxyethyl Phosphorylcholine Polymer Nanofibers Prepared via Electrospinning for Biomedical Materials. *Journal of Applied Polymer Science*, *131*(14). https://doi.org/10.1002/app.40606

Uyar, T., & Besenbacher, F. (2008). Electrospinning of uniform polystyrene fibers: The effect of solvent conductivity. *Polymer*, *49*(24), 5336–5343. https://doi.org/10.1016/j.polymer.2008.09.025

Vacanti, C. (2006). The history of tissue engineering. *Journal of Cellular and Molecular Medicine*, *1*(3), 569–576. https://doi.org/10.2755/jcmm010.003.20

Vacanti, J. P., & Vacanti, C. A. (2013). The History and Scope of Tissue Engineering. In *Principles of Tissue Engineering: Fourth Edition* (Fourth Edi). Elsevier. https://doi.org/10.1016/B978-0-12-398358-9.00001-X

Vaz, C. M., van Tuijl, S., Bouten, C. V. C., & Baaijens, F. P. T. (2005). Design of scaffolds for blood vessel tissue engineering using a multi-layering electrospinning technique. *Acta Biomaterialia*, *1*(5), 575–582. https://doi.org/10.1016/j.actbio.2005.06.006

Vonbrunn, E., Mueller, M., Pichlsberger, M., Sundl, M., Helmer, A., Wallner, S. A., … Lang-Olip, I. (2020). Electrospun PCL/PLA Scaffolds Are More Suitable Carriers of Placental Mesenchymal Stromal Cells Than Collagen/Elastin Scaffolds and Prevent Wound Contraction in a Mouse Model of Wound Healing. *Frontiers in Bioengineering and Biotechnology*, *8*(December), 1–16. https://doi.org/10.3389/fbioe.2020.604123

Vroman, I., & Tighzert, L. (2009). Biodegradable polymers. *Materials*, *2*(2), 307–344. https://doi.org/10.3390/ma2020307

Wang, H. M., Chou, Y. T., Wen, Z. H., Wang, Z. R., Chen, C. H., & Ho, M. L. (2013). Novel Biodegradable Porous Scaffold Applied to Skin Regeneration. *PLoS ONE*, *8*(6), 2–12. https://doi.org/10.1371/journal.pone.0056330

Wang, T., Ji, X., Jin, L., Feng, Z., Wu, J., Zheng, J., He, N. (2013). Fabrication and Characterization of Heparin-Grafted Poly-L-lactic acid−Chitosan Core−Shell Nanofibers Scaffold for Vascular Gasket. *ACS Applied Materials and Interfaces*, *5*, 3757–3763. https://doi.org/dx.doi.org/10.1021/am400369c

Wang, W., Hu, J., He, C., Nie, W., Feng, W., Qiu, K., … Wang, G. (2015). Heparinized PLLA/PLCL nanofibrous scaffold for potential engineering of small-diameter blood vessel: Tunable elasticity and anticoagulation property. *Journal of Biomedical Materials Research - Part A*, *103*(5), 1784–1797. https://doi.org/10.1002/jbm.a.35315

Wise, S. G., Byrom, M. J., Waterhouse, A., Bannon, P. G., Ng, M. K. C., & Weiss, A. S. (2011). A multilayered synthetic human elastin/polycaprolactone hybrid vascular graft with tailored mechanical properties. *Acta Biomaterialia*, *7*(1), 295–303. https://doi.org/10.1016/j.actbio.2010.07.022

World Health Organization. (2020). Cardiovascular Diseases. Retrieved from https://www.who.int/health-topics/cardiovascular-diseases/#tab=tab_1

Wu, D., Lin, D., Zhang, J., Zhou, W., Zhang, M., Zhang, Y., … Lin, B. (2011). Selective localization of nanofillers: Effect on morphology and crystallization of PLA/PCL blends. *Macromolecular Chemistry and Physics*, *212*(6), 613–626. https://doi.org/10.1002/macp.201000579

Wu, J., Hu, C., Tang, Z., Yu, Q., Liu, X., & Chen, H. (2018). Tissue-engineered Vascular Grafts: Balance of the Four Major Requirements. *Colloids and Interface Science Communications*, *23*(February), 34–44. https://doi.org/10.1016/j.colcom.2018.01.005

Wu, Y., Qin, Y., Wang, Z., Wang, J., Zhang, C., Li, C., & Kong, D. (2018). The regeneration of macro-porous electrospun poly(ε-caprolactone) vascular graft during long-term in situ implantation. *Journal of Biomedical Materials Research - Part B Applied Biomaterials*, *106*(4), 1618–1627.

https://doi.org/10.1002/jbm.b.33967

Xiang, S., Feng, L., Bian, X., Zhang, B., Sun, B., Liu, Y., Chen, X. (2019). Toughening modification of PLLA with PCL in the presence of PCL-b-PLLA diblock copolymers as compatibilizer. *Polymers for Advanced Technologies*, *30*(4), 963–972. https://doi.org/10.1002/pat.4530

Xue, L., & Greisler, H. P. (2003). *Biomaterials in the development and future of vascular grafts*. 472–480. https://doi.org/10.1067/mva.2003.88

Yalcin Enis, I., & Gok Sadikoglu, T. (2018). Design parameters for electrospun biodegradable vascular grafts. *Journal of Industrial Textiles*, *47*(8), 2205–2227. https://doi.org/10.1177/1528083716654470

Yalcin Enis, I., Horakova, J., Gok Sadikoglu, T., Novak, O., & Lukas, D. (2017). Mechanical investigation of bilayer vascular grafts electrospun from aliphatic polyesters. *Polymers for Advanced Technologies*, *28*(2), 201–213. https://doi.org/10.1002/pat.3875

Yalcin, I., Horakova, J., Mikes, P., Sadikoglu, T. G., Domin, R., & Lukas, D. (2016). Design of Polycaprolactone Vascular Grafts. *Journal of Industrial Textiles*, *45*(5), 813–833. https://doi.org/10.1177/1528083714540701

Yang, S. kyeong, Shafiq, M., Kim, D., Park, C., Jung, Y., & Hyun, S. (2016). Characterization and preparation of bioinspired resorbable conduits for vascular reconstruction. *Macromolecular Research*, *24*(4), 371–379. https://doi.org/10.1007/s13233-016-4042-4

Yao, Q., Cosme, J. G. L., Xu, T., Miszuk, J. M., Picciani, P. H. S., Fong, H., & Sun, H. (2017). Three dimensional electrospun PCL/PLA blend nanofibrous scaffolds with significantly improved stem cells osteogenic differentiation and cranial bone formation. *Biomaterials*, *115*, 115–127. https://doi.org/10.1016/j.biomaterials.2016.11.018

Yi, S., Ding, F., Gong, L., & Gu, X. (2017). Extracellular Matrix Scaffolds for Tissue Engineering and Regenerative Medicine. *Current Stem Cell Research & Therapy*, *12*(3), 233–246. https://doi.org/10.2174/1574888X11666160905092

Zamani, M., Khafaji, M., Naji, M., Vossoughi, M., Alemzadeh, I., & Haghighipour, N. (2017). A Biomimetic Heparinized Composite Silk-Based Vascular Scaffold with sustained Antithrombogenicity. *Scientific Reports*, *7*(1), 1–14. https://doi.org/10.1038/s41598-017-04510-1

Zdraveva, E., Fang, J., Mijovic, B., Lin, T., Rayleigh, Lord, & Morton, W. J. (2017). Electrospun Nanofibers. In *Structure and Properties of High-Performance Fibers* (pp. 267–300). https://doi.org/10.1016/B978-0-08-100550-7.00011-5

Zhai, W., Ko, Y., Zhu, W., Wong, A., & Park, C. B. (2009). A study of the crystallization, melting, and foaming behaviors of polylactic acid in compressed CO2. *International Journal of Molecular Sciences*. https://doi.org/10.3390/ijms10125381

Zhalmuratova, D., La, T. G., Yu, K. T. T., Szojka, A. R. A., Andrews, S. H. J., Adesida, A. B., Chung, H. J. (2019). Mimicking "j-Shaped" and Anisotropic Stress-Strain Behavior of Human and Porcine Aorta by Fabric-Reinforced Elastomer Composites. *ACS Applied Materials and Interfaces*, *11*(36), 33323–33335. https://doi.org/10.1021/acsami.9b10524

Zhang, F., Bambharoliya, T., Xie, Y., Liu, L., Celik, H., Wang, L., King, M. W. (2021). A hybrid vascular graft harnessing the superior mechanical properties of synthetic fibers and the biological performance of collagen filaments. *Materials Science and Engineering C*, *118*(May 2020), 111418. https://doi.org/10.1016/j.msec.2020.111418

Zhang, Y., Yoo, J. J., & Atala, A. (2020). Tissue engineering: bladder and urethra. In *Principles of Tissue Engineering* (pp. 845–862). INC. https://doi.org/10.1016/b978-0-12-818422-6.00048-4

Zhao, L., Li, X., Yang, L., Sun, L., Mu, S., Zong, H., Zhang, Q. (2021). Evaluation of remodeling and regeneration of electrospun PCL/fibrin vascular grafts in vivo. *Materials Science and Engineering C*, *118*(August 2020). https://doi.org/10.1016/j.msec.2020.111441

Zhao, N., Lv, Z., Ma, J., Zhu, C., & Li, Q. (2019). Fabrication of hydrophilic small diameter vascular foam scaffolds of poly(ε-caprolactone)/polylactic blend by sodium hydroxide solution. *European Polymer Journal*, *110*(August 2018), 31–40. https://doi.org/10.1016/j.eurpolymj.2018.11.011

Zhao, Y., Eng, G., Lee, B. W., Radisic, M., & Vunjak-Novakovic, G. (2020). Cardiac tissue engineering. In *Principles of Tissue Engineering* (pp. 593–616). INC. https://doi.org/10.1016/b978-0-12-818422-6.00033-2

Zhou, J., Cao, C., Ma, X., & Lin, J. (2010). Electrospinning of silk fibroin and collagen for vascular tissue engineering. *International Journal of Biological Macromolecules*, *47*(4), 514–519. https://doi.org/10.1016/j.ijbiomac.2010.07.010

Zhu, Caihong, Zhu, J., Wang, C., Chen, R., Sun, L., & Ru, C. (2018). Wrinkle-Free, Sandwich, Electrospun PLGA/SF Nanofibrous Scaffold for Skin Tissue Engineering. *IEEE Transactions on Nanotechnology*, *17*(4), 675–679. https://doi.org/10.1109/TNANO.2018.2801569

Zhu, Chenhui, Fan, D., Duan, Z., Xue, W., Shang, L., Chen, F., & Luo, Y. (2009). Initial investigation of novel human-like collagen/chitosan scaffold for vascular tissue engineering. *Journal of Biomedical Materials Research - Part A*, *89*(3), 829–840. https://doi.org/10.1002/jbm.a.32256

Zhu, R. T., Tan, M. H., Zhang, P., Zhang, L., Chen, X. M., & Yang, F. (2014). Morphological structure and thermal property of PLA/PCL nanofiber by electrospinning. *Advanced Materials Research*, *1048*(C), 418–422. https://doi.org/10.4028/www.scientific.net/AMR.1048.418

Zussman, E. (2011). Encapsulation of cells within electrospun fibers. *Polymers for Advanced Technologies*, *22*(3), 366–371. https://doi.org/10.1002/pat.1812

CURRICULUM VITAE

Name Surname : Janset Öztemur

EDUCATION :

- **B.Sc.** **:** 2018. Istanbul Technical University. Textile Eng.

PROFESSIONAL EXPERIENCE AND REWARDS:

- 2019-2021. Research Assistant at Istanbul Technical University. Textile Technologies and Design Faculty

PUBLICATIONS AND PRESENTATIONS ON THE THESIS:

- **Oztemur. J..** Yalcin-Enis. I. (2021) Development of biodegradable webs of PLA/PCL blends prepared via electrospinning: Morphological. chemical. and thermal characterization. J Biomed Mater Res B Appl Biomater. 109(11):1844-1856. doi: 10.1002/jbm.b.34846. Epub 2021 Apr 13. PMID: 33847451.

- **Oztemur J..** Yalcin-Enis. I. (2021) Morphological Analysis of Fibrous Webs Electrospun from Polycaprolactone. Polylactic acid and Their Blends in Chloroform Based Solvent Systems. *Materilas Today: Proceedings.* 46(6) 2161-2166. https://doi.org/10.1016/j.matpr.2021.02.638.

- **Oztemur. J..** Yalcin-Enis. İ. (2020). The Potential Use of Fibrous Webs Electrospun from Polylactic Acid/Poly Ɛ-Caprolactone Blends in Tissue Engineering Applications. C. Civi. T. Yilmaz (Ed). Engineering and Architecture Sciences (pp. 213-234). Montenegro: IVPE. ISBN 978-9940-46-034-1

- **Oztemur. J..** Yalcin-Enis. İ. (2020). The Role of Biopolymer Selection in the Design of Electrospun Small Caliber Vascular Grafts to Replace the Native Arterial Structure. A. Hayaloğlu (Ed). Theory Research in Engineering (pp.167-192). Ankara: Gece Kitaplığı. ISBN 978-625-7243-79-7

- Ozdemir. S.. **Oztemur. J..** Sezgin. H.. Yalcin-Enis. İ.. 2021. Investigation of Polymer Concentration on Physical and Morphological Properties of PLLA Based Fibrous Structures. International Conference on Radiation Applications. 5-6 September 2021 (online conference)

- **Oztemur. J..** Yalcin-Enis. İ.. 2021. Fabrication and Physical Characterization of Biodegradable Fibrous Mats From Polylactic Acid and Polycaprolactone Blends Designed for Tissue Engineered Scaffolds. iNano Congress. 25-26 January 2021 (online conference)

OTHER PUBLICATIONS. PRESENTATIONS AND PATENTS:

- **Oztemur. J..** Sezgin. H. & Yalcin Enis. I. (2021) Design of an Impact Absorbing Composite Panel from Denim Wastes and Acrylated Epoxidized Soybean Oil based Epoxy Resins. Textile and Apparel. 31 (3). 229-234. DOI: 10.32710/tekstilvekonfeksiyon.910676

- **Oztemur. J..** Sezgin. H.. Yalcin-Enis. İ.. 2021. Effect of Blending Ratio on Morphological. Design of an Impact Absorbing Green Composite. Sustainable Materials and Practices for Built Environment (SMPBE). 25 November 2021 (online conference)